

The University of Maine

DigitalCommons@UMaine

Electronic Theses and Dissertations

Fogler Library

Summer 8-18-2023

Endothelial Interleukin-17 Receptor D (IL17RD) Promotes Western Diet-Induced Aortic Myeloid Cell Infiltration

Shivangi Pande

University of Maine, shivangi.pande@maine.edu

Follow this and additional works at: <https://digitalcommons.library.umaine.edu/etd>



Part of the [Cell Biology Commons](#), [Immunopathology Commons](#), and the [Molecular Biology Commons](#)

Recommended Citation

Pande, Shivangi, "Endothelial Interleukin-17 Receptor D (IL17RD) Promotes Western Diet-Induced Aortic Myeloid Cell Infiltration" (2023). *Electronic Theses and Dissertations*. 3838.

<https://digitalcommons.library.umaine.edu/etd/3838>

This Open-Access Dissertation is brought to you for free and open access by DigitalCommons@UMaine. It has been accepted for inclusion in Electronic Theses and Dissertations by an authorized administrator of DigitalCommons@UMaine. For more information, please contact um.library.technical.services@maine.edu.

**ENDOTHELIAL INTERLEUKIN-17 RECEPTOR D (IL17RD) PROMOTES WESTERN DIET-
INDUCED AORTIC MYELOID CELL INFILTRATION**

by

Shivangi Pande

B.Sc., University of Mumbai, India, 2010

M.Sc., University of Mumbai, India, 2012

A DISSERTATION

Submitted in Partial Fulfillment of the

Requirements for the Degree of

Doctor of Philosophy (in Biomedical Sciences)

The Graduate School

The University of Maine

August 2023

Advisory Committee:

Sergey Ryzhov, Faculty Scientist II, MaineHealth Institute for Research, Co-Advisor
Igor Prudovsky, Faculty Scientist II, MaineHealth Institute for Research, Co-Advisor
Robert Friesel, Faculty Scientist III, MaineHealth Institute for Research, External Advisor
Calvin Vary, Faculty Scientist III, MaineHealth Institute for Research
Pradeep Sathyanarayana, Senior R&D Manager, IDEXX Laboratories
Robert Gundersen, Professor (retired) & Dept Chair, MBMS, The University of Maine

© 2023 Shivangi Pande

All Rights Reserved

ENDOTHELIAL INTERLEUKIN-17 RECEPTOR D (IL17RD) PROMOTES WESTERN DIET-INDUCED AORTIC MYELOID CELL INFILTRATION

By Shivangi Pande

Thesis Co-Advisors: Dr. Sergey Ryzhov and Dr. Igor Prudovsky, Dr. Robert Friesel (external)

An Abstract of the Thesis Presented
in Partial Fulfillment of the
Requirements for the
Degree of Doctor of Philosophy
(in Biomedical Science)
August 2023

ABSTRACT: The Interleukin-17 (IL17) family is a group of cytokines implicated in the etiology of several inflammatory diseases. Interleukin-17 receptor D (IL17RD), also known as Sef (similar expression to fibroblast growth factor), belonging to the family of IL17 receptors, has been shown to modulate IL17A-associated inflammatory phenotypes. The objective of this study was to test the hypothesis that IL17RD promotes endothelial cell activation and consequent monocyte adhesion. We utilized primary human aortic endothelial cells and demonstrated that RNAi targeting of IL17RD suppressed transcript levels by 83% compared to non-targeted controls. Further, RNAi knockdown of IL17RD decreased the adhesion of THP-1 cells onto a monolayer of aortic endothelial cells in response to IL17A. Additionally, we determined that IL17A did not significantly enhance the activation of canonical MAPK and NF κ B pathways in endothelial cells and further did not significantly affect the expression of VCAM-1 and ICAM-1 in aortic endothelial cells, which is contrary to previous findings. We also determined the functional relevance of our findings *in vivo* by comparing the expression of VCAM-1 and ICAM-1 and leukocyte infiltration in the aorta in Western diet-fed *Il17rd* null versus wild-type mice. Our results showed that although *Il17rd* null mice do not have significant alteration in aortic expression of VCAM-1 and ICAM-1 in endothelial cells, they exhibit a decreased accumulation

of proinflammatory monocytes and neutrophils, suggesting that endothelial IL17RD enhances myeloid cell accumulation in a CAM-independent manner *in vivo*. We further assessed the pathophysiological relevance of our findings by initiating atherosclerosis in global and endothelial cell-specific *Il17rd* loss of function mouse models using an AAV-mPCSK9 approach. Our results suggest that although endothelial *Il17rd* does not affect the aortic lesion area, *Il17rd* modulates circulating levels of IL23 and IL27. Collectively, our results underscore a critical role for *Il17rd* in the regulation of WD-induced myeloid cell infiltration and proinflammatory cytokines *in vivo*.

ACKNOWLEDGEMENTS

There are several people who have contributed immensely to teaching me how to be a scientist and were instrumental in enabling me to reach my goals. First and foremost, I would like to express my sincere gratitude to my thesis advisors, Dr. Robert Friesel, Dr. Sergey Ryzhov, and Dr. Igor Prudovsky, as well as for giving me an opportunity to pursue my doctoral studies in their laboratories, for providing necessary direction to keep me focused on my research track as well as fostering independence of thought.

Secondly, I am extremely thankful to the Graduate School of Biomedical Science and Engineering (GSBSE) at The University of Maine, especially Dr. Lenard Kaye, Dr. Clarissa Henry, Dr. David Neivandt, Jennifer Chiarell, Zhen Zhang, and Tammy Crosby, for providing me with the opportunity to pursue my doctoral studies and funding the first two years of my studies. I would also like to specifically thank the Maine Economic Improvement Fund (MEIF) for granting me financial assistance via the University of Maine's Michael J. Eckardt Dissertation Fellowship for the academic year 2017-2018 to perform this research. I would also like to thank the MaineHealth administration, including Dr. Elizabeth Jacobs, Dr. Don St. Germain, Dr. Adriana Rosato, and Dr. Thomas Gridley, for providing all requisite resources during the course of my scientific training. I would also like to express my gratitude to my committee members, Dr. Calvin Vary, Dr. Pradeep Sathyanarayana, and Dr. Robert Gundersen, for critically assessing my work and providing valuable insight to refine my experimental methodology. Additionally, I would like to thank Dr. Lucy Liaw for providing valuable experimental and scientific resources and her guidance.

I will forever be grateful to Dr. Xuehui Yang for investing her valuable time and effort in providing me with all necessary hands-on technical training and for assisting me with performing major experiments. In addition, I would like to thank the managers of the MHIR Core Facilities, including the Histology Core, Molecular Phenotyping Core, Microscopy Core, Flow Cytometry C

ore, Physiology Core, and Research Laboratory Services Core for providing me with all necessary equipment and training to perform my experimental procedures.

I would also like to sincerely thank all current and past students at the GSBSE and Tufts, especially Dr. Deepthi Muthukrishnan, Matthew Siviski, Connor Murphy, Chenhao Yang, and Dr. Jessica Davis-Knowlton as well as all my colleagues at MHIR, especially Dr. Robert Koza, Dr. Rea Koza, Crystal Coombs, and Lindsey Gower for lending their professional expertise and providing personal encouragement during the various phases of graduate school. In addition, I would also like to thank several non-scientific staff members from MHIR, including Elisabeth Bergst from Staff Services, Karen Corts and Claire Stull from Operations, and Derek Nowek from Information Systems, for lending their professional expertise to facilitate my work.

To the most important people in my life, my family, my parents Madhu (Mamma) and Ravindra Kumar Pande (Baba), and my uncle Vinod Kumar Pande (Chachu); I fall short of words to express what you'll mean to me. Thank you for your resolute belief in my abilities, for being my steadfast support system, and my home. I am who I am only because of you. A special mention to my paternal grandparents Smt. Kamladevi (Dadi) and Shri Laxminarayan Pande (Babuji), I have felt your presence and blessings in every aspect of my life, and I know that your sacrifices have paved the way for me to be able to pursue my career aspirations. Another special mention to my maternal grandparents Smt. Savitri (Nani) and Shri Suraj Prasad Dwivedi (Nana), and my paternal great-grandfather Shri Hiralal Tiwari (Nanaji), you'll have had a profound effect on my upbringing that has enabled me to reach this stage of my life and career. To my brother Manoj Dwivedi (Pappu bhaiya), thank you for anchoring me when I was faced with life's curveballs, for sharing life's responsibilities, and propelling me forward toward my PhD. A distinctive mention to Karen Corts, Dr. Rakesh Verma and Navin Chopra uncle; you, along with my immediate family, are the shoulders on which I stand, and I consider you all as bona fide members of my family. Another special mention to all my friends, especially Dr. Ambreen Sayed, Dr. Shreya Shah, Dr.

Anupa Hinduja, Dr. Sonali Harchandani, Ritika Jhangiani, and Dr. Devina Savant, thank you for motivating me and standing by me when times were difficult.

DEDICATION

To my parents, Ravindra Pande and Madhu Pande, for their unwavering love and support, and for making me the person I am today. Every achievement of my life has been possible only because of your blessings and sacrifice.

TABLE OF CONTENTS

ACKNOWLEDGEMENTS.....	iii
DEDICATION.....	vi
LIST OF TABLES.....	xi
LIST OF FIGURES.....	xii
LIST OF ABBREVIATIONS.....	xiv
SPECIFIC AIMS.....	xviii
1. REVIEW OF THE LITERATURE.....	1
1.1 The cardiovascular system.....	1
1.1.1 Overview of the cardiovascular system.....	1
1.1.2 Structure, function and cellular composition of blood vessels	1
1.1.3 Endothelial cells.....	4
1.1.3.1 Endothelial cells during vascular homeostasis.....	4
1.1.3.2 Endothelial cell heterogeneity.....	6
1.2 Atherosclerosis and cardiovascular disease.....	9
1.2.1 Epidemiology of cardiovascular disease.....	9
1.2.2 Atherosclerosis.....	10
1.2.2.1 Endothelial cell activation.....	12
1.2.3 Animal models of atherosclerosis.....	14
1.3 IL17 signaling family.....	15
1.3.1 IL17 cytokines.....	16
1.3.1.1 IL17A signaling pathway.....	17
1.3.2 IL17 receptor family.....	17
1.3.2.1 IL17RD (SEF).....	18
1.3.2.2 Structure and conformation of IL17RD (SEF).....	19

1.3.2.3	Expression pattern of IL17RD (SEF).....	21
1.3.2.4	SEF (IL17RD) regulation of FGF and IL17 signaling pathways.....	22
1.3.3	IL17 signaling during pathological conditions.....	27
1.3.3.1	The contribution of IL17 cytokines to cardiovascular disease.....	27
1.3.3.2	The role of IL17RD (SEF) during disease.....	28
1.3.3.2.1	IL17RD (SEF) during inflammatory disease.....	28
1.3.3.2.2	IL17RD (SEF) during disorders of vascular remodeling.....	29
1.4	Summary and significance of our study.....	29
2.	MATERIALS AND METHODS	30
2.1	<i>In vitro</i> experiments.....	30
2.1.1	Cell culture, siRNA transfection and <i>in vitro</i> stimulation.....	30
2.1.2	RNA extraction, cDNA preparation and RT-qPCR analysis.....	31
2.1.3	Immunoblotting.....	32
2.1.4	Monocyte adhesion assay.....	35
2.2	<i>In vivo</i> experiments.....	35
2.2.1	Mice.....	35
2.2.1.1	KST223.....	37
2.2.1.2	Il17rd f/f.....	37
2.2.2	Tamoxifen injection.....	41
2.2.3	AAV-mPCSK9 ^{D374Y} injection.....	41
2.2.4	Diet feeding.....	41
2.2.5	Physiological measurements.....	41
2.2.6	Glucose Tolerance Test.....	42
2.3	<i>Ex vivo</i> experiments.....	42
2.3.1	Blood and serum collection.....	42
2.3.1.1	Hematological analysis, serum metabolite and cytokine analysis.....	42

2.3.2 Tissue harvest and processing.....	43
2.3.2.1 Preparation of aortic cell suspension and flow cytometry analysis	43
2.3.2.2 Histological sectioning	47
2.3.2.3 Oil Red O staining.....	47
2.3.2.4 Calculation of plaque area and lipid deposition	48
2.3.2.5 X-gal staining	48
2.4 Statistical analysis.....	49
3. RESULTS.....	50
3.1 Expression of IL17RD in human aortic endothelial cells.....	50
3.2 Knockdown efficiency of IL17RD in HAECs by siRNA transfection.....	51
3.3 Role of IL17RD in IL17A–induced adhesion of monocytes.....	52
3.4 IL17A does not stimulate VCAM-1 and ICAM-1 expression in HAECs.....	54
3.5 IL17A does not significantly induce activation of the NFκB and MAPK pathways in HAECs.....	55
3.6 <i>Il17rd</i> is expressed in aortic cell subpopulations <i>in vivo</i>	59
3.7 Validation of <i>Il17rd</i> null mouse model.....	61
3.8 Loss of <i>Il17rd</i> decreases weight gain and proportion of body fat in male mice upon 14-week WD feeding.....	62
3.9 Loss of <i>Il17rd</i> does not affect glucose metabolism.....	65
3.10 Effect of loss of <i>Il17rd</i> on the levels of circulating IL17A and cholesterol in male and female mice upon WD feeding.....	66
3.11 Loss of <i>Il17rd</i> decreases levels of FGF21 upon 14-week WD feeding.....	68
3.12 Loss of <i>Il17rd</i> decreases myeloid cell infiltration into the mouse aorta.....	69
3.13 Loss of <i>Il17rd</i> does not significantly affect the aortic endothelial expression levels of VCAM-1 and ICAM-1 upon WD feeding.....	72

3.14	Loss of <i>Il17rd</i> does not significantly affect the aortic endothelial expression levels of IL17RA and IL17RC upon WD feeding.....	74
3.15	<i>Il17rd</i> is expressed in atherosclerotic lesions in male mice <i>in vivo</i>	76
3.16	Loss of <i>Il17rd</i> does not affect atherosclerotic plaque formation <i>in vivo</i>	78
3.17	Analysis of atherogenesis in endothelial cell-specific <i>Il17rd</i> loss of function mice.....	79
3.18	Circulating levels of IL23 and IL27 are altered in endothelial cell-specific <i>Il17rd</i> knockout mice during atherosclerosis.....	81
4.	DISCUSSION AND FUTURE PERSPECTIVES	85
5.	REFERENCES	88
6.	BIOGRAPHY OF THE AUTHOR	99

LIST OF TABLES

Table 1: siRNA target sequences.....	31
Table 2: List of primary antibodies used for immunoblotting assays.....	34
Table 3: List of secondary antibodies used for immunoblotting assays.....	34
Table 4: Number of mice used in experimental analyses.....	36
Table 5: List of primers used in this study.....	40
Table 6: List of antibodies used for flow cytometry analysis.....	45

LIST OF FIGURES

Figure 1: Visual representation of putative structural and functional domains encoded by IL17RD (Sef) isoforms.....	20
Figure 2: Schematic diagram depicting modulation of the FGF signaling cascade by different isoforms of hSEF.....	24
Figure 3: Schematic diagram depicting IL17RD (Sef) regulation of the IL17 signaling cascade and associated disease relevance.....	26
Figure 4: Generation of endothelial cell specific <i>Il17rd</i> loss-of-function mice.....	38
Figure 5: Flowchart for gating strategy used for <i>in vivo</i> flow cytometry analysis.....	46
Figure 6: Analysis of <i>Il17rd</i> expression in human endothelial cells and THP-1 cells by RT-qPCR.....	50
Figure 7: Knockdown efficiency of IL17RD in HAECs by siRNA transfection.....	51
Figure 8: siRNA-driven down-regulation of <i>IL17RD</i> in human endothelial cells suppresses the adhesion of THP-1 cells.....	53
Figure 9: IL17RD promotes monocyte adhesion in HAECs in an ICAM-1- and VCAM-1-independent manner.....	55
Figure 10: Effect of <i>IL17RD</i> inactivation on the activity of downstream signaling cascades in human endothelial cells stimulated with IL17A.....	57
Figure 11: <i>Il17rd</i> is expressed in aortic cell subpopulations <i>in vivo</i>	60
Figure 12: Validation of <i>Il17rd</i> null mouse model.....	62
Figure 13: Loss of <i>Il17rd</i> decreases weight gain and proportion of body fat in male mice upon 14 week WD feeding.....	64
Figure 14: Loss of <i>Il17rd</i> does not affect glucose metabolism.....	66
Figure 15: Effect of loss of <i>Il17rd</i> on the levels of circulating IL17A and cholesterol levels in male and female mice upon WD feeding.....	67
Figure 16: Loss of <i>Il17rd</i> decreases levels of FGF21 upon 14-week WD feeding.....	69

Figure 17: Loss of <i>Il17rd</i> decreases myeloid cell infiltration into the mouse aorta.....	71
Figure 18: Loss of <i>Il17rd</i> does not affect the level of VCAM-1 and ICAM-1 expression on aortic endothelial cells.....	73
Figure 19: Loss of <i>Il17rd</i> does not significantly affect the aortic endothelial expression levels of IL17RA and IL17RC upon WD feeding.....	75
Figure 20: <i>Il17rd</i> is expressed in atherosclerotic lesions in male mice <i>in vivo</i>	77
Figure 21: Loss of <i>Il17rd</i> does not affect atherosclerotic plaque formation <i>in vivo</i>	78
Figure 22: Efficiency of <i>Cdh5-CreERT2</i> mice.....	80
Figure 23: Endothelial specific deletion of <i>Il17rd</i> regulates atherosclerotic plaque formation.....	81
Figure 24: Circulating levels of IL23 and IL27 are altered in endothelial cell-specific <i>Il17rd</i> knockout mice during atherosclerosis.....	83

LIST OF ABBREVIATIONS

AAV: adeno-associated virus
ACS: acute coronary syndromes
AJ: adherens junctions
AML: Acute monocytic leukemia
ApoB: apolipoprotein B
ApoE: apolipoprotein E
ATCC: American Type Culture Collection
BEC: blood endothelial cells
BSA: Bovine Serum Albumin
CAM: cell adhesion molecules
CD: Chow diet
COUPTFII: chicken ovalbumin upstream transcription factor II
CMC: Chronic mucocutaneous candidiasis
DAPI: 4',6-diamidino-2-phenylindole
DEXA: dual-energy x-ray absorptiometry (DEXA)
DII4: Delta-like canonical Notch ligand 4
dPBS: Dulbecco's Phosphate Buffered Saline
EBM-2: Endothelial Basal Media-2
ECM: extracellular matrix
EEL: external elastic lamina
EGM-2: Endothelial Cell Growth Medium-2
ERK: Extracellular Regulated Kinase
eNOS: endothelial nitric oxide synthase
EphB4: ephrin receptor B4
EuMMCR: European Mouse Mutant Cell Repository

F-actin: Filamentous actin

FBS: Fetal Bovine Serum

FGF: Fibroblast Growth Factor

FGFR: FGF receptor

fl/fl: flox/flox

FLPo: Flp recombinase

FRT: flippase recognition target

$\gamma\delta$: Gamma delta T cells

GFP: Green Fluorescent Protein

GJ: gap junctions

GTT: Glucose Tolerance Test

HAEC: Human Aortic Endothelial cells

HDL: high density lipoproteins

HEPES: ((4-(2-hydroxyethyl)-1-piperazineethanesulfonic acid)

HRP: Horseradish peroxidase

HSPG: heparin sulfate proteoglycan

Ig, Immunoglobulin

ICAM-1, Intercellular adhesion molecule-1;

IEL: internal elastic lamina

IL17A, Interleukin-17 A

IL17RA, Interleukin-17 Receptor A

IL17RC, Interleukin-17 Receptor C

IL17RD, Interleukin-17 Receptor D

ILC3: type 3 innate lymphoid cells

I.Q.R, Interquartile range

JNK, c-Jun N-terminal kinase

LEC: Lymphatic ECs

LDL: low density lipoproteins

LDLR: LDL receptors

LYVE-1: lymphatic vascular endothelial hyaluronan receptor-1

MAPK: Mitogen activated protein kinase

MI: myocardial infarction

NF- κ B: Nuclear Factor kappa light chain enhancer of activated B cells

NKT: natural killer T-cells

NO: nitric oxide

NMR: Nuclear Magnetic Resonance

NT: non-targeting scrambled

OCT: Optimal Cutting temperature compound

ORF: open reading frame

Ox-LDL: oxidized LDL

pA: polyadenylation site

PAD: peripheral arterial disease

PCSK9: proprotein convertase subtilisin/kexin type 9

PECAM-1: platelet endothelial cell adhesion molecule-1

Prox1: prospero-related homeobox domain 1

PVAT: Perivascular adipose tissue

PI3K: Phosphoinositide 3 kinase

RA: rheumatoid arthritis

RTK: Receptor Tyrosine Kinase

RPMI, Roswell Park Memorial Institute

SA: splice acceptor

SMC: smooth muscle cells

Sox18: SRY-related HMG-box 18

S.D.: Standard Deviation

Sef: Similar expression to FGF

SEFIR: Sef/IL17R

TEM: transendothelial migration

Th17 cells, type 17 T-helper T-cells

TJ: tight junctions

TNF: Tumor Necrosis Factor

TRAD: TNF receptor associated factor

VCAM-1: Vascular cell adhesion molecule

VE-cadherin: Vascular endothelial cadherin

VEGFR2: Vascular endothelial growth factor 2

VLA-4: very late antigen-4

VVO: vesiculo-vacuolar organelles

vWF: von Willebrand Factor

WHHL: Watanabe hereditary hypercholesterolemic

WT: Wild Type

WD: Western Diet

SPECIFIC AIMS

Aim 1: Determine whether IL17RD regulates IL17A-induced expression of endothelial cell (EC) adhesion molecules (CAM) and leukocyte adhesion *in vitro*.

Hypothesis: IL17RD promotes IL17A-induced activation of downstream p38 MAPK signaling pathway in human ECs to regulate the expression of endothelial CAM molecules and promote monocyte adhesion *in vitro*.

Aim 2: Examine the role of IL17RD regulates aortic EC activation and leukocyte infiltration during inflammatory conditions *in vivo*.

Hypothesis: IL17RD promotes *in vivo* aortic EC expression of CAM molecules and myeloid cell infiltration upon WD feeding in mice.

Aim 3: Investigate whether IL17RD regulates hypercholesterolemia-induced atherosclerotic plaque formation *in vivo*.

Hypothesis: Endothelial IL17RD promotes atherosclerotic plaque formation in a mouse model of hypercholesterolemia-induced atherogenesis.

CHAPTER 1: REVIEW OF THE LITERATURE

1.1 The cardiovascular system

1.1.1 Overview of the cardiovascular system

The vertebrate circulatory system is an intricate and complex organ system that functions to transport respiratory gases, nutrition, metabolites, and secretory molecules, as well as provide immune surveillance for the efficient homeostatic functioning of the body. The cardiovascular system, along with the lymphatic system, form the two integral circuits which invasively traverse the body to form the circulatory system. The cardiovascular system includes the heart, blood, and blood vessels, in which the heart functions as an anatomical pump to propel blood into vessels. These vessels serve as a conduit for the circulation of blood containing various metabolites and effectors throughout the body. The lymphatic system consists of the lymph, lymph vessels, and lymph nodes, and lymphoid organs such as bone marrow, spleen, and thymus; and collects exudate and interstitial fluid which filters out from the arteries and capillary beds within the hematopoietic system (1).

Within the cardiovascular system, the circulatory circuits are further subdivided into the circulatory system into pulmonary and systemic circulations. The pulmonary circulatory system functions to provide oxygenated blood, specifically from the lung to the heart, whereas the systemic circulatory system pumps oxygenated blood from the heart to the other organ systems (1).

1.1.2 Structure, function and cellular composition of blood vessels

Blood vessels are classified into arteries, arterioles, capillaries, venules, and veins; based on their size, structure, and function. Functionally, arteries and arterioles (except pulmonary artery) serve as conduits for oxygenated blood, whereas venules and veins (except pulmonary vein)

serve as carriers of deoxygenated blood. The layout of vessels within the circulatory system follows a hierarchical branching network. In the systemic circuit, the dorsal aorta is the major arterial blood vessel that arises from the left atrium of the heart and subsequently divides into major arteries. These arteries further divide into smaller arterioles and capillaries to extensively traverse all organs and facilitate the exchange of nutrients, gases, and metabolites to meet their nutritive and respiratory needs, as well as collect secretions such as enzymes, hormones, and growth factors for transport to target tissues. The deoxygenated blood containing various secretions then drains from capillary beds into venules which feed into large veins (except the pulmonary vein), which subsequently drain into the inferior vena cava and ultimately into the right atrium of the heart for reoxygenation via the pulmonary circulation. Under homeostatic conditions, blood flows within the vessels in a pulsatile manner in a linear direction parallel to the long axis of the vessels (2).

The cardiovascular system is the first organ system to be established in the developing embryo and is initiated with the *de novo* formation of blood vessels termed vasculogenesis, which occurs at E7.5 in mice (3) and E14.5 in humans (4). The process initiates with the appearance of bipotent precursor cells known as hemangioblasts derived from mesodermal progenitor cells and which can differentiate into endothelial cells and hematopoietic cells. These hemangioblasts coalesce in 2 distinct areas around the yolk sac to form “blood islands” and establish two “angioblastic cords” which lumenize and anastomose to form the primitive vascular plexus alongside concurrent development of the heart and establishment of a definitive hematopoietic system and leading to the onset of circulation (5). This plexus then undergoes remodeling to expand and establish a functional vascular network through the process of “angiogenesis”, which is the formation of new vessels from existing vessels in response to chemokine gradients (6, 7). The process of angiogenesis entails the development and extension of F-actin (filamentous actin) filled membranous protrusions from a specialized type of vascular cells, termed endothelial cells (ECs) (8) (reviewed later) . The ECs that respond to proangiogenic

signals by extending filopodia are termed “tip cells”, whereas the other endothelial cells elongate, lumenize, and anastomose to establish the vessel by forming “stalk cells” (8) (discussed later). The ECs then lumenize and anastomose to establish a functional vascular network and recruit mesenchymal cells to the growing vessel, which differentiate into smooth muscle cells (SMCs) or pericytes to mature the growing vessel, leading to the establishment of a functional vascular network (7).

In terms of its ultrastructure, mature blood vessels are arranged into 3 concentric layers radiating outward from the lumen, sequentially tunica intima, tunica media, and tunica externa, which function to maintain vascular tone. The tunica intima forms the innermost layer of the blood vessel. It is comprised of an innermost continuous monolayer of ECs, surrounded by a subendothelial layer consisting of mesodermal cells and extracellular matrix (ECM) molecules such as collagen, laminin, fibronectin and heparin sulfate proteoglycan (HSPGs) called the basement membrane. This is surrounded by a basal layer of elastic tissue lamella known as internal elastic lamina (IEL) which separates it from the tunica media. The tunica media is the middle layer of the blood vessel, comprised of several layers of vascular smooth muscle cells (pericytes in the case of capillaries) and an extracellular matrix comprised of collagen and elastin fibers. It is separated from the tunica externa by the external elastic lamina (EEL). The tunica externa (tunica adventitia) forms the outermost structural layer of the blood vessel, consisting predominantly of extracellular matrix components such as fibroblasts, mast cells, as well as extensive neuronal and vascular networks (vasa vasorum), and a surrounding layer of perivascular adipose tissue (PVAT) (9).

Structurally, the major difference between the major types of blood vessels lies in their size, the thickness of vessel walls, primarily the tunica media, and lumen diameter. Arteries and veins (macrovasculature) have a diameter from 100 μm to 2.5 cm, arterioles and venules have a diameter between 8 μm to 100 μm , whereas capillaries have a diameter of less than 8 μm . Arteries and arterioles have a small lumen and thick medial layer to accommodate the

circulatory pressure of ejection of blood from the heart, whereas most capillaries are characterized by a single layer of endothelial cells and a basement membrane to facilitate the exchange of materials and the absence of tunica media and tunica externa layer. Since veins transport blood in the absence of ejector pressure from the heart, they have a thinner medial layer and larger lumen. However, veins are interspersed with valves to prevent the backward flow of blood into organs as well as to transport blood upwards into the heart against gravitational force. Although arteries typically do not have such valves throughout their structure, the major arteries (pulmonary and dorsal aorta) are characterized by valves at the juncture of the beginning of the vessel and the heart to ensure unidirectional flow of blood under ejector circulatory pressure (9, 10).

1.1.3 Endothelial cells

1.1.3.1 Endothelial cells during vascular homeostasis

ECs are a specialized type of cells that form a dynamic monolayer interface encircling the vessel lumen in the form of an endothelial layer or endothelium. Depending on the characteristics of the originating vessel, the dimensions of mature ECs lie within a range of 50-70 μm in length, 10-30 μm in width, and 100 nm–10 μm in thickness. During development, ECs are derived from hemangioblasts within the mesodermal layer in the developing embryo, which populate micro and macro vessels to form the largest vascular system in the body, numerically translating to an average of 10,000 billion cells occupying a surface area of approximately 1000 μm^2 (11, 12) Under physiological conditions, ECs have ellipsoidal nuclei and exhibit an apical–basolateral polar orientation. They are longitudinally arranged in a coaxial planar alignment parallel to the direction of blood flow (13). The apical side of the endothelium oriented towards the vessel lumen is overlaid with a thick layer of glycoproteins and proteoglycans termed the glycocalyx, which primes it to withstand the force of fluid shear stress on the luminal side of the

vessel, whereas the basolateral side regulates interaction with the pericytes and IEL to maintain vessel wall integrity (14, 15).

The endothelium primarily functions as a dynamic semi-permeable membrane is to regulate vascular homeostasis under conditions of laminar shear stress. In this context, multiple endogenous properties of the endothelium (sensory, anti-inflammatory, and secretory) contribute to its primary function of maintaining vascular homeostasis. ECs function to provide a semi-permeable barrier between circulating blood and surrounding vascular tissue to regulate platelet and leukocyte adherence to intimal cells (anti-inflammatory properties), integrate and transduce hemodynamic stimuli from circulating blood (sensory properties) and synthesize and store metabolites such as prostacyclins, endothelin, nitric oxide (NO) and vWF (von Willebrand Factor) (secretory properties) (12, 13)

Endothelial cells store vWF or Factor-VIII in granular structures known as Weibel-Palade bodies, which are exclusively characteristic of ECs. Due to its extensive range of intrinsic properties, ECs have the ability to control several processes such as coagulation and fibrinolysis, vasomotor tone, blood viscosity and blood pressure, vascular tone and dilation, immunomodulation, and tissue vascularization by angiogenesis (11, 12, 16)

An influx of biomolecules and cellular structures across the endothelium occurs via two primary mechanisms, namely transcellular transport and paracellular transport. Transcellular transport involves the transcytosis of large biomolecules, ligands, and hormones into the interstitium via caveolae-rich structures termed vesiculo-vacuolar organelles (VVO) (17). Paracellular transport involves the recruitment of intercellular junctional complexes, namely gap junctions (GJ), tight junctions (TJ), and adherens junctions (AJ) which are interspersed along the length of the monolayer (17, 18). GJ function as channels between adjacent ECs to regulate the transport of water, ions, and small metabolites across the monolayer, whereas TJ and AJ maintain EC integrity. Specifically, tight junctions regulate the distribution of cytoskeletal and membranous lipoprotein complexes to maintain EC planar cell polarity, whereas AJs function to facilitate EC

intracellular and intercellular communication through calcium-dependent homophilic receptor interactions (17-19)

The distribution of AJ and TJ and interaction between them regulates the integrity of the monolayer and are specific to each vascular bed. Each junction is characterized by specific markers, claudin and occluding proteins are associated with tight junctions, wherein Vascular endothelial cadherin (VE-cadherin) and platelet endothelial cell adhesion molecule-1 (PECAM-1) are markers mostly associated with AJs. In addition to the intercellular junctional complexes, ECs also possess clathrin-coated pits and clathrin vesicles, which regulate endocytic macromolecule and receptor trafficking within the cell (11, 14, 18, 20).

Given the above-mentioned unique features and markers of ECs, commonly used markers of endothelial cells include VE-cadherin, vWF, PECAM-1, endothelial nitric oxide synthase (eNOS), and Vascular endothelial growth factor 2 (VEGFR2) (11).

1.1.3.2 Endothelial cell heterogeneity

Endothelial cells (EC) demonstrate significant plasticity and environmental adaptability resulting in diversity in morphological, functional, and transcriptomic properties, which result in a range of EC outputs in permeability, expression of specific endothelial markers, and layout of tight and adherens junctions. This consequent phenotypic, structural, molecular, and functional heterogeneity is defined under the purview of EC heterogeneity (21).

Principally, ECs populate vasculature carrying either blood or lymph, based on which they are classified as blood endothelial cells (BEC) or Lymphatic ECs (LEC). All ECs are derived from hemangioblasts (11, 12) (discussed previously) and exhibit significant diversity in size, phenotype, structure, function, and molecular signature as a factor of location, which is discussed below. Whereas LECs express the transcription factor prospero-related homeobox domain 1 (Prox1), VEGFR-3, lymphatic vascular endothelial hyaluronan receptor-1 (LYVE-1),

and the membrane glycoprotein podoplanin. Similar to BECs, LECs also exhibit extensive diversity in molecular signature, structure, and function depending on the size and location of the vessel, which is beyond the scope of this review and has been covered elsewhere (22-25). Multiple factors, such as the size of the vessel, the location in a specific organ, exposure to microenvironmental cues, and biophysical forces contribute to EC heterogeneity. EC heterogeneity can be expressed as a characteristic output signature of several parameters, such as molecular signature, number of tight junctions, continuity of the endothelial monolayer, presence of fenestrae, and size and density of VVOs, in an organ-specific manner (26).

Size: In terms of size, ECs from different organs exhibit a diversity of fundamental properties based on the diameter of originating vessel. Macrovascular ECs are those that populate large vessels, including aortae, cardinal vein, and umbilical aorta and vein, whereas those derived from arterioles, venules, and capillaries, are classified as microvascular ECs e.g.: heart (cardiac), skin (dermis) lung (pulmonary) and brain (cerebral) endothelial cells. Usually, large arteries and arterioles are characterized by well-defined tight junctions with fewer VVOs, whereas capillaries and venules have loosely defined tight junctions and numerous VVOs to facilitate the exchange of metabolites and transcellular outflux (20). However, the characteristics of ECs in each vascular bed are determined by organ-specific cues.

Arterial and venous ECs: Molecularly, arterial ECs express markers such as VEGFR2, EphrinB2, Delta-like canonical Notch ligand 4 (Dll4), Jagged1, and Dll1. Capillary ECs expressing the highest levels of VEGFR2 extend filopodia to migrate towards vascular cues such as VEGF-A gradient to form tip EC, which lead angiogenesis (8). The cells that express the highest levels of VEGFR2 form tip cells and also express other specific molecular markers such as Dll4, VEGFR3, NRP1, and PDGF-BB (8). The Dll4 expressed by the tip cells then laterally binds to adjacent ECs to suppress the expression of VEGFR2 in these cells via Dll4/Notch signaling to suppress the tip cell phenotype in these cells. These arterial ECs with suppressed VEGFR2 expression are called stalk cells and express high levels of Jagged1 and

Dll1. These ECs proliferate and extend the length of the vessel to arrange and form a lumen to eventually establish a vessel structure. Whereas venous ECs express the transcription factor chicken ovalbumin upstream transcription factor II (COUPTFII) and ephrin receptor B4 (EphB4) (27, 28). Further, COUPTFII promotes the expression of Prox1 through SRY-related HMG-box 18 (Sox18) to give rise to LECs (6, 10).

Structural heterogeneity: ECs exhibit a significant degree of structural heterogeneity to adapt to the functions of the originating organ. Based on this aspect, the endothelial layer can be continuous or discontinuous. A continuous endothelial layer is one in which the ECs are anchored to an intact basement membrane and are characterized by the presence of several TJ. Further, based on the presence of membranous transcellular pores known as fenestrae that perforate EC intercellular junctions, continuous endothelium can be subdivided into fenestrated or nonfenestrated continuous endothelium. Microvasculature of organ systems such as the cardiac, cerebral, and pulmonary is continuous and nonfenestrated; however, heterogeneity may still be observed amongst these organs to dynamically adapt to the function of each organ system e.g. cardiac and skeletal capillary beds have fewer tight junctions and a high number of caveolae for transporting water and small solutes by transcytosis and endothelial layer within the cerebral microvasculature has numerous tight junctions and few caveolae to stringently maintain neuronal homeostasis in the face of dynamic alterations in blood constitution. In contrast, organ systems associated with requirements for increased permeability, such as secretory glands, digestive systems, and excretory systems, have a continuous and fenestrated endothelium with sparsely interspersed tight junctions to regulate water and solute balance. The discontinuous endothelium is characterized by a discontinuous, largely sinusoidal, and fenestrated endothelial layer anchored onto a poorly developed basement membrane leading to the formation of intercellular junctions for endocytosis and translocation of nutrients, metabolites, and large macromolecules across the endothelial layer. It is characteristic of

organs with high metabolic activity and cellular turnover rates, including liver, bone marrow, and spleen (11, 14, 16, 20).

In addition to heterogeneity arising from organ-specific cues, ECs are also functionally adaptable to a localized microenvironment to represent a phenotype that is an integrated output of external spatiotemporal factors such as biomechanical forces as well as exposure to growth factors and cytokines that also contribute to the heterogeneous nature of ECs, which can often lead to segments with phenotypic and molecular heterogeneity within the same organ (29). For example, single-cell transcriptomic analysis of aortic cell subpopulations revealed multiple distinct subsets of ECs associated with remodeling and metabolism, wherein each subpopulation expresses specific genes associated with specific endothelial cell functions. This suggests functional segregation and heterogeneity of ECs even within the same organ, representing the capability of each individual EC to dynamically adapt to a localized microenvironment (11, 26).

1.2 Atherosclerosis and cardiovascular disease

1.2.1 Epidemiology of cardiovascular disease

Cardiovascular disease is the predominant cause of death worldwide, which translates into a numerical figure of approximately 17.8 million individuals and is expected to rise to more than 22 million by the year 2030. Within the United States, cardiovascular-related mortalities surpass the incidence of cancer, with approximately 850,000 deaths attributable to cardiovascular disease in the year 2017, and the incidence is higher in middle to low-income countries due to premature mortality on account of socioeconomic factors (30). In addition, the expenses incurred due to medical intervention and treatment lead to a significant economic burden to the affected families, reflected by an annual collective cost of \$351.3 billion for the year 2014-2015. Several strategies have been developed over the past few years for effective management of

risk parameters of cardiovascular disease. These include monitoring and effective management of health factors such as exercise and physical activity and maintenance of healthy body weight, quality of diet and nutritional intake, regulation of blood pressure as well as and lifestyle behaviors such as salt/alcohol/tobacco consumption, and metabolic parameters such as blood levels of cholesterol, triglycerides and blood glucose (30). Although current intervention strategies have advanced enough to decrease the risk of morbidity and mortality, there remains a significant risk of residual disease, which can lead to impairment (31).

1.2.2 Atherosclerosis

Atherosclerosis is a pathological condition characterized by the accumulation of lipid-filled, multicellular lesions within the tunica intima of medium and large-sized arterial blood vessels, known as an atherogenic plaque or atheroma (31). Progressive lesion buildup along with maladaptive cellular response within the vessel leads to the development of occlusive fatty streaks, which impede blood flow resulting in vessel stenosis and tissue hypoxia, resulting in the development of clinical sequelae such as aneurysm formation, aortic rupture, and organ ischemia. These events consequently act as a prelude to the development of chronic complications such as angina pectoris and peripheral arterial disease (PAD) and/or acute coronary syndromes (ACS) such as myocardial infarction (MI) and cerebrovascular strokes, which might have debilitating or lethal consequences (31).

From a biological perspective, atherosclerosis is a multifaceted disease comprised of genetic, metabolic, environmental and hemodynamic factors. The pathophysiological manifestation of the disease is a manifestation of chronic systemic inflammatory conditions, resulting as a cumulative outcome of dysregulated cellular lipoprotein metabolism and cellular response of the vessel wall, leading to the formation of lipid laden multicellular fibrous structures. Etiologically, the disease can be divided into 3 stages, namely initiation, progression, and development of complications, and is primarily caused by pathologically elevated levels of cholesterol-containing

lipoproteins in circulation (32, 33). Depending on their density, these lipoproteins are primarily classified as low-density lipoproteins (LDL) and high-density lipoproteins (HDL), of which LDL functions as the predominant cholesterol carrier and the principal initiator of atherosclerosis and development of fatty streaks (31) (34). LDL-Cholesterol is usually transported in the blood as a core of lipid (cholesteryl ester) rich globules encircled by a hydrophilic coating comprised of phospholipids, unesterified cholesterol, and apolipoprotein B (apoB). The mechanism of uptake of circulating LDL-C is via LDL receptors (LDLR), which bind apoB leading to internalization and endocytosis of LDL. A circulating enzyme called PCSK9 (proprotein convertase subtilisin/kexin type 9), secreted predominantly by the liver and by the intestine and kidneys to a lesser degree, inhibits the recycling of LDLRs and promotes their degradation within hepatocytes, effectively increasing the levels of circulating cholesterol (34).

In addition to physiologically elevated levels of LDL-Cholesterol, exposure to other inflammatory risk parameters such as hyperglycemia, hypertension, inflammatory cytokines and disturbed blood flow leads to disruption of the integrity of the endothelial layer. The functionally impaired ECs facilitate the penetration of LDL, as well as leukocytes from the blood into the vessel wall, wherein the LDL undergoes chemical oxidation to form oxidized-LDL (ox-LDL), and monocytes differentiate into aortic macrophages, and these together form the fatty streak. Progression of atherosclerosis occurs when the ox-LDL particles are endocytosed by scavenger receptors expressed by the macrophages, thereby transforming into cholesterol-rich foam cells, which synthesize inflammatory cytokines and matrix metalloproteinases (MMPs) (31). These inflammatory mediators transform smooth muscle cells from a quiescent, contractile state to an aberrant proliferative, synthetic phenotype which contributes to the formation of foam cells and also synthesizes ECM macromolecules comprising the fibrous cap, which determines the plaque's susceptibility to withstand denudation under turbulent flow in advanced plaques (15). As the disease progresses, the cellular components of the plaque, including ECs, smooth muscle cells, and macrophages, undergo apoptosis, and impaired efferocytosis of the cellular

debris leads to the formation of a necrotic core, which accrues upon the building plaque. The secreted MMPs modulate the breakdown and remodeling of collagen within the cap, increasing the vulnerability of the lesion to biomechanical forces of blood flow (33). Thus, each plaque is a multicellular heterogeneous structure, depending on cellular composition, stage of progression, as well as remodeling due to exposure to external factors such as sustained inflammatory insults and circulatory hemodynamic forces, leading to inter and intra-individual plaque heterogeneity (15).

The final stages of atherosclerosis entail the development of clinical complications due to plaque complexity and eventual rupture. Progressive enlargement in lesion size infringes upon the vessel lumen, restricting blood supply and leading to tissue ischemia and necrosis. In case of plaque rupture, exposure of cellular components of the plaque to blood flow initiates the clotting cascade, leading to thrombus formation, which precedes strokes and myocardial infarctions (15, 32).

1.2.2.1 Endothelial cell activation

Depending on the surrounding milieu, ECs undergo acute (type I) or chronic (type II) activation response. Acute responses comprise transient changes in physiological parameters, including microvascular permeability and resistance in response to inflammatory mediators, and mostly involve transcellular mechanisms (17).

Whereas chronic response encompass sustained alterations in EC phenotype and function in response to stimulation with biological agents such as cytokines, pathogen products, or turbulent hemodynamic forces, termed endothelial cell dysfunction or endothelial cell activation. This activation initiates a series of events involving leukocyte arrest, rolling, and trans-endothelial migration (TEM), designated as the leukocyte adhesion cascade (35). ECs that are exposed to multidirectional flow patterns, such as those at vessel branch points, and those

exposed to elevated shear stress, such as valvular endothelial cells, exhibit polygonal geometries and undergo an erosion of the glycocalyx layer. As a result, these ECs are most susceptible to impairments in barrier function, forming atherosclerosis-prone regions (15). Morphologically, ECs transform into cuboidal geometries and undergo molecular and cellular changes, including activation of proinflammatory signaling cascades and alterations in the expression and synthesis of cellular markers and chemokines, resulting in enduring changes in permeability which consequently promote leukocyte recruitment and TEM (13). Leukocyte transmigration across the EC occurs predominantly by employing a paracellular mode of transport, with a few microvascular beds employing transcellular mechanisms (35). The EC cellular markers associated with leukocyte TEM include immunoglobulin-like adhesion molecules, including cellular adhesion molecules (CAM) such as vascular cell adhesion molecule-1 (VCAM-1) and intercellular adhesion molecule-1 (ICAM-1). Other molecules involved in this process include cell surface lectins: endothelial and platelet selectin (36). A brief description of relevant EC activation markers is given below:

VCAM-1: Vascular cell adhesion molecule-1 (VCAM-1) or CD106 is an immunoglobulin-like glycoprotein ligand that is predominantly expressed in endothelial cells as well as other cell types as an inducible adhesion ligand, and was shown to be significantly induced upon exposure to proinflammatory cytokines and mediators in ECs (13, 37). VCAM-1 has been shown to primarily bind with high affinity to mononuclear leukocytes constitutively expressing the receptor very late antigen-4 (VLA-4, alternatively designated as integrin $\alpha 4\beta 1$), as well as with integrin $\alpha 4\beta 7$ expressing lymphocytes and galectin-3 expressing eosinophils with weaker affinity (38). Mechanistically, VCAM-1/VLA-4 binding has been shown to facilitate leukocyte rolling, adhesion, and TEM in a protein kinase C α (PKC α)/ protein tyrosine phosphatase 1B (PTP1B) dependent manner, consequently impairing EC cellular junctions and permeability (39). Furthermore, upregulation of EC VCAM-1 expression has been shown to be associated

with the EC layer in several human and mouse models of atherosclerosis and is therefore used as a principal marker representing endothelial cell activation (37, 40).

ICAM-1: Intracellular adhesion molecule-1 (ICAM-1) or CD54 is a transmembrane protein belonging to the immunoglobulin family, which is inducibly expressed in endothelial as well as multiple other cell types, including epithelial cells and immune cells (41). The cognate receptors for ICAM-1 include leukocyte receptors β 2-integrins lymphocyte function-associated antigen 1 (LFA-1) CD11a/CD18) and macrophage antigen 1 (Mac-1; CD11b/CD18). Structurally, ICAM-1 consists of five extracellular immunoglobulin domains, which ensure receptor dimerization and engagement with cognate receptors to facilitate leukocyte TEM, followed by a transmembrane and cytoplasmic domain (41). ICAM-1 has been shown to promote EC activation in a MAPK-dependent manner, as well as induce cytoskeletal rearrangement and leukocyte trafficking and migration in a cell context-dependent manner dependent via the activation of Protein kinase C-Rho-GTPase, AMPK/ Calcium- CaMMK and Src kinases (42). Consistent with this, in vitro and in vivo data have shown that ICAM-1 promotes the infiltration of monocytes, lymphocytes, and neutrophils into atherosclerosis-prone regions. In view of its potent effector function, ICAM-1 is used as a cell activation marker denoting EC activation along with VCAM-1 (40).

1.2.3 Animal models of atherosclerosis

Animal models that have been commonly used for atherosclerosis studies include mice, rabbits, and pigs, as well as nonhuman primates such as monkeys (43). Pig and rabbit models of atherosclerosis include wild-type domestic species such as the New Zealand white rabbit and domestic farm pig as well as mutant hypercholesterolemic models such as the Watanabe hereditary hypercholesterolemic (WHHL) rabbits and hyper-LDL cholesterolemia pig models that develop atherosclerosis on a cholesterol-rich diet whereas non-human primate models of atherosclerosis include the African Green, Rhesus, and cynomolgus monkeys. All these models

develop atherosclerotic plaques when maintained on a cholesterol-rich diet for a minimum duration of 18-24 months, thus proving to be cost and labor-intensive. (44-46).

Mice are the most commonly used model organisms for atherosclerosis studies due to advancements in gene targeting approaches which enable the generation of transgenic mice having global as well as conditional gene deletions and insertions (43). Additionally, the short gestation time for mice (21 days), as well as the availability of mutant atherosclerosis-prone mouse models such as the apolipoprotein E (ApoE) knockout mouse strain (47) and LDL receptor (Ldlr) knockout mouse (48) allow the study of the effect of specific genes through the generation of multiple mutant mouse models, thus providing an economically and timely efficient experimental means for atherosclerosis studies (43). Further, recent technological advancements demonstrated that injection of a single dose of adeno-associated vector (AAV) based gain-of-function formulation of the PCSK9 virus (AAV-PCSK9^{D374Y}) into wild-type (WT) mice induced hyperlipidemia and led to the formation of atherosclerotic plaques, addressing the economic and time limitations associated with intercrossing for generation of complex mutant atherosclerosis-prone mice (49). In this context, of the several strains of mice used for performing atherosclerosis studies, the C57BL/6 mouse model has been shown to be most susceptible to hyperlipidemia and the formation of lesions in studies of vascular inflammation and atherosclerosis (49-51).

1.3 IL17 signaling family

Cytokines are small proteins that function as intercellular mediators by initiating signaling responses within cellular networks. The IL-17 signaling family consists of six structurally related ligands (IL17A - F) and five cognate receptors (IL17RA - IL17RE) (52). All receptors from this family are single-pass transmembrane proteins characterized by the presence of conserved domains, specifically an extracellular fibronectin type III domain and an intracellular SEFIR motif, which form the structural basis of similarity between receptors from this family (52). The

SEFIR domain of IL17 receptors recruits and interacts with the SEFIR domain of the cytosolic adapter protein Act1 to activate the canonical IL-17 dependent MAPK and NFκB pathways, which forms the functional basis of similarity of all receptors belonging to this family (52, 53). IL17 receptors exist as homodimers and as heterodimers and have been shown to interact via the SEFIR domain in certain cellular contexts (54). Structurally, cytokines belonging to this family adopt a unique cysteine knot fold architecture and exist in physiological states as homodimers and as heterodimers with other IL17 cytokines and often bind to homo and heterodimeric IL17 receptor complexes, increasing the complexity of cytokine-receptor interactions (55).

1.3.1 IL17 cytokines

Elevated levels of IL17 family cytokines have been observed in a host of several diseases, however, the most significant associations between elevated IL17 levels have been observed in the context of inflammatory diseases, including oral candidiasis, host-pathogen interactions, autoimmune disease, and allergic responses (55, 56). IL17A is often found in a heterodimeric conformation with IL17F, and induces similar downstream pathway activation as well as phenotypic outputs as IL17A, albeit with lesser efficiency. In addition to IL17A, IL17C, and IL17E have also been shown to modulate allergic responses, as well as host defense in autoimmune diseases (56). IL17C is primarily secreted by epithelial cells and has been shown to promote inflammation in these tissues, as well as mediate epithelial-neuronal crosstalk during injury and disease (56). IL17E secreted by intestinal tuft cells and thymic epithelial cells has also been shown to have an important role in facilitating a type II immune response to parasitic infections. IL17B is principally secreted by immune cells and has been associated with inflammation and oncogenic transformation in tissues of epithelial origin (56). The function of IL17D still needs further elucidation, however, initial studies suggest that it is associated with an inflammatory

phenotype during leukocyte infiltration during cancer. Within the IL17 family, IL17A remains the best-characterized cytokine with respect to the function and pathophysiology of the disease, whereas the receptor for IL17D remains undefined (55).

1.3.1.1 IL17A signaling pathway

IL17A is a pleiotropic proinflammatory cytokine that is associated with a wide spectrum of inflammatory diseases, including rheumatoid arthritis, psoriasis, cancer and cardiovascular disease. The principal source of IL17 is a specific subpopulation of CD4⁺ T-helper cells, designated as type 17 T-helper T-cells (Th17) cells. Other sources of IL-17 include $\gamma\delta$ T-cells, natural killer T-cells (NKT), IL-17-producing CD8⁺ T-helper cells (Tc17 cells), type 3 innate lymphoid cells (ILC3s), and certain myeloid cells (57). Structurally, IL-17A is closely related to IL-17F and is found in a homodimeric or heterodimeric form with IL-17F. The physiological receptor for IL17A comprises an obligate homodimeric complex of IL17RA and IL17RC, however, heterotrimeric complexes of IL17RA/IL17RC/IL17RD have also been reported in certain cellular contexts (58). Upon IL17A stimulation, IL17RA recruits the ubiquitin ligase adapter protein Act1, which then targets the adapter protein TNF receptor-associated factor-6 (TRAF6) to recruit Transforming growth factor beta Activated Kinase (TAK) to activate downstream MAPK (ERK, p38, and JNK) pathway as well as the NF κ B pathway through IKK (I κ B kinase), which comprises the canonical arm of IL17 signaling. Act1 also recruits the adapter proteins TRAF2 (TRAF2) and TRAF5 to activate the noncanonical arm of IL17 signaling to regulate mRNA stability of target genes in a cellular context-dependent manner.

1.3.2 IL17 receptors

In terms of receptor characterization, IL17RA has remained the best-characterized receptor from this family and has been shown to form an obligate heterodimer with IL17RC to modulate signaling downstream of homo and heterodimeric forms of IL17A and IL17F, showing

preferential binding for IL17A(59). The physiological ligand for IL17RD remained uncharacterized. However IL17RD has been shown to modulate signaling downstream of IL17A by forming a heterotrimeric complex with IL17RA/IL17RC to promote a psoriatic inflammatory phenotype downstream of IL17A. There are several gaps with respect to its modulation of IL17A signaling in other contexts. IL17RA has also been shown to bind to IL17RB and IL17RC to mediate IL17B, IL17C and IL17E signaling. The receptor for IL17D remains unidentified, IL17RD has been shown to modulate cellular response downstream of IL17A as well as IL17F, although the response to IL17F was significantly weaker (54). IL17B has been shown to bind to a heterodimeric form of IL17RB with another as yet uncharacterized IL17 receptor (53). Most interaction studies have delineated a central role for IL17RA in mediating responses downstream of multiple cytokines within this family (52, 53).

1.3.2.1 Interleukin-17 Receptor D (SEF)

Interleukin-17 receptor D (IL17RD), originally designated as *Sef* (similar expression to *fgf*), was discovered during a high throughput in situ hybridization screening of zebrafish and frog embryos. *Sef* expression was demonstrated to be regulated by fibroblast growth factor (FGF) signaling during zebrafish, frog, and chick development, wherein it was shown to regulate FGF-induced Extracellular Regulated Kinase (ERK) activation and associated developmental phenotypes, thus implicating SEF as a feedback inhibitor of FGF signaling (60-62).

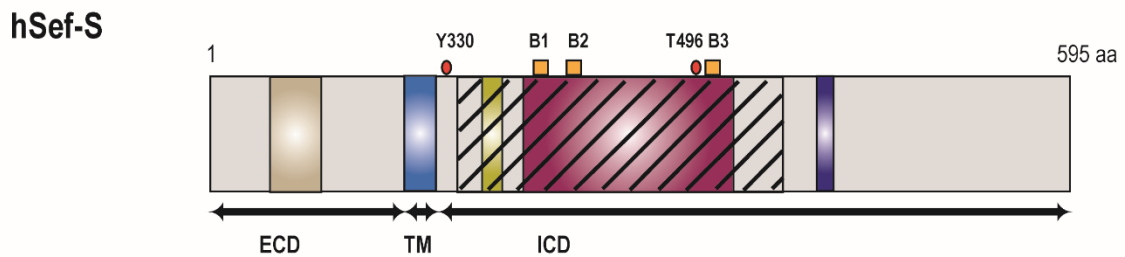
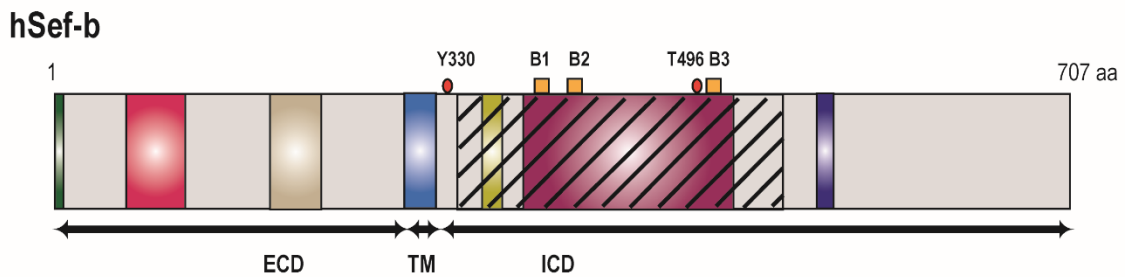
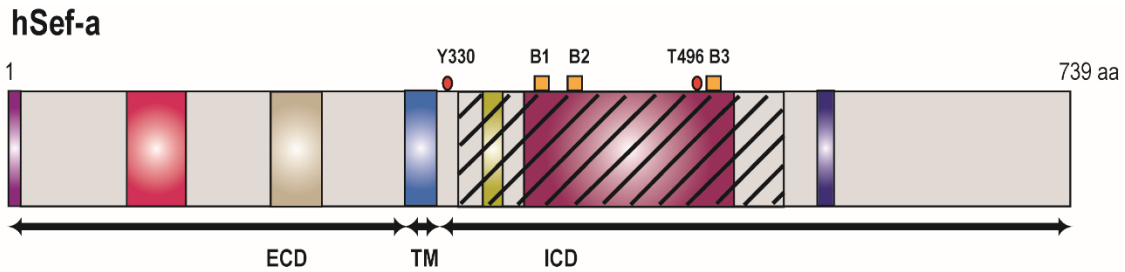
Subsequently, mouse and human orthologs of *SEF* (*IL17RD*) were also determined to affect FGF as well as several other signaling pathways to regulate a wide range of biological processes. Since the cytoplasmic domain of SEF contains sequence and structural similarity interleukin 17 receptors (SEFIR, SEF/IL17R domain), *SEF* was designated as *IL17RD* (60, 63).

1.3.2.2 Structure and conformation of IL17RD (SEF)

Structurally, human SEF is a type I transmembrane protein that is evolutionarily conserved among vertebrates and is encoded by a single locus on chromosome 3p14.3 in humans (60, 61, 63). The mRNA consists of 13 exons encoding a polypeptide product of 739 amino acids comprised of a 26-residue amino-terminal signal peptide, followed by a 272 amino acid extracellular domain, a short transmembrane domain consisting of 20 amino acids, and a 420 amino acid intracellular domain(63) (Figure 1). The extracellular domain of SEF consists of a signal peptide, an immunoglobulin-like domain, and a fibronectin type III repeat. The extracellular region is followed by a short, single-span transmembrane domain, and a cytoplasmic domain containing a highly conserved SEFIR segment, designated based on sequential and structural homology with the cytoplasmic domain of interleukin-17 receptors. The SEFIR domain contains a putative TNF receptor-associated factor 6 (TRAF6) binding site; and a TIR (Toll/Interleukin-1 Receptor) subdomain containing three conserved putative TIR binding motifs or “boxes”. The SEFIR domain is followed by a proline-rich putative Src homology 3 (SH3) binding domain (60, 61, 63-66). A visual representation of the Sef (IL17RD) protein containing the putative interactive domains is shown in Figure 1.

Within the cell, SEF (IL17RD) expression has been localized mainly to the plasma membrane (63, 67), although it has also been observed in the Golgi apparatus (68, 69) and in early and recycling endosomes (perinuclear structures) (70) in overexpression systems. Physiologically, SEF has been shown to exist in monomeric, dimeric as well as oligomeric forms, showing a preference for oligomerization (63, 71). In its dimeric form, SEF exists as a homodimer as well as in heterodimeric forms with FGFR1 (through its extracellular, transmembrane, and intracellular domain), FGFR2 (via its extracellular, transmembrane, and intracellular) (72), IL17RA (predominantly through its SEFIR domain) (54), TNFR2 (via its extracellular domain) (73) TLR3 (partly through its SEFIR domain) and TLR4 (partly through its SEFIR domain) and with Epidermal Growth Factor Receptor(EGFR) (70). The homomeric interactions between SEF

molecules were independent of the SEFIR domain of IL17RD, indicating that this domain might play a role in facilitating heterotypic interactions with other SEFIR-containing receptors, whereas the transmembrane domain might facilitate homotypic interactions (71).



- Signal peptide
- Immunoglobulin-like domain
- Fibronectin type III domain
- Transmembrane region
- TRAF6 binding domain
- SEF/IL17R (SEFIR) region
- Toll/IL-1R (TIR) region
- SH3 domain
- hSefb unique sequence
- Conserved signaling residues
- SEFIR/TIR signaling "box" sequences

Figure 1: Visual representation of putative structural and functional domains encoded by IL17RD (SEF) isoforms.

IL17RD (Sef) is comprised of an extracellular domain, a transmembrane domain, and an intracellular domain which are delimited by the arrows. hSEF-a (IL17RD) contains a signal peptide sequence (residues 1-26) immediately upstream of the extracellular domain (residues 27-299). Within the extracellular domain are conserved subdomains, including an immunoglobulin-like domain (residues 89-126) and a fibronectin type III domain (residues 199-281). The extracellular domain is followed by a short transmembrane domain (residues 300-319). The intracellular domain (residues 320-739) contains a Sef/IL17R homology region (SEFIR) (residues 335-564) which contains a TRAF6 binding subdomain (residues 348-352) and a Toll/IL1R (TIR) subdomain (residues 355-508). The SEFIR domain is followed by a putative SH3 domain (residues 567-578) followed by a short cytoplasmic tail (residues 579-739). The conserved tyrosine 330 (Y330) and threonine 496 (T496) residues are indicated, and the three short sequences “boxes”, indicated as B1 for Box1 (residues 357-362), B2 for Box2 (residues 377-381) and B3 for Box3 (residues 500-503). hSEF-b is a cytosolic variant that lacks first 42 residues, including the signal peptide, which are replaced by 10 new amino acids. hSEF-S is translated from an alternate initiation codon downstream of the hSEF-a initiation codon and therefore lacks the signal peptide and immunoglobulin domain, thus remaining in the cytoplasm.

1.3.2.3 Expression pattern of IL17RD (SEF)

Several studies have performed expression analyses to characterize SEF levels in various organs. The *hSEF-a* isoform is more ubiquitously expressed in various organs. Predominantly, *hSEF-a* has been shown to be expressed in epithelial tissues such as gonads, breast, small intestine, eyes, and skin keratinocytes. High levels have also been observed in endothelial cells as well as throughout the brain (including the hypothalamus and pituitary), kidney, bone, spinal

cord, skeletal muscle, heart, and nerves (Schwann cells) (63, 74-76). Moderate expression of *SEF* has been observed in the small intestine, tonsils, spleen, adenoids, and the liver, whereas low levels have been observed in the adrenal gland, peripheral blood leukocytes, smooth muscle cells, lung, bladder, pancreas, adipose, and spleen (63, 76). With respect to *hSEF-b*, the expression pattern is more restricted, with high levels observed in the thyroid and testes, moderate in the brain, and low levels in endothelial cells (76). The expression of the *hSEF-S* has not been extensively characterized, with the adrenal medulla being the only known organ system (64, 76).

1.3.2.4 IL17RD (SEF) regulation of FGF and IL17 signaling pathways

FGF: All three isoforms of SEF have been shown to bind to FGFR by coimmunoprecipitation analysis and affect the activation of different effector molecules downstream of FGF (67, 76, 77). The transmembrane form of SEF (*hSEF-a*) has been determined to inhibit the FGF signaling pathway to suppress its mitogenic response. Studies from our laboratory revealed that the transmembrane form of mouse *Sef* (*mSef*) co-immunoprecipitated with FGFR1 to inhibit FGF-induced RAF, MEK, and ERK activation, as well as AKT activation (67). SEF has also been shown to regulate the activation of stress pathways downstream of FGF2, specifically the p38 Mitogen-activated protein kinase (p38 MAPK) and the c-Jun N-terminal kinase (JNK) pathways, in a manner dependent on cellular context (72, 78). The interaction of SEF with FGFR is independent of ligand stimulation, FGFR dimerization, and FGFR kinase activity (67). Further, receptor crosslinking analysis determined that the extracellular as well as transmembrane domains of SEF interact with the transmembrane FGF receptor, with most of the interaction facilitated by the transmembrane region of SEF (67). Thus, the interaction between FGFR1 and SEF might occur at multiple sites on both receptors. Further, one of the cytosolic isoforms of SEF, *hSEF-b*, was shown to restrict the proliferative response of FGF, specifically at the level of ERK activation, by interfering with its phosphorylation (76, 78),

whereas the hSEF-S isoform was shown to regulate FGF induced mitogenesis in an ERK independent manner (77). mRNA expression analyses have shown that human ECs express high levels of the transmembrane isoform (*hSEF-a*) and moderate levels of the cytosolic isoform (*hSEF-b*) (63, 76). Mechanistically, hSEF-a has been shown to suppress the phosphorylation of FGF-induced ERK and p38 MAPK in apoptotic endothelial cells without affecting the activation of the JNK pathway (72), whereas the specific function of hSef-b in endothelial cells still remains to be elucidated. These results indicate that the varied mode of action of SEF on FGF downstream signaling cascades might be attributable to cell type-specific mechanisms governed by cellular source of origin (epithelial versus mesenchymal), contextual factors as well as isoform-specific effects (76, 79, 80). A diagrammatic summary of the role of IL17RD in the context of FGF signaling is shown in Figure 2.

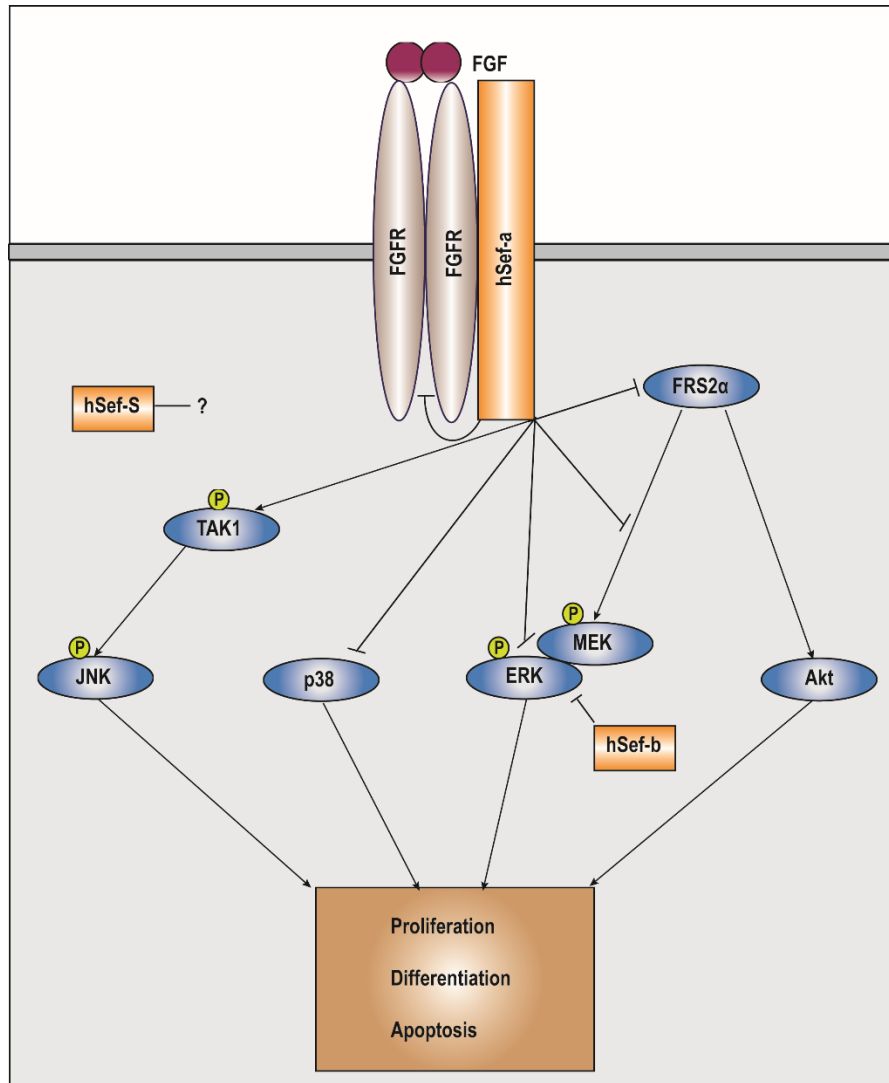


Figure 2: Schematic diagram depicting modulation of the FGF signaling cascade by different isoforms of hSEF. The transmembrane form of Sef (hSEF-a), physically associates with FGFR1 and FGFR2 to restrict FGFR kinase activation and subsequent FRS2 α phosphorylation upon FGF stimulation. By inhibiting FGFR-mediated FRS2 α tyrosine phosphorylation as well as subsequent adaptor protein activation, the ERK and AKT pathways are attenuated. hSEF-a is also reported to bind to the MEK-ERK complex without inhibiting activation of its components but impedes dissociation and nuclear translocation of ERK and, thus, activation of its downstream targets. Conversely, the cytosolic hSef-b isoform specifically

Figure 2(continued)

restricts ERK phosphorylation. hSef-a also regulates the activation of the p38 MAPK pathway in a cell type-specific manner; and promotes the activation of the JNK pathway by associating with TAK1. The cytosolic hSef-S isoform regulates cellular proliferation through an undefined mechanism.

IL17A: Although SEF was identified and named due to its association with FGF signaling, it was designated as a member of the IL17 receptor family (IL17RD) based on sequence homology with other IL17 receptors (60, 63). Rong et al. showed that IL17RD mediated IL17A induced downstream pathway activation in a homodimeric as well as in a heterodimeric state with IL17RA (81) (Figure 3). Additional investigative studies revealed that the interaction between IL17RA and IL17RD occurred independent of IL17 stimulation through multiple sites on both receptors, with most of the interaction occurring via the intracellular SEFIR domain (54, 81). Further, IL17RD was shown to function as a modulator of IL17-induced downstream effector pathways in primary mouse embryonic fibroblasts (MEFs) and bone marrow-derived macrophages (BMDMs) (54) and as a physiological receptor for IL17A to differentially regulate expression of IL17A target genes in keratinocytes (58). Loss of IL17RD decreased IL17-induced activation of the p38 MAPK pathway to consequently downregulate the expression of Macrophage Inflammatory Protein2 (MIP-2). This was accompanied by a slight increase in the activation of the ERK pathway and no significant effect on the activation of the JNK pathway (54). However, in the same context, loss of IL17RD significantly enhanced IL17-induced NF- κ B activation to upregulate the expression of IL6 (54). In another cellular context, loss of IL17RD in keratinocytes significantly decreased IL17A-induced activation of p38 MAPK and JNK to differentially regulate IL17A-induced chemokine expression. This was accompanied by a slight decrease in ERK activation and a slight increase in NF- κ B activation (58). Taken together, these

results suggest that IL17RD associates with the IL17RA/IL17RC receptor complex to bind to and modulate IL17A signaling in a cellular context-dependent manner. A diagrammatic representation of the role IL17RD in the context of IL17A signaling is shown in Figure 3.

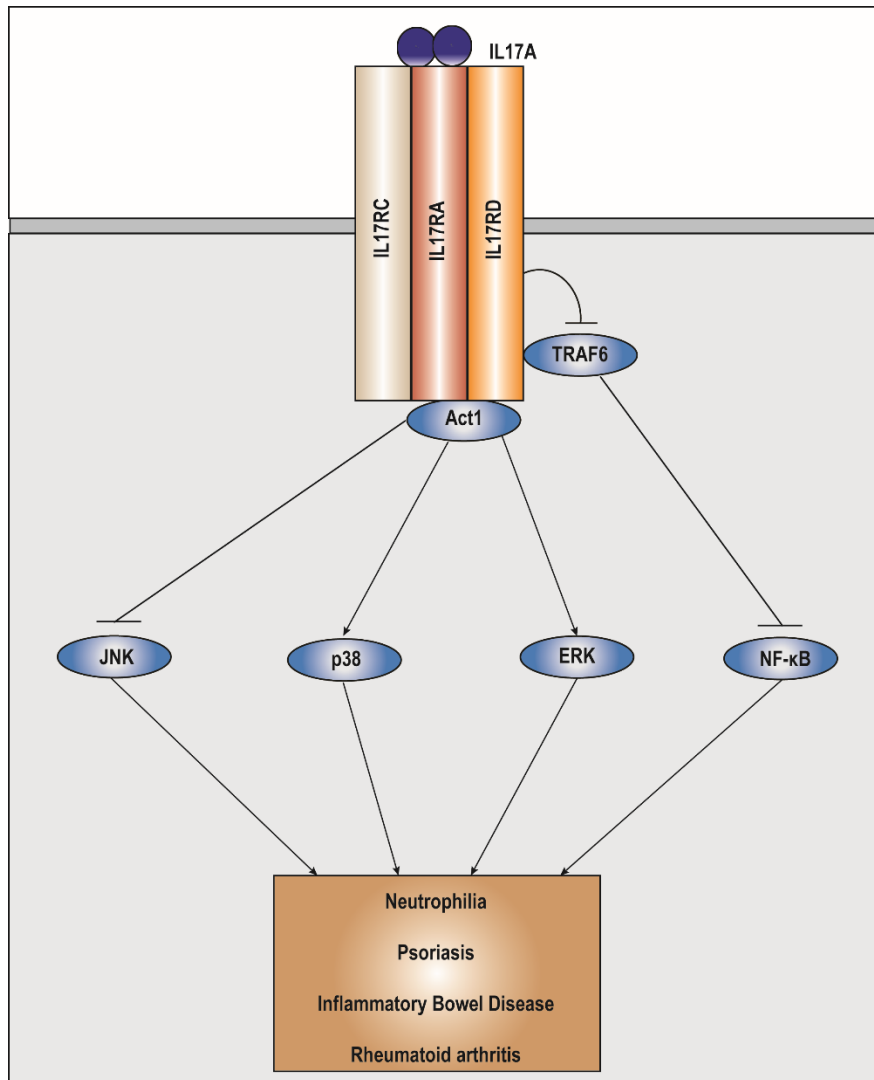


Figure 3: Schematic diagram depicting IL17RD (Sef) regulation of the IL17 signaling cascade and associated disease relevance. IL17RD binds to IL17RA in a cell type-dependent manner to regulate IL-17 signaling. Upon binding of IL17A to the IL17RA/IL17RC/IL17RD receptor complex, IL17RD modulates the recruitment of adapter proteins ACT1 and TRAF6 to

Figure 3 (continued)

the receptor complex. IL17RD subsequently regulates the polyubiquitination of TRAF6, as well as the activation of predominantly the p38 MAPK and the ERK, JNK, and NF- κ B pathways to differentially regulate the expression of target genes. Consequently, genetic perturbations and disruptions in IL17RD expression have been associated with several inflammatory diseases and immunomodulatory phenotypes associated with the IL17 signaling superfamily.

1.3.3 IL17 signaling during pathological conditions

IL17A evolved as an orchestrator of protective response to infectious diseases, primarily Chronic mucocutaneous candidiasis (CMC) caused by the fungus *C. albicans*, and has also been shown to defend against other fungal and bacterial infections, including *Cryptococcus*, *Klebsiella*, and *Staphylococcus* (57). Subsequently, IL17A levels were found to be elevated in several inflammatory and autoimmune diseases, including psoriasis, arthritis, multiple sclerosis, ankylosing spondylitis, systemic lupus erythematosus, and Crohn's disease (55). In vivo, IL17A functions downstream of IL23. Anti-IL17A antibodies have been approved for the treatment of psoriasis, whereas trials are currently underway for ankylosing spondylitis (55) and have been approved for psoriatic arthritis (82). Furthermore, IL17A has also been shown to promote neutrophilia in the context of inflammatory diseases such as pulmonary and peritoneal neutrophilia through IL17RD (54). Recent studies have also implicated elevated IL17A levels to be associated with the development of cardiovascular comorbidities in patients suffering from these diseases, leading to several studies focused on characterizing the role of IL17 during atherosclerotic plaque formation.

1.3.3.1 The contribution of IL17 cytokines to cardiovascular disease

Several studies have characterized the role of IL17A in terms of atherosclerotic plaque formation. However, the role of IL17A is still undefined, with studies demonstrating IL17A to

have a proatherogenic, anti-atherogenic, or no effect on plaque formation (83). Elevated IL17A levels have been observed in mouse models of atherosclerosis, and anti-IL17 antibodies have attenuated plaque formation in atherosclerosis-prone *Apoe*^{-/-} mice. Furthermore, knockout of IL17A in *Apoe*^{-/-} mice significantly decreased atherogenic plaque formation upon weeks of western diet feeding. However, contrary knockout of IL17A was shown to enhance plaque formation in *Apoe*^{-/-} mice. Reasons for the discrepancy in results include duration of high-fat feeding, dietary constituents, as well as mouse husbandry (83, 84). *In vitro*, IL17A has been shown to activate ECs by regulating the expression of EC adhesion molecules and promote leukocyte adhesion through the p38 MAPK pathway (83, 85).

1.3.3.2 The role of IL17RD (SEF) in disease

Genetic alterations in *IL17RD* and dysregulation in its expression have been associated with a wide array of conditions, including cancer, neuroendocrine, inflammatory as well as diseases involving vascular remodeling, and are often accompanied by impairments in known IL17RD signaling partners (86). A concise overview of the role of IL17RD in inflammatory disease and in disorders of vascular remodeling is given below.

1.3.3.2.1 IL17RD (SEF) during inflammatory disease

SEF (IL17RD) during inflammatory disease: Dysregulation in IL17RD expression have been associated with a wide array of conditions, including inflammatory diseases, carcinogenesis, neuroendocrine disorders, and diseases associated with cellular remodeling, and are often accompanied by impairments in known IL17RD signaling partners. Interactions between IL17RD and its associated ligands have been shown to have clinical pathological relevance in patients suffering from rheumatoid arthritis(87), COVID-19 (88), Crohn's disease (89), and psoriasis (58). IL17RD has also been shown to play a crucial role in fostering an immunoprotective response to systemic inflammation in mice by regulating chemokine expression, suggesting that it may play

an important role in regulating host response to pathogen exposure (66). In another study utilizing a mouse model of *in vivo* cytokine induction, Mellett, et al., showed that loss of *Il17rd* decreased peritoneal and pulmonary neutrophilia in response to IL17A through differential regulation of chemokine expression (54). In a different cellular context, loss of *Il17rd* in keratinocytes was also shown to partially suppress imiquimod (IMQ) induced psoriasis by decreasing IL17A-induced infiltration of neutrophils and $\gamma\delta$ T cells into the epidermal layer of the skin and regulating keratinocyte expression of *Il23* (58).

1.3.3.2.2 IL17RD (SEF) during disorders of vascular remodeling

Potentially pathogenic mutations in *IL17RD* have also been associated with non-syndromic cerebral arteriovenous malformations (BAVMs), and have been implicated in EC dysfunction, along with dysregulations of members of RTK and BMP signaling superfamily (90, 91).

1.4 Summary and significance of our study

The above disease correlations underscore an important role for IL17RD in modulating inflammatory phenotypes and EC dysfunction by regulating cellular response in response to multiple individual cytokines. However, since IL17RD interacts with multiple pathways within its interactive network, its role as a signaling scaffold for the assembly of various receptor complexes and their respective interacting proteins to generate signaling outputs still remains to be defined. Given the ubiquitous pattern of its expression, further investigation using animal models and tissue-specific gene targeting is required to define its mode of action in regulating the crosstalk between its known interacting partners *in vitro* and *in vivo* to aid in understanding its diagnostic and therapeutic implications. We aim to address some of these questions in our experimental investigation, as highlighted in subsequent sections.

CHAPTER 2: MATERIALS AND METHODS

2.1 *In vitro* experiments

2.1.1 Cell culture, siRNA transfection, and *in vitro* stimulation

Human Aortic Endothelial Cells (HAEC; catalog no: CC-2535, Lot no: 20TL231227) and Human Umbilical Vein Endothelial Cells (HUVEC; catalog no: CC-2519, Lot no: not available) were obtained from Lonza (Portsmouth, NH) and used up to passage 8 in all experiments. HAECs and HUVECs were cultured on plates coated with 0.2% gelatin (Sigma; St. Louis, MO; catalog no: G9391) in Endothelial Cell Growth Medium-2 (EGM-2; Lonza, catalog no: CC-3162) for the majority of the experiments. The immortalized THP-1 monocytic cells were obtained from American Type Culture Collection (ATCC; Manassas, Virginia, catalog no: TIB-202) and maintained in Roswell Park Memorial Institute – 1640 media (RPMI-1640; HyClone; Logan, UT; catalog no: SH30027) containing 10% FBS, 20mM 4-2-hydroxyethyl-1-piperazineethanesulfonic acid (HEPES; Sigma; catalog no: H4034), 1mM sodium pyruvate (Thermo Fisher; Waltham, MA; catalog no: 11360070) and 50 μ M β -mercaptoethanol (Sigma; catalog no: M6250). THP-1 cells were maintained at a concentration of 0.3 - 0.9 x 10⁶ cells/ml and split every three days. For qPCR analysis, HAECs and HUVECs were grown to 100% confluence and used for qPCR analysis (see RNA and RT-qPCR procedure in subsequent sections).

For siRNA transfection, HAECs were grown to 50-60% confluence and transfected with 25 nM IL17RD targeting (Horizon Discovery; Lafayette, CO, catalog no: L-007946-02) or 25 nM non-targeting scrambled control (Horizon Discovery; catalog no: D-001810-10) ON-TARGETplus SMARTpool siRNA using 2 μ l/ml of RNAiMax (Thermo Fisher; catalog no: 13778075) in Opti-MEM Reduced Serum Medium (ThermoFisher; catalog no: 31985070) for 6 hours (sequences provided in Table 1). The cells were then washed with Dulbecco's Phosphate Buffered Saline (without calcium and magnesium) (dPBS; HyClone; catalog no: SH30028) and allowed to

recover in fresh EGM-2 for 48 hours before being used for the indicated experiments. Efficiency of RNAi suppression was evaluated by qPCR.

For experiments involving analysis of endothelial activation markers expression, HAECs transfected with NT or IL17RD siRNA were stimulated with 100 ng/ml recombinant human IL17A (Advent Bio; Elk Grove, IL; catalog no: 11694) or vehicle control (0.2% Bovine Serum Albumin, BSA; Sigma; catalog no: 10735086001) for 24 hours. For short-term signaling studies, HAECs were cultured in Endothelial Basal Media-2 (EBM-2; Lonza; catalog no: CC-3156) for 8 hours to deplete growth factor activity before being stimulated with IL17A for the indicated time points. Each experiment with HAECs was performed three independent times.

Table 1: siRNA target sequences

siRNA Target	Sequence
NT SMARTpool	UGGUUUACAUGUGACUAA, UGGUUUACAUGUUGUGUGA, UGGUUUACAUGUUUUCUGA, UGGUUUACAUGUUUUCUA
IL17RD SMARTpool	GUGUGAUGAUAAAUGGUAA, GAGAGUGACUUCUGCCUAA, ACUACAAGCUCAAGCACGA, UCGACGGACCAGACAGAAA

2.1.2 RNA extraction, cDNA preparation and qRT-PCR analysis

For cells, the total RNA was extracted from cells using the RNEasy mini kit (Qiagen; Germantown, MD; catalog no: 74106). For tissues, aortas from *Il17rd*^{-/-} and *Il17rd*^{+/+} were homogenized in TriReagent (Molecular Research Center Inc.; Cincinnati, OH; catalog no: TR 118), following which the RNA was extracted using the RNeasy Mini Kit as previously described in (92). Extracted RNA was quantified using the Nanodrop 1000 UV-Vis Spectrophotometer (Thermo Scientific). 1µg of the extracted RNA was reverse transcribed into cDNA using qScript cDNA SuperMix (BioRad; catalog no: 1708890), following which the reaction mixture was diluted in a ratio of 2ng cDNA: 1 µl of nuclease-free water. The diluted cDNA was then used for qPCR analysis for use in qPCR analysis using AzuraQuant Green Fast qPCR Mix (AzuraQuant;

Raynham, MA; catalog no: AZ-2101). The program used for performing qPCR was as follows: Enzyme activation at 95°C for 2 minutes, followed by denaturation at 95°C for 5 seconds, followed by annealing with gene-specific primers (Table 3) at 60°C for 30 seconds for 40 cycles. Changes in transcript levels were determined as fold change relative to control ($2^{-\Delta\Delta Ct}$ method). Briefly, average Ct values from the housekeeping reference gene (β -actin) for the experimental condition were subtracted from average threshold (Ct) values of the indicated gene for each experimental condition (ΔCt). The normalized Ct value of each experimental condition was then subtracted from the normalized Ct value from the vehicle control to obtain a relative difference in transcript levels ($\Delta\Delta Ct$). 2 to the power of the negative value of the difference was used to obtain fold-change values.

2.1.3 Immunoblotting

Cells were washed with dPBS and lysed in an appropriate volume of 2X SDS sample buffer containing 0.5M Tris-HCl pH 6.8 (Thermo Fisher, catalog no: A144), 10% β -mercaptoethanol, 4% SDS (Sigma; catalog no: S7920), 20% glycerol (Sigma; catalog no: G22020), 0.02% bromophenol blue (Sigma; catalog no: B8026) on ice. The samples were homogenized by sonication and further denatured by boiling at 95°C for 5 minutes. For immunoblotting, proteins were loaded into 8% or 10% SDS-polyacrylamide gels made using Trizma (Sigma; T6066), 30% acrylamide (BioRad; Hercules, CA; catalog no: 1610156), SDS, APS (Sigma; catalog no: A3778), TEMED (Sigma; catalog no: T9281). The samples were separated by electrophoresis and transferred onto nitrocellulose membranes (BioRad; catalog no: 162-0115) at 16 V for 120 minutes in transfer buffer containing 25 mM Tris, 192 mM glycine (Sigma; catalog no: G8898), 0.0002% SDS and 20% methanol (Millipore Sigma; catalog no: MX0485). The membranes were then blocked in a solution of 5% nonfat milk in Tris buffer saline –Tween-20 (TBS-T), containing 50 mM Tris-HCl pH 7.4, 150 mM NaCl (Sigma; catalog no: S3014); 0.05% Tween 20 (Sigma;

catalog no: P1379) for 2 hours at room temperature. The membrane was then probed with the indicated primary antibodies (See Table 2) in 5% BSA in TBS at dilutions indicated in Table 2, at 4 °C overnight. The primary antibody was then washed off with TBS-T, and the membranes were further incubated with the corresponding horseradish peroxidase (HRP)-conjugated secondary antibodies (Table 3) for 2 hours at room temperature. The membranes were washed for 30 minutes each with TBS-T and detected by autoradiography using chemiluminescent substrate (West Pico, Millipore Sigma; catalog no: WBKLS0500) obtained by mixing Substrate Peroxide solution and Substrate Luminol Reagent (1:1). For analysis, the indicated protein(s) was determined based upon migration of prestained molecular weight standards (Bio-Rad; catalog no: 1610394).

The densitometric intensity of each protein was calculated using the measure feature in ImageJ. The raw values were obtained by subtracting the densitometric intensity of each experimental condition from the background intensity on the same blot. The raw values were then normalized to loading control (Total ERK, Total p38, Total JNK, Total p65, Total Akt or β -actin as indicated) for each experimental condition and further normalized to unstimulated siNT control to obtain relative densitometric intensity quantification.

Table 2: List of primary antibodies used for immunoblotting assays

Target antigen	Vendor	Catalog number	Working dilution
pERK	Cell Signaling Technology	4370	1:1000
Total ERK	Cell Signaling Technology	9102	1:1000
pAkt	Cell Signaling Technology	9271	1:1000
Total Akt	Cell Signaling Technology	4691	1:1000
pp38	Cell Signaling Technology	9211	1:1000
Total p38	Cell Signaling Technology	8690	1:1000
pJNK	Cell Signaling Technology	9251	1:500
Total JNK	Cell Signaling Technology	9252	1:1000
pp65	Cell Signaling Technology	3033	1:1000
Total p65	Cell Signaling Technology	8242	1:1000
β -Tubulin	Cell Signaling Technology	86298	1:5000
GAPDH	Cell Signaling Technology	2118	1:5000
VCAM-1	Cell Signaling Technology	13662	1:5000
ICAM-1	Cell Signaling Technology	4915	1:500
β -actin	Sigma	8226	1:5000

Table 3: List of secondary antibodies used for immunoblotting assays

Target antigen	Vendor	Catalog number	IB working dilution
Goat anti-mouse IgG, HRP-linked	Bio-Rad	1706516	1:5000
Goat anti-rabbit IgG, HRP-linked	Bio-Rad	1706515	1:5000

2.1.4 Monocyte adhesion assay

HAECs were transfected with *NT* or *IL17RD* siRNA according to the procedure described in the preceding sections. The cells were allowed to recover in fresh EGM-2 for 24 hours and were then seeded at a density of 10^5 cells per well of a 96-well plate. The cells were allowed to attain confluence for 24 hours before being stimulated with vehicle control (0.2% BSA) or recombinant IL17A (100 ng/ml) for 24 hours. THP-1 cells, at a concentration of 3×10^5 cells/well, were labeled with 20 μ M Calcein Red-Orange (ThermoFisher; catalog no: 34851) for 30 minutes in EBM-2. The labeled THP-1 cells were washed twice with EBM-2 and subsequently added to endothelial cells cultured in EBM-2 for 1 hour. The adherent cells were then washed twice with dPBS (with calcium and magnesium) (HyClone; catalog no: SH30264), and the number of adherent monocytes was quantitatively determined by spectrophotometric measurement at 580 nm using Glomax[®] Microplate Reader (Promega; Fitchburg, WI) using a standard curve with a known number of THP-1 cells. The absorbance of labeled THP-1 cells was subtracted from the absorbance of the endothelial monolayer. The wells were then imaged using EVOS M5000 (Thermo Fisher) Inverted fluorescent microscope.

2.2 *In vivo* experiments

2.2.1 Mice

All experimental procedures on mice used in our experiments were performed according to protocols reviewed and approved by the MaineHealth Institute for Research (MHIR) Institutional Animal Care and Use Committee (IACUC, protocol #2104). All mice were housed in a pathogen-free environment under light (14:10 hour light: dark cycle), temperature (70°F), and humidity (55%) controlled conditions for all our experiments. We used groups of 4-8 groups of male and female mice for all our experiments. The size of the experimental cohorts is given in Table 4.

Mouse models that were used in the experiments described in our studies include C57BL/6 mice (The Jackson Laboratory; Bar Harbor, ME; catalog no: 000664), the *I117rd* null strain (*Kst223*); mouse strains with a conditional allele for *I117rd* (*I117rd f/f*); mouse codon-optimized FLP recombinase *FLPo* mice (The Jackson Laboratory; catalog no: 012930), *VE-cadherin* endothelial specific tamoxifen-inducible Cre recombinase (*Cdh5-CreERT2*) mice (93, 94), the *Rosa26-Stopfl/fl- tdTomato* mice (The Jackson Laboratory; catalog no: 007914; (95)) and intercross combinations of these lines. All mice strains were backcrossed onto the C57BL/6 genetic background for at least ten generations. For our experimental purposes, we used male and female mice. Mice were euthanized by isoflurane inhalation (Dechra Veterinary Products; Overland Park, KS) followed by cervical dislocation, consistent with the guidelines of the Panel on Euthanasia of the American Veterinary Medical Association.

Table 4: Number of mice used in experimental analyses

<i>In vivo</i> experiment	Sex	Genotype	Diet	
			CD	WD
Analysis of <i>I117rd</i> expression	Males	<i>C57BL6/J</i>	6	-
	Females	<i>C57BL6/J</i>	6	-
Aortic leukocyte infiltration analysis	Males	<i>I117rd +/+</i>	8	6
		<i>I117rd -/-</i>	6	7
	Females	<i>I117rd +/+</i>	8	8
		<i>I117rd -/-</i>	5	5
Aortic endothelial VCAM-1 and ICAM-1 expression	Males	<i>I117rd +/+</i>	8	8
		<i>I117rd -/-</i>	5	6
	Females	<i>I117rd +/+</i>	8	8
		<i>I117rd -/-</i>	8	8
Atherosclerosis	Males	<i>I117rd +/+</i>	4	4
		<i>I117rd -/-</i>	4	5
	Males	<i>I117rd ECWT</i>	-	5
		<i>I117rd ECKO</i>	-	8

2.2.1.1 KST223

The *Kst223* (*Il17rd*^{-/-}) mutant cell line was generated by gene trap technology as described by Leighton et al. (96), resulting in the insertion of the *GT1TMpfs* vector into the third intron of the endogenous *Il17rd* locus on an FVB background. The mutant mice contain a fusion of β -geo within intron 3 at nucleotide 332 (97). These mice have been validated by our laboratory as well as by others (97-99). The mice were backcrossed on to the C57BL/6 genetic background for at least 10 generations for our experiments. Mice were genotyped by PCR amplification of tail DNA with a three-primer combination: Int3-F2 and Int3-R1 for the wild-type band and Int3-F2 and GTR1 specific for the *Kst223* insertion band as previously described (97, 99) (see Table 5). A representative validation of the genotype of the mice is indicated in Figure 10. Wild-type littermates were used as experimental controls (*Il17rd*^{+/+}).

2.2.1.2 *Il17rd* f/f

The *Il17rd*^{f/f} ES cells were obtained from the European Mouse Mutant Cell Repository (EuMMCR). Recombination between the homology arms of the targeting construct modifies the intron by introducing 2 additional genetic elements flanked by flippase recognition target (*FRT*) sites: an exon consisting of a splice acceptor site (*SA*), a LacZ reporter gene cassette (*LacZ*) and an SV40 poly-adenylation site (*pA*); and a transcriptional unit containing the neomycin resistance gene selection marker (*Neo*) driven by the human β -Actin promoter (*BactP*) on a C57BL6 background. These mice were then intercrossed with *FLPo* mice, which restores the mutant *Il17rd* allele containing exons 6 and 7 flanked by *loxP*- sites. *Cre*-mediated recombination between *loxP* sites results in the deletion of exons 6 and 7 which consequently results in a frameshift deletion to encode a mutant *Il17rd* protein. The resulting mice were screened for insertion by PCR of genomic DNA using the primers and founder lines validated by genotyping using. A schematic representation of the construct for the mouse is described in

Figure 4, along with the location of primers and strategy used for genotyping. The sequences of primers are given in Table 5.

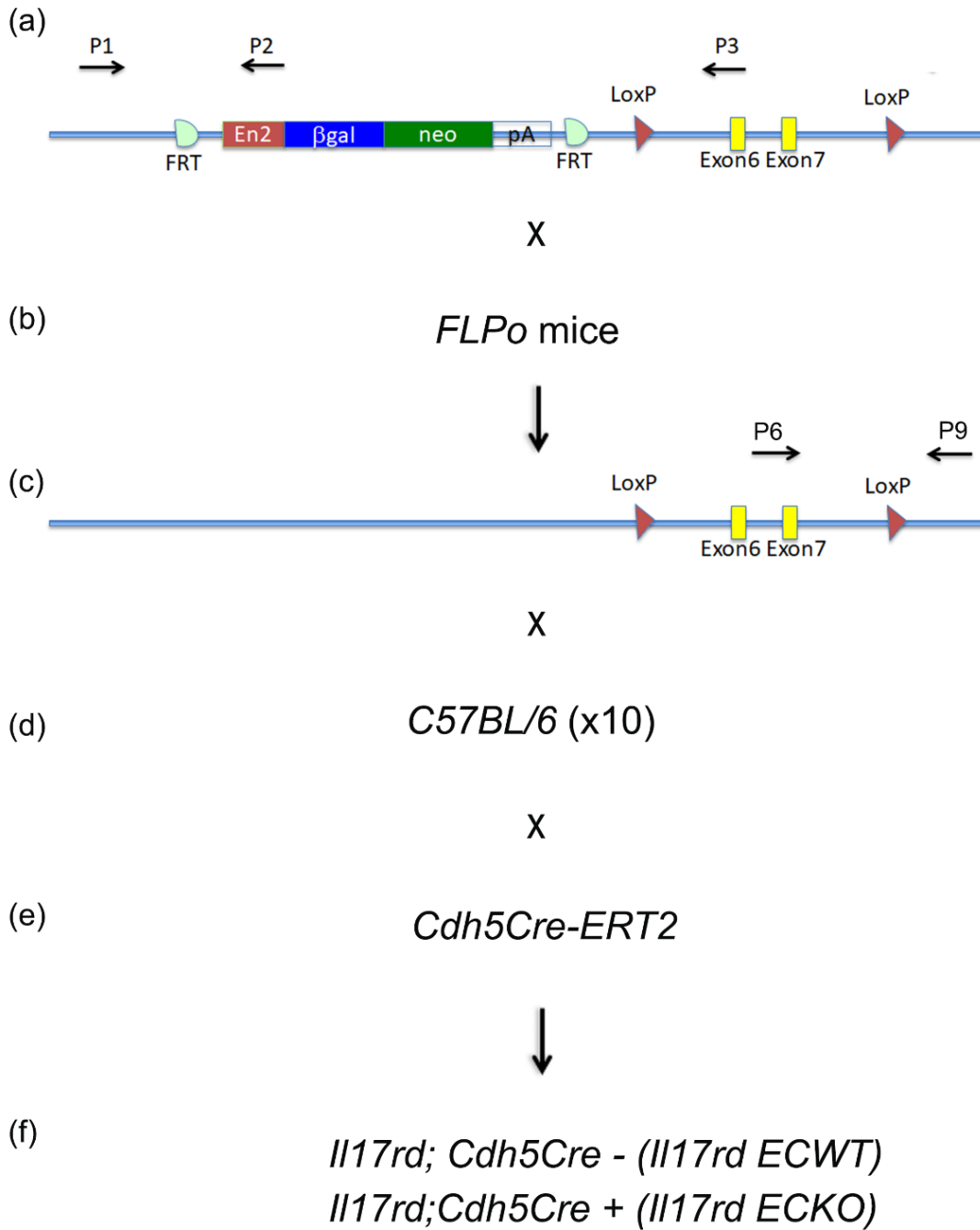


Figure 4: Generation of endothelial cell specific *Il17rd* loss-of-function mice: (a) The mutant *Il17rd^{dff}* allele contains an exon consisting of a splice acceptor site (*SA*), a LacZ reporter gene cassette (*LacZ*) and an SV40 poly-adenylation site (*pA*); and a transcriptional unit containing the neomycin resistance gene selection marker (*Neo*) driven by the human β -Actin promotor (*BactP*) on a C57BL6 background, followed by a mutant construct containing loxP flanked exons 6 and 7. Primers P1 and P2 amplify the wild type construct without Flp deletion (236bp), primers P1+P3 encompass the loxP flanked exons 6 and 7 (with Flp deletion: 500bp, without Flp deletion: 7000bp) (b) The mutant mice were then intercrossed with *FLPo* expressing mice, which excises the *SA-IRES-LacZ* and the *BactP-Neo* gene which restores the mutant *Il17rd* allele containing exons 6 and 7 flanked by *loxP*- sites. These mice were then intercrossed with C57BL/6 mice for 10 generations, and were genotyped using primers P6 and P9 (280bp for floxed allele vs. 216 bp for non floxed allele). These mice were then intercrossed with Cdh5Cre-ERT2 mice to generate mice containing endothelial-cell specific *Il17rd* loss-of-function mice.

Table 5: List of primers used in this study

Primer	Sequence
Human IL17RD forward	5'-CTGCGGGTAGCTGAAGGTAG-3'
Human IL17RD reverse	5'-AGCTTTGGCACCTTGTATGG-3'
Human β -actin forward	5'-AGAAAATCTGGCACCACACC-3'
Human β -actin reverse	5'-GTCTCAAACATGATCTGGG-3'
Int3 -F2 (forward) (<i>Kst223</i>)	5'-GCCAAGCCTTGATATGACAAAC-3'
Int3-R1 (wild-type)(<i>Kst223</i>)	5'-TTATGAGTCATTCTCCAGCCCG-3'
GTR1 (mutant) (<i>Kst223</i>)	5'-GGTCTTTGAGCACCAGAGGACATC-3'
P1 (<i>Il17rd ff</i>)	5'-GCGCAACGCAATTAATGATA-3'
P2 (<i>Il17rd ff</i>)	5'-CGTGGCTTTGATACCACCTC-3'
P3 (<i>Il17rd ff</i>)	5'-ATCCGTTTCAAGCAAGGAGA-3'
P6 (<i>Il17rd ff</i>)	5'- CTGACTCACTCACCCTGTCC-3'
P9 (<i>Il17rd ff</i>)	5'-GCCCTAGGTTCTCCACCTCTA -3'
Cre forward	5'-GCATTACCGGTCGATGCAACGAGTG-3'
Cre reverse	5'-GAACGCTAGAGCCTGTTTTGCACGTT-3'
R26F2 (Forward)	5'-AAAGTCGCTCTGAGTTGT-3'
R523 (wild-type)	5'-GGAGCGGGAGAAATGGAT-3'
R26R (mutant)	5'-GCTATGAACTAATGACCCCG-3'

2.2.2 Tamoxifen injection

Tamoxifen (Sigma; catalog no: T5648) was dissolved at a concentration of 10 mg/ml in corn oil (Sigma; catalog no: C8267). Male *Il17rd f/f; Cdh5CreERT2* mice between the ages of 8-10 weeks were injected intraperitoneally with 1 mg tamoxifen per mouse per day for 5 consecutive days. After injection, the mice were housed for two weeks to ensure Cre-mediated recombination.

2.2.3 AAV-mPCSK9^{D374Y} injection

Adeno-associated viral construct of PCSK9 containing a gain-of-function mutation D374Y under the control of the HCRApoE/hAAT promoter was obtained from the Boston Children's Hospital viral core. Mice were then retro-orbitally injected with 10^{11} genome copies of AAV-mPCSK9^{D374} in 50 μ L of 0.9% saline under isoflurane anesthesia.

2.2.4 Diet feeding

8-11 week old mice of the indicated genotypes were fed a western diet (WD) comprising high fat (21.2%), high cholesterol (0.21%), and no sodium cholate (Research Diets; New Brunswick, NJ; catalog no: D12079B) or standard chow diet (CD; Envigo; Indianapolis, IN; catalog no: T-2918) *ad libitum* for 14 weeks as indicated.

2.2.5 Physiological measurements

Mice that were fed with WD or CD were weighed weekly. After 14 weeks of WD or CD feeding, body composition was determined by dual-energy x-ray absorptiometry (DEXA) using the PIXImus densitometer (GE Medical Lunar, Madison, WI) and Mini Spec Nuclear Magnetic

Resonance (NMR, Bruker, Billerica, MA) as described in (92). Body composition results were represented as a proportion of body weight.

2.2.6 Glucose Tolerance Test

Mice were fasted for 12 hours and weighed the next morning. Fasting glucose levels were measured by a glucometer (AccuChek, Aviva Plus) from blood extracted from the tail, following which the mice were injected intraperitoneally with a D-glucose source (1 mg glucose/g body weight). Blood glucose concentration was then measured at 30, 60, and 120 minutes post-injection.

2.3 Ex vivo experiments

2.3.1 Blood and serum collection

For analysis of *Il17rd* expression in circulating leukocytes, blood was treated with 0.5M citrate buffer (Thermo Fisher, catalog no: J62918.AK) before being stained with respective antibodies for flow cytometry (see procedure below).

For obtaining differential leukocyte count, blood was collected from the mice by retroorbital bleeding technique into EDTA Microtainer tubes (BD Biosciences; Franklin Lake, NJ; catalog no: 367856). For analysis of circulating cholesterol and IL17, mice were fasted for 4 hours. Whole blood was centrifuged at 2500 rpm for 15 minutes, and the supernatant was collected to obtain serum. All hematological and serum assays were performed in singlicate.

2.3.1.1 Hematological analysis, serum metabolite and cytokine analysis

Blood collected into EDTA Microtainer tubes was and was immediately analyzed by ProcyteDx Hematology Analyzer (Idexx, Westbrook, ME) to obtain circulating hematological parameters.

Levels of circulating cholesterol levels were measured using the Total cholesterol kit (Cell BioLabs; San Diego, CA; catalog no: STA-384) according to the manufacturer's instructions. Circulating levels of IL17A were determined using the R&D Quantikine™ HS Mouse IL-17 Immunoassay (R&D Systems, Minneapolis, MN, catalog no: MHS170) according to the manufacturer's instructions. Levels of circulating FGF21 were determined by ELISA (R & D Systems, cat no MF2100), whereas circulating levels of proinflammatory cytokines were determined using the LegendPlex mouse inflammation panel (BioLegend cat no: 740150) according to the manufacturer's instructions.

2.3.2 Tissue harvest and processing

Post euthanasia, the peritoneal and thoracic cavities of the mouse were exposed, and the left ventricle of the heart was perfused with PBS. The organs of the respiratory (lungs, trachea) and the digestive (stomach, intestine, and liver) systems were removed from the thoracic and abdominal cavities to expose the heart, diaphragm, and kidneys. The aorta and aortic branches (brachiocephalic and carotid arteries) were then dissected from the heart until the aortic bifurcation according to the procedure described in (100).

2.3.2.1 Preparation of aortic cell suspension and flow cytometry analysis

HAECs were fluorescently labeled with PE-conjugated anti-IL17RD antibody (R&D; catalog no: FAB2275P; 3 μ l/10⁶ cells) in FACS buffer (PBS + 2% BSA + 2mM EDTA) for 20 minutes. Cells were washed and labeled with 4',6-diamidino-2-phenylindole (DAPI; 0.04 μ g/ml; Thermo Fisher; catalog no: 62248) for assessment of cell viability. Briefly, viable cells were gated and quantified for mean fluorescence intensity (MFI) of IL17RD (PE). The MFI of unlabeled cells was subtracted from the MFI of the labeled cells to obtain Δ MFI.

For *in vivo* aortic flow cytometry, the aorta was dissected until the thoracoabdominal branch, and the surrounding perivascular and periaortic lymph nodes were removed. The aorta was then subjected to flow cytometry analysis according to the procedure described in (101). Briefly, the aorta was digested using an enzyme cocktail mixture of 10 mg/ml collagenase type II (Worthington Biochemical, Lakewood, NJ, catalog no: LS004174) and 5 mg/ml Dispase Type II (Sigma, catalog no: D4693) for 30 min at 37°C. For our experiments involving analysis of *in vivo* aortic EC, we combined samples from 2 mice to account for the low number of endothelial cells. The cell suspension was then incubated with anti-mouse CD16/CD32 (BD Biosciences, catalog no: 553140) to block Fc receptors, followed by staining with the indicated antibodies (see Table 6) in FACS buffer for 20 minutes. The cells were then stained with DAPI for assessment of cell viability before being analyzed by flow cytometry for the indicated markers. Flow cytometry data were collected using the MACSQuant Analyzer 10 (Miltenyi; Gaithersburg, MD) and analyzed using the FlowJo software (BD Biosciences). For analysis, viable singlet cells were gated into immune and non-immune cells by quantifying the number of CD45^{pos} and CD31b^{pos} cells (antibody list in Table 6). The mean expression level (Δ MFI) of ICAM-1, VCAM-1, IL17RA, and IL17RC was obtained in CD31^{pos} cells in the non-immune cell fraction by subtracting the MFI of unlabeled cells from the MFI of the labeled cells.

For immune cells in the aorta and blood, the myeloid cell population was obtained in the CD45^{pos} cells by gating the number of CD11b^{pos} cells. The number of neutrophils in the aorta was quantified by gating the number of Ly6G^{pos} within the CD11b^{pos} myeloid cells. The Ly6G^{neg} cell population was then gated for Ly6C^{pos} cells to obtain the number of monocytes infiltrated into the aorta. Cells expressing MHCII, F4/80, and CD11c were defined as macrophages. For analysis of *Il17rd* expression in blood, viable singlet cells were gated into CD11b^{pos} myeloid cells. The list of antibodies used for flow cytometry analysis is shown in Table 6. A flowchart showing the gating strategy is shown in Figure 5.

Table 6: List of antibodies used for flow cytometry analysis

Antibody	Target species	Clone	Company
IL17RD	Mouse	309822	R&D
IL17RA	Mouse	448	R&D
IL17RC	Mouse	2270	R&D
CD45	Mouse	30-F11	Biolegend
CD11b	Mouse	M1/70	Biolegend
Ly6G	Mouse	1A8	Biolegend
Ly6C	Mouse	HK1.4	Biolegend
MHCII	Mouse	M5/114/15.2	Biolegend
F480	Mouse	BM8	Biolegend
CD11c	Mouse	N418	eBioscience
VCAM-1	Mouse	429	Biolegend
ICAM-1	Mouse	YN1/1.7.4	Biolegend
Sca1	Mouse	E13-161.7	Biolegend
IL17RD	Human	FAB2275	R&D

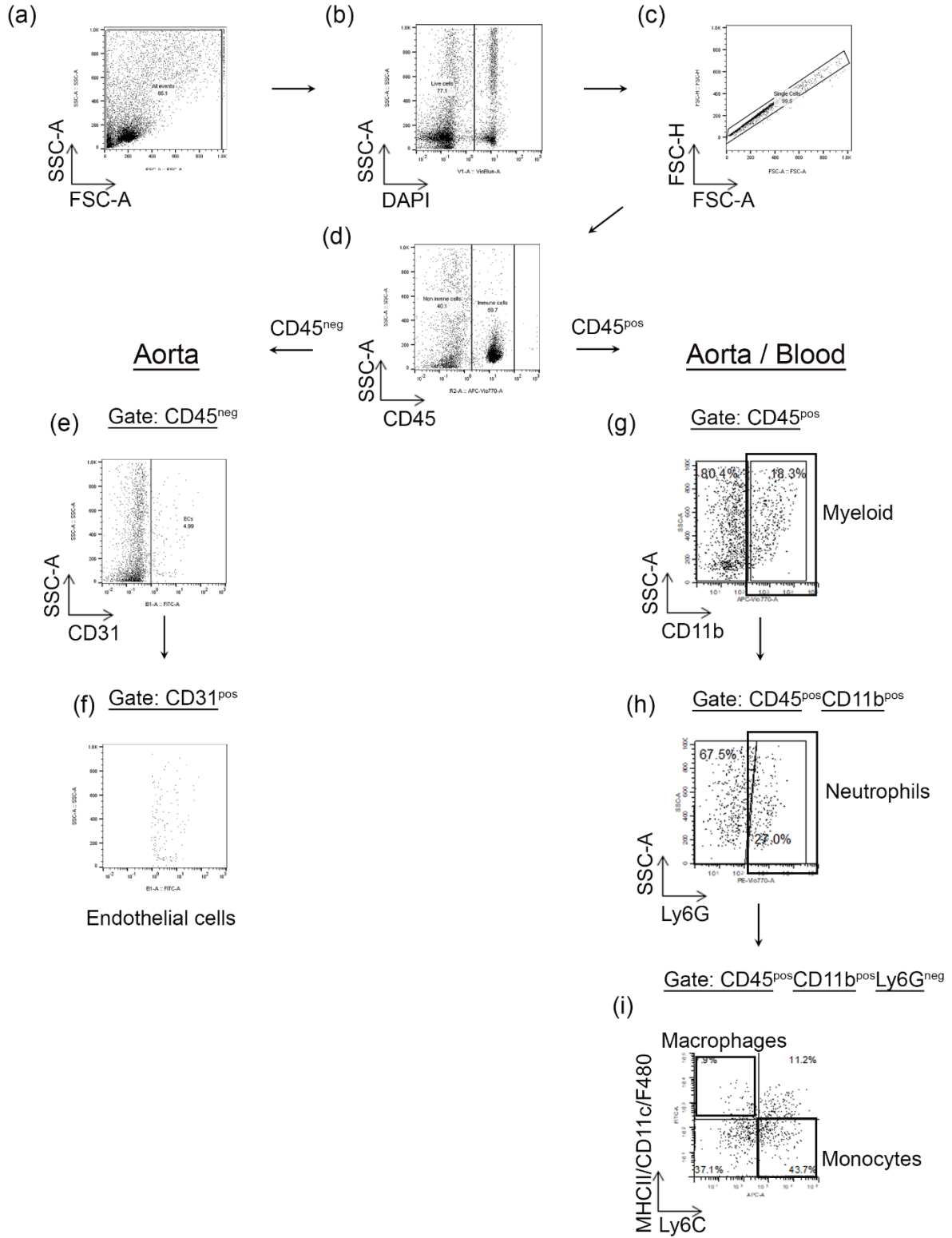


Figure 5: Flowchart for gating strategy used for *in vivo* flow cytometry analysis.

(a,b) Live/dead cells were obtained from the analyzed cell population by staining with DAPI. (c) The live DAPI^{neg} cells were then gated into singlets using FSC-A vs. FSC-H. (d) The cells were then gated into CD45^{pos} immune and CD45^{neg} non-immune cells. (e,f) Endothelial cells were defined as CD31 expressing cells within CD45 negative population. The cell surface expression of IL17RD, ICAM-1, VCAM-1, IL17RA, and IL17RC in CD31 endothelial cells was characterized using delta mean fluorescence intensity (Δ MFI) by subtracting the MFI of unlabeled cells from the MFI of the labeled cells. (g) For leukocyte analysis in the aorta and the blood, the CD45^{pos} cells were analyzed for the number of CD11b^{pos} myeloid cells. (h) The neutrophils were defined as Ly6G^{pos} within the CD11b^{pos} cells. (i) The proinflammatory monocytes, and macrophages were defined as Ly6C^{pos} cells and MHCII/F480/CD11c cells within the Ly6G^{neg} cell population.

2.3.2.2 Histological sectioning

The harvested aorta was fixed in formalin overnight and cut into two segments, the upper segment of the heart containing the heart atria and 1mm of the ascending aorta were cryopreserved in optimal cryopreservation temperature compound (O.C.T; Tissue Tek; Torrance, CA; catalog no: 4583) for histological analysis in the plane of the aortic root according to the procedures described in (100). Calculation of plaque area and lipid deposition was performed according to the procedure described in subsequent sections below.

2.3.2.2.1 Oil Red O staining

Aortic root sections were immersed in a solution of 0.7% Oil Red O in absolute propylene glycol at 60°C. Excess stain was washed off from the tissue by differentiating the slides in 85% propylene glycol, following which the slides were counterstained with Gill's III Haematoxylin. Lipid

accumulation in the aortic root was analyzed by imaging 3 sections per mouse and calculating the average Oil Red O positive area by ImageJ.

2.3.2.2.2 Calculation of plaque area and lipid deposition

To obtain measurements, we used 3-4 sections per mouse for quantification of plaque area, each placed at 100 μ m from the appearance of aortic root leaflets. A microscale (1mm) was used to set the scale for all image calculations. Each plaque was traced using the freehand drawing tool in ImageJ, and the area was obtained using the Measure feature. The total aortic area, including plaques, was outlined to obtain the total aortic area. The relative total area occupied by all plaques in each aorta was represented as a proportion of the total aortic area.

2.3.2.3 X-gal staining

Freshly isolated aortic root was placed in X-gal fixing buffer (1% formaldehyde, 0.2% glutaraldehyde in X-gal wash buffer (dPBS with calcium and magnesium, 0.5M EGTA, 0.04% magnesium chloride, 0.02% NP40, 0.01% sodium deoxycholate)). The tissue was subsequently cryopreserved in an O.C.T solution. 5 μ m thick sections of the tissue were then placed in X-gal working solution consisting of 40mg/ml X-gal (Thermo Fisher; catalog no: B1690), 5mM potassium ferricyanide (Sigma, catalog no: 702587), 5 mM potassium ferrocyanide (Sigma; catalog no: 60279), 2mM magnesium chloride (Sigma; catalog no: M8266) at 37C for 8-16 hours. The sections were then counterstained with nuclear fast red solution (Sigma; catalog no: N3020) for 10 minutes.

2.4 Statistical analysis

Data were tested for normality using the Shapiro-Wilk test. Data sets with the normal distribution of variables were analyzed for statistical significance using Student's unpaired t-test for comparisons between 2 experimental groups or two-way analysis of variance (ANOVA) with Sidak's post-hoc test and are presented as Mean \pm Standard Deviation (S.D) for more than 2 experimental groups. Data sets which were significantly departed from normality by the Shapiro-Wilk test were tested for statistical significance using the Mann-Whitney test for comparisons between 2 experimental groups or two-way analysis of variance (ANOVA) with Sidak's post-hoc test after logarithmic transformation of variables and represented as Median \pm Interquartile range (I.Q.R). A p-value of less than 0.05 was considered significant for all our statistical tests.

CHAPTER 3: RESULTS

3.1 Expression of IL17RD in human aortic endothelial cells.

We first determined the expression of IL17RD in Human Aortic Endothelial Cells (HAECs) and in the THP-1 human monocytic cell line using RT-qPCR. Because IL17RD is highly expressed in human umbilical vein endothelial cells (HUVECs) (63, 102), the total RNA isolated from these cells was used as a positive control. As shown in Figure 6, we observed that HAECs express significantly higher levels of IL17RD compared to HUVECs, whereas THP-1 cells express IL17RD at significantly lower levels as compared to HAECs. Thus, our results demonstrate high levels of IL17RD mRNA expression in primary human aortic endothelial cells.

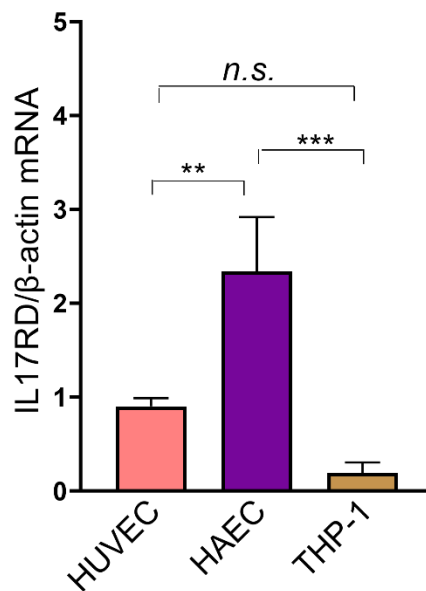


Figure 6: Analysis of *Il17rd* expression in human endothelial cells and THP-1 cells by RT-qPCR. HUVEC and HAEC cells at passage 5 were grown to confluence and harvested. THP-1 cells were harvested at a concentration of $0.3-0.9 \times 10^6$ cells/ml. Total RNA was isolated from the cells and was reverse transcribed for analysis of IL17RD expression by RT-qPCR. Graphs representing quantification of IL17RD mRNA normalized to β -actin in HUVEC, HAEC, and THP-1 cells.

3.2 Knockdown efficiency of IL17RD in HAECs by siRNA transfection.

To suppress IL17RD levels in HAECs, we transfected 50-60% confluent HAECs with *IL17RD* siRNA, or *NT* scrambled control siRNA and assessed IL17RD mRNA levels and cell-surface protein 72 hours after transfection. As shown in Figure 7a, transfection of HAECs with *IL17RD* siRNA resulted in an 83% decrease in IL17RD mRNA expression compared to HAECs transfected with *NT* siRNA. We further quantified cell surface expression of IL17RD in *NT* or *IL17RD* siRNA transfected HAECs by flow cytometry, however, we found a large variability in cell surface expression of IL17RD and the absence of *siIL17RD* effect (Figure 7b), raising concerns about the specificity of anti-human IL-17RD antibody (clone FAB2275P).

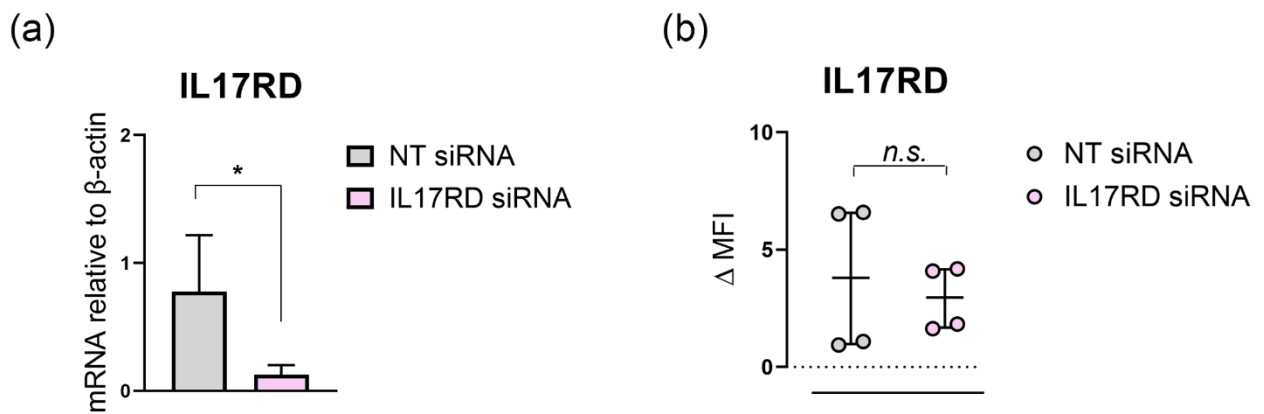


Figure 7: Knockdown efficiency of IL17RD in HAECs by siRNA transfection. HAECs were grown to 50-60% confluence and transfected with NT or IL17RD siRNA for 6 hours (a) Graphs representing quantification of IL17RD mRNA expression by RT-qPCR in HAECs transfected with *siNT* or *siIL17RD* after 72h (b) Quantification of cell-surface IL17RD expression in HAECs transfected with *siNT* or *siIL17RD* 72 hours post-transfection. Data were analyzed using the Mann-Whitney test. Results are presented as Median \pm I.Q.R

3.3 Role of IL17RD in IL17A–induced adhesion of monocytes.

Next, we assessed the role of IL17RD in the modulation of IL17A-induced aortic EC-monocyte interaction, specifically with respect to the adhesion of monocytes onto the endothelial monolayer (83). We used THP-1 cells as a human monocytic cell line model that does not express IL17RD (Figure 1a). Next, we stimulated *siNT* or *siIL17RD* transfected HAECs with IL17A or vehicle control *in vitro* for 24 hours and added THP-1 cells fluorescently labeled with Calcein Orange-Red for 1 hour. As shown in Figures 8b and 8c, *siIL17RD* transfected HAECs had significantly decreased the adhesion of THP-1 cells to the endothelial monolayer compared to *siNT* transfected HAECs in response to IL17A stimulation. Thus, our results indicate that IL17RD promotes monocyte adhesion to the endothelial monolayer *in vitro*.

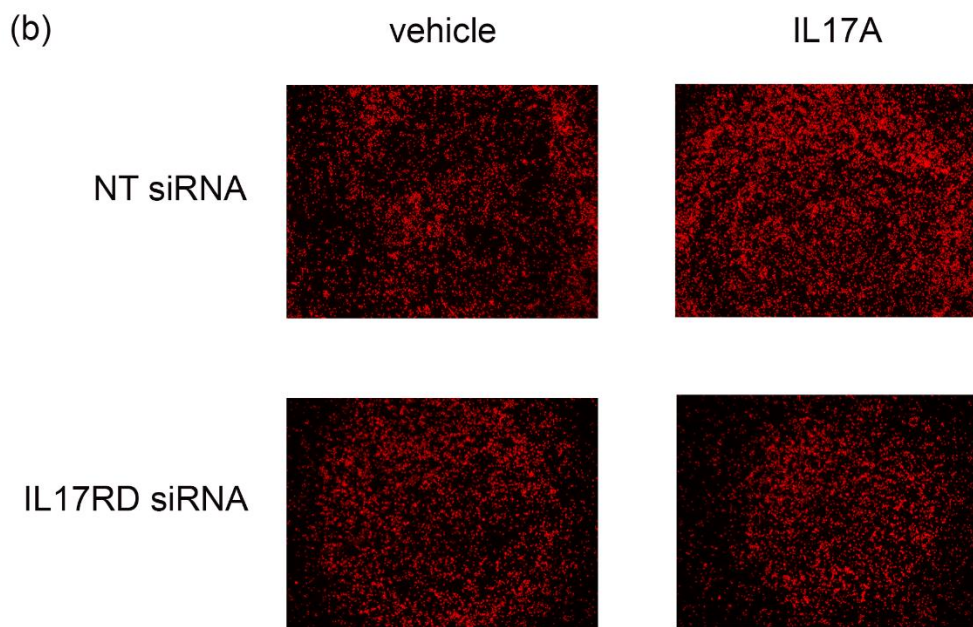
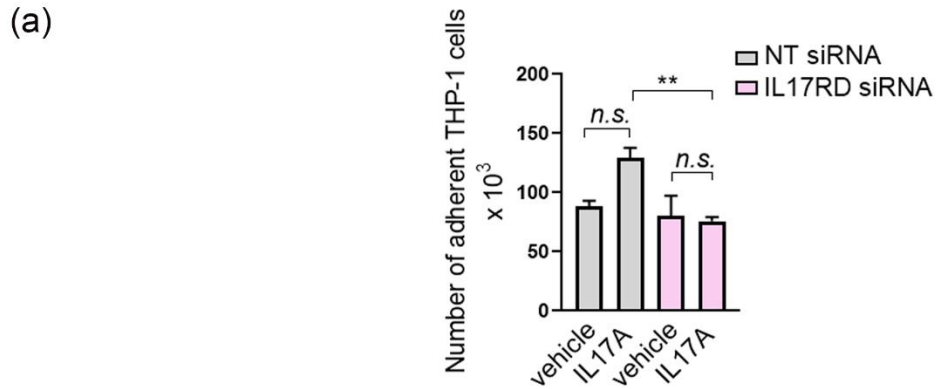


Figure 8: siRNA-driven down-regulation of *IL17RD* in human endothelial cells suppresses

the adhesion of THP-1 cells. HAECs were grown to 50-60% confluence and transfected with

NT or *IL17RD* siRNA for 6 hours (a) Quantification of adhesion of fluorescently labeled THP-1

cells to confluent monolayer of vehicle (0.2% BSA) or IL17A treated *siNT* or *siIL17RD*

transfected HAECs after IL17A treatment for 24 hours. Data are representative of n=5

replicates. (b) Representative fluorescence micrograph images of experimental wells from (b)

taken at original 40X magnification. Data were analyzed by two-way ANOVA with Sidak's

Figure 8 (continued)

post-hoc test. Results in panel (a) are presented as Mean \pm S.D., results in panel (b) are presented as Median \pm I.Q.R. For results in panel (a), data was analyzed with two-way ANOVA using absolute values, log transformed values did not demonstrate statistical significance in the *NT* group. * $p < 0.05$, ** $p < 0.005$

3.4 IL17A does not stimulate VCAM-1 and ICAM-1 expression in HAECs.

Next, we investigated whether IL17RD regulates EC activation downstream of IL17A. In order to determine this, we analyzed the expression of endothelial cell adhesion molecules, specifically VCAM-1 and ICAM-1 in *siNT* or *siIL17RD* transfected HAECs stimulated with IL17A for 24-hours. As shown in Figure 9a-c, immunoblot analyses of NT and IL17RD transfected HAECs showed that stimulation of HAECs with IL17A did not induce any difference in the expression of VCAM-1 and ICAM-1, and further suppression of *IL17RD* did not affect the expression of VCAM-1 and ICAM-1 upon treatment with vehicle or IL17A, suggesting that IL17RD increases IL17A induced monocyte adhesion in HAECs independent of upregulated VCAM-1 and ICAM-1 expression.

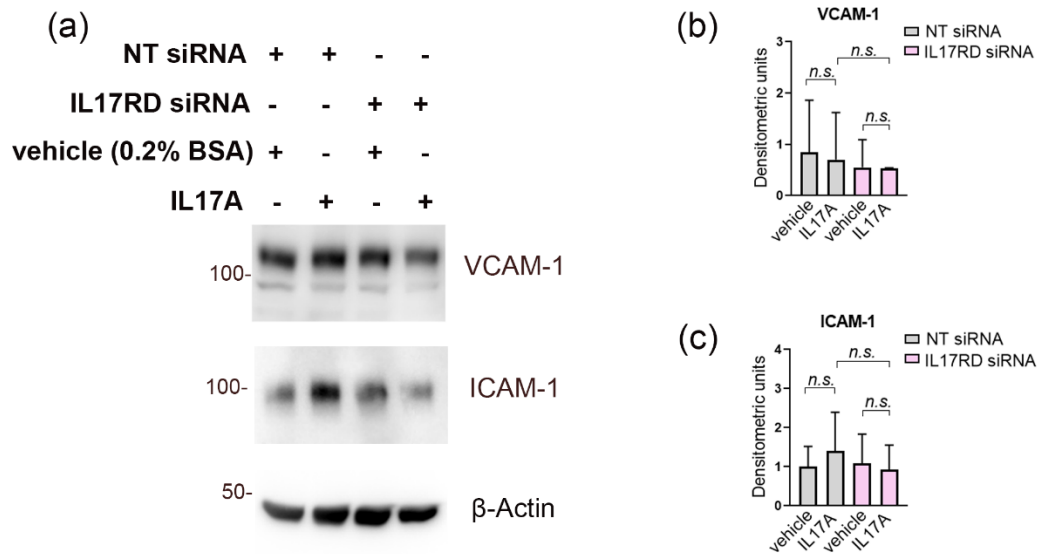


Figure 9: IL17RD promotes monocyte adhesion in HAECs in an ICAM-1- and VCAM-1-independent manner. (a) Representative immunoblots of protein expression of endothelial markers VCAM-1 (120 kDa) and ICAM-1 (92 kDa) in *siNT* or *siIL17RD* transfected HAECs treated with either vehicle control (0.2% BSA) or IL17A (100 ng/ml) for 24 hours. Figure (a) is representative of $n=3$ independent experiments. (b,c) Graphs representing densitometric quantification of $n=3$ independent experiments normalized to β -actin (45 kDa). Results in panel (b) are presented as Median \pm I.Q.R, results in panel (c) are presented as Mean \pm S.D. Data were analyzed using two-way ANOVA with Sidak's post-hoc test.

3.5 IL17A does not significantly induce activation of the NF κ B and MAPK pathways in HAECs.

Since IL17RD has been shown to modulate IL17A-induced activation of the downstream p38 and NF- κ B pathways, we hypothesized that IL17RD regulates the activation of signaling cascades downstream of IL17A in endothelial cells. To investigate this, we determined IL17A-induced activation of known IL17RD signaling effector pathways in *siNT* or *siIL17RD* treated

HAECs, including ERK (67) Akt (67, 78), JNK (79), p38 (54, 58) and NF- κ B pathways (69, 71).

As shown in Figures 10a-g, immunoblot analyses showed that IL17A stimulation did not induce a significant increase in the activation of the ERK, p38, JNK, Akt, and NF- κ B pathways in

HAECs. Further, depletion of IL17RD did not affect the activation of either pathway, suggesting

that IL17RD promotes IL17A-induced monocyte adhesion independent of activation of canonical signaling pathways in HAECs.

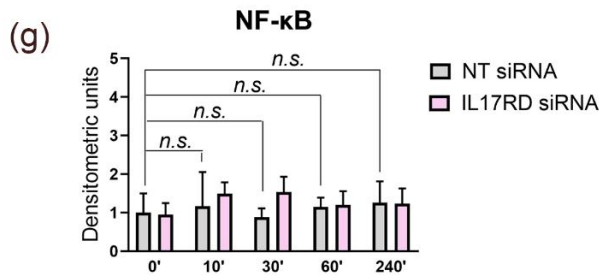
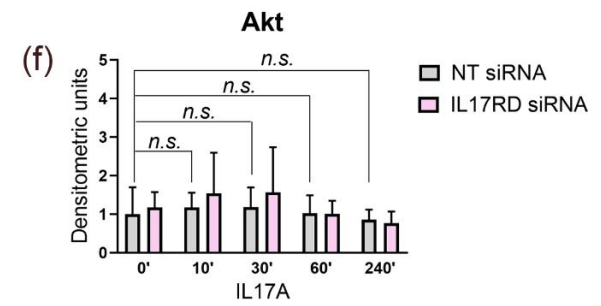
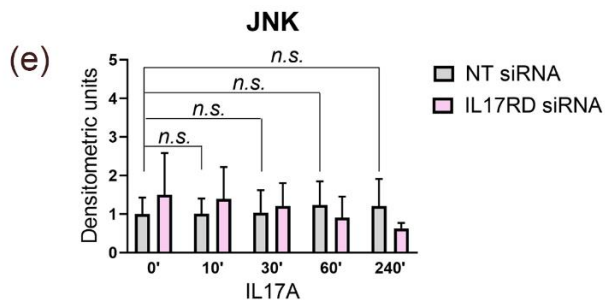
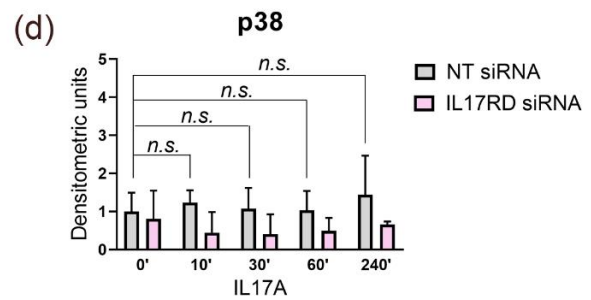
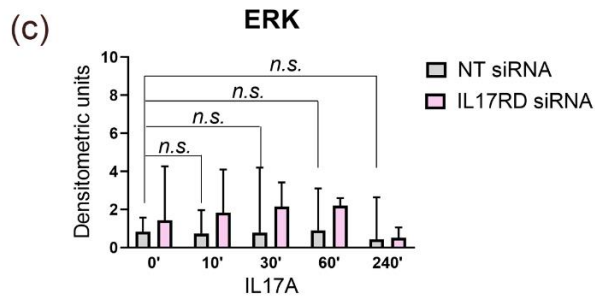
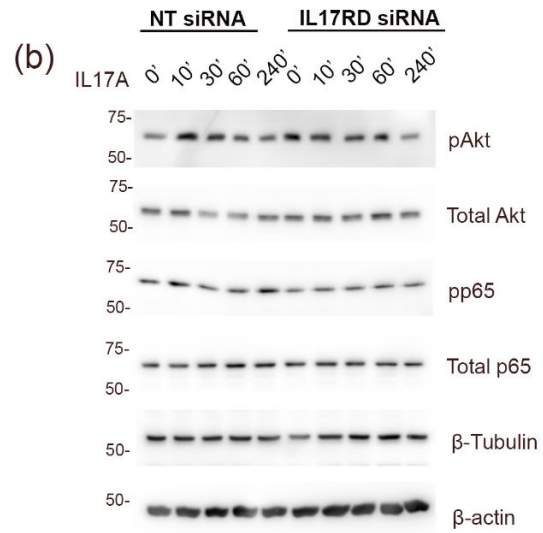
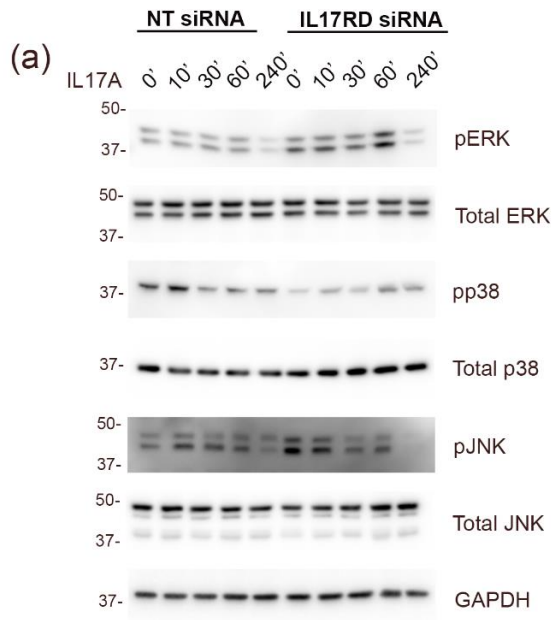


Figure 10: Effect of *IL17RD* inactivation on the activity of downstream signaling cascades in human endothelial cells stimulated with IL17A. (a) Representative immunoblots depicting the activation of ERK (42, 44 kDa), p38 (40 kDa) and JNK (46,54 kDa) MAPK pathways and (b) PI3K/Akt (60 kDa) and NF- κ B (65 kDa) pathways in *siNT* or *siIL17RD* transfected HAECs treated with IL17A (50 ng/ml) for the indicated time points. Figures (a, b) are representative of n=3 independent experiments. (c-g) Graphs representing densitometric quantification of blots from n=3 independent experiments normalized to total ERK (42,44 kDa), total p38 (40 kDa), total JNK (46,54 kDa), total Akt (60 kDa) and total NF- κ B (65 kDa) as indicated on each graph. Graphs (c-g) represent the quantification of n=3 replicates. Results in panels c and d are presented as Median \pm I.Q.R, results in panels e,f and g are presented as Mean \pm S.D. Data were analyzed using two-way ANOVA with Sidak's post-hoc test.

3.6 *I17rd* is expressed in aortic cell subpopulations *in vivo*.

Next, we sought to investigate the *in vivo* relevance of our findings of *I17rd* promotion of monocyte attachment. For this purpose, we initially characterized *I17rd* expression in aortic cell subpopulations and in circulating blood leukocytes in peripheral blood in male and female C57BL/6 mice by flow cytometry as per the gating strategy in Figure 5. As represented in the histograms in Figures 11a and 11b, we observed expression of *I17rd* in aortic endothelial cells and Sca1^{pos} fibroblasts, whereas we did not detect any expression of *I17rd* in CD45^{pos} myeloid cells in the blood as represented in the histograms in Figures 11c and 11d. The quantification of relative differences in mean fluorescence intensity of *I17rd* expression within the above-mentioned aortic cellular subpopulations and leukocytes in males is represented in Figure 11e. We obtained similar results in females, as shown in Figure 11f, suggesting that *I17rd* expression *in vivo* is independent of biological sex. Collectively, our results suggest that in the context of the aorta-leukocyte interaction, the expression of *I17rd* is restricted to aortic cell subpopulations, specifically endothelial cells, and fibroblasts.

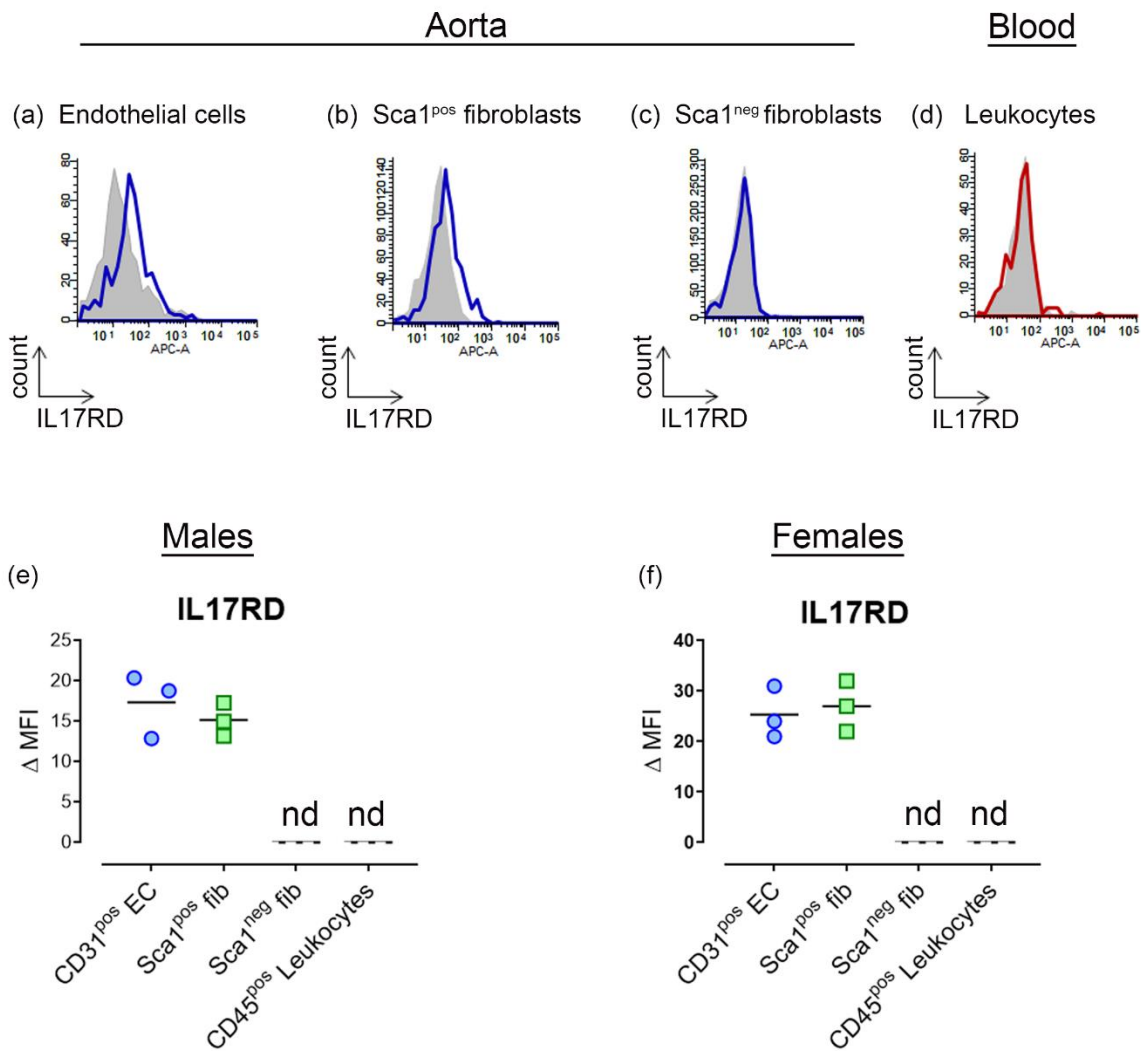


Figure 11: *Il17rd* is expressed in aortic cell subpopulations *in vivo*. Single-cell suspensions of aortas and blood leukocytes were obtained from 8-week-old male and female C57BL/6J mice (n=6 mice/group). Analysis of cell surface *Il17rd* expression in circulating blood and aortic cell suspensions by flow cytometry. Representative histogram of *Il17rd* expression in (a) CD31^{pos} ECs (blue) as compared to unstained controls (grey) (b) CD31^{neg} Sca1^{pos} fibroblasts (blue) endothelial cells as compared to unstained controls (grey) (c) CD31^{neg} Sca1^{neg} fibroblasts (blue) endothelial cells as compared to unstained controls (grey) (d) CD45^{pos} leukocytes (red) as compared to unstained controls (grey). Quantification of *Il17rd* expression on the cell surface of

Figure 11 (continued)

ECs, Sca1^{pos}, Sca1^{neg} fibroblasts, and leukocytes in (e) males and (f) females. Each data point is representative of aortic ECs combined from 2 mice. Results are presented as Mean \pm S.D; nd - not detected.

3.7 Validation of *I17rd* null mouse model.

In order to determine the role of *I17rd* in regulating endothelial cell activation and leukocyte infiltration *in vivo*, we first determined the knockout efficiency of *I17rd* knockout mice. These mice have been previously characterized by our lab (99) as well as by others (97). We validated the genotype of the mice by genotyping as shown in Figure 12a. We further validated the *I17rd* transcript in aortic preparations using primers specific for the N- and C- termini of *I17rd* as shown in Figure 12b. As shown in Figures 12c, both the N- and C-termini appeared to be conserved in *I17rd* $+/+$ mice, whereas *I17rd* $-/-$ mice, the N-terminus appeared to be conserved, whereas no expression of the C-terminus was observed in these mice, thus validating our mouse model.

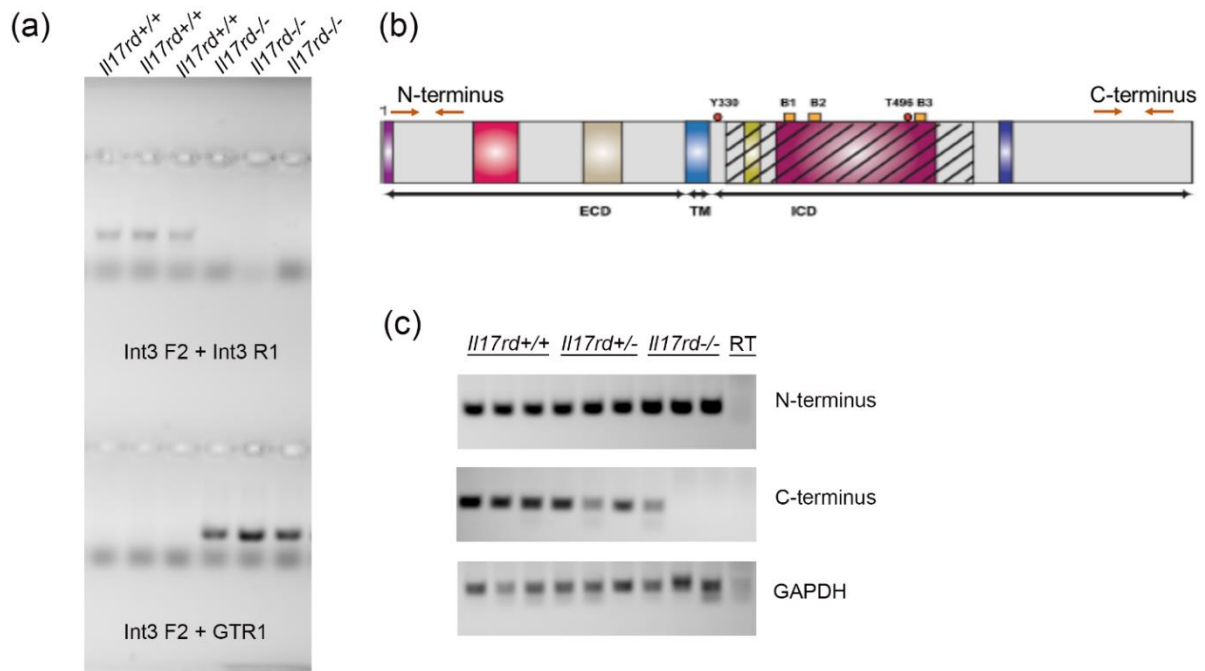


Figure 12: Validation of *Il17rd* null mouse model.

(a) Representative genotyping for validation of *Il17rd* null mice. Representative agarose gel image of PCR amplification of DNA from tail samples of *Il17rd*^{+/+} and *Il17rd*^{-/-} mice using the primer combination Int3-F2 and Int3-R1 for wild-type band, Int3-F2 and GTR1 specific for *Kst223* mutant band (97, 99) (b) Diagrammatic representation of the location of primers specific for N- and C- terminus of *Il17rd*. (c) mRNA expression of N- and C- terminus *Il17rd* in aortas from *Il17rd*^{+/+}, *Il17rd*^{+/-} and *Il17rd*^{-/-} mice. Diagram in panel (b) is from (86).

3.8 Loss of *Il17rd* decreases weight gain and proportion of body fat in male mice upon 14-week WD feeding.

To evaluate *in vivo* extent of leukocyte infiltration and *in vivo* aortic EC expression of VCAM-1 and ICAM-1, we used 8-10 week-old mice male and female global *Il17rd* null mice (96) or

littermate wild-type (*Il17rd* +/+) mice and fed them with WD or CD for 14 weeks. We initially assessed physiological parameters in these mice. As shown in Figure 13a, male *Il17rd*^{-/-} mice were characterized by significantly lower body weight upon 14 weeks of WD feeding as compared to male *Il17rd*^{+/+} mice, whereas female *Il17rd*^{-/-} mice showed no differences in body weight compared to *Il17rd*^{+/+} mice upon 14 weeks of WD feeding as shown in Figure 13b. The cohorts of *Il17rd*^{-/-} and *Il17rd*^{+/+} mice that were maintained on CD showed no difference in body weight upon 14 weeks of feeding either in males, as shown in Figure 13c, or in females, as shown in Figure 13d. Thus, our results suggest that *Il17rd* promotes weight gain upon WD feeding in male mice. Next, we analyzed body composition in our experimental groups. As shown in Figure 13e, in male mice, WD feeding increased the proportion of body fat in *Il17rd*^{+/+} mice as compared to CD-fed mice consistent with previous literature (103), whereas *Il17rd*^{-/-} mice were resistant to increase in gain of body fat upon WD feeding as compared to CD-fed mice. Further, *Il17rd*^{-/-} mice had significantly decreased body fat proportion as compared to WD fed *Il17rd*^{+/+} mice. In females, WD feeding did not change body fat composition (103), and deletion of *Il17rd* did not lead to any significant changes in body fat proportion upon CD or WD feeding, as shown in Figure 13f. Concurrently, WD feeding decreased the proportion of lean mass in male *Il17rd*^{+/+} mice as compared to CD-fed mice, whereas *Il17rd*^{-/-} mice did not show any difference in lean mass proportion upon 14 week WD feeding. Further, male *Il17rd*^{-/-} mice had significantly increased proportion of lean body mass as compared to *Il17rd*^{+/+} mice upon 14 week WD feeding as shown in Figure 13g. Whereas in females, we observed no difference in lean mass proportion upon WD feeding either in *Il17rd*^{+/+} or in *Il17rd*^{-/-} mice as shown in Figure 13h. Thus, our results suggest that *Il17rd* promotes weight gain and accumulation of body fat in male mice upon 14 week WD feeding.

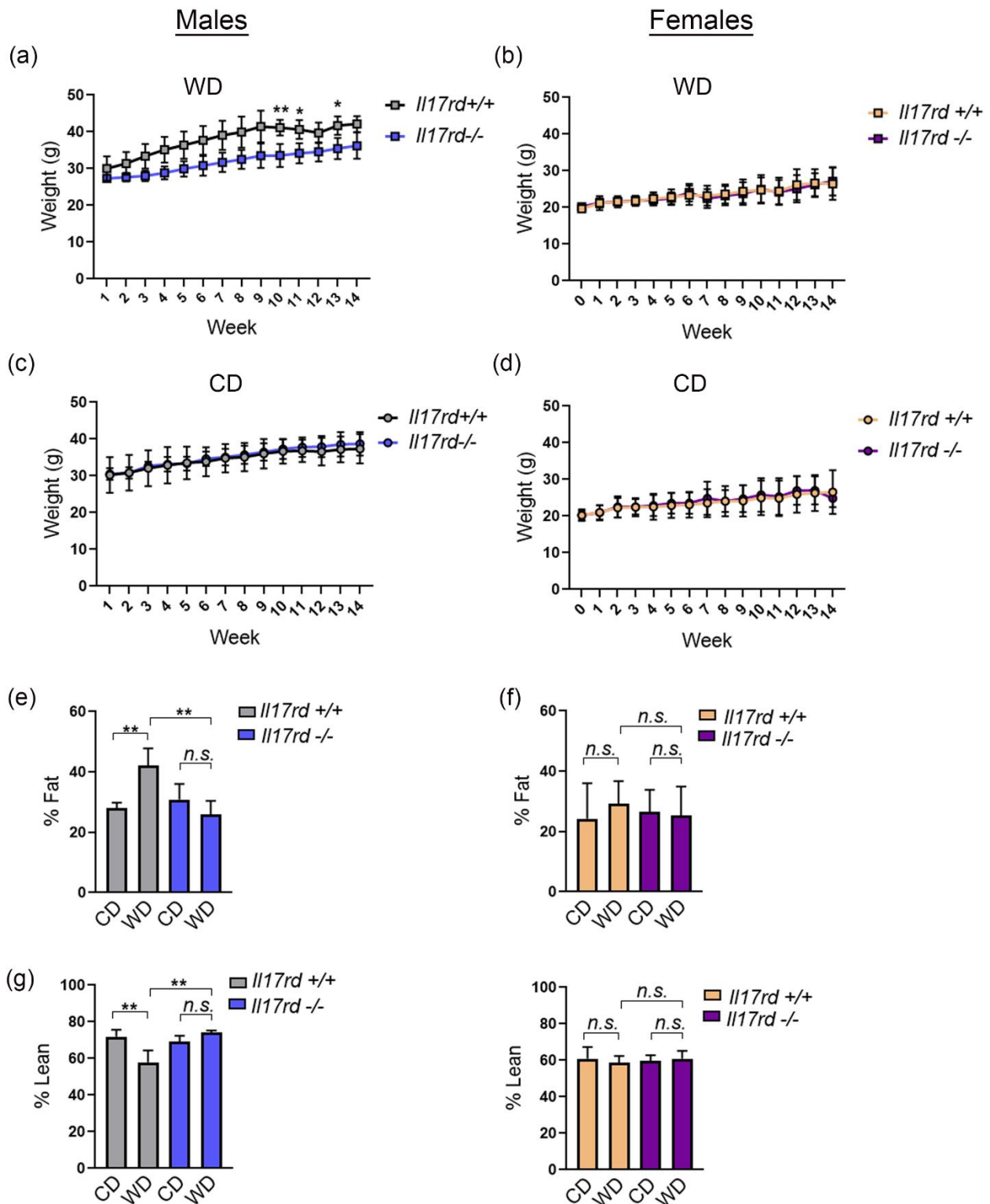


Figure 13: Loss of *Il17rd* decreases weight gain and proportion of body fat in male mice upon 14 week WD feeding. Weekly weight of 8-10 week old (a) male and (b) female *Il17rd*^{-/-}

Figure 13 (continued)

and *I17rd+/+* mice upon 14-week WD feeding. Weekly weight of 8-10 week old (c) male and (d) female *I17rd-/-* and *I17rd+/+* mice upon 14 week of WD or CD feeding. Body fat proportion in (e) males and (f) females *I17rd-/-* and *I17rd+/+* after 14 weeks WD or CD feeding. The proportion of lean mass in (g) males and (h) females *I17rd-/-* and *I17rd+/+* after 14 weeks of WD or CD feeding. Data were analyzed using two-way ANOVA with Sidak's post-hoc test. Results in panels (a-d, f, h) are presented as Mean \pm S.D., results in panels (e,g) are presented as Median \pm I.Q.R * $p < 0.05$, ** $p < 0.005$. n=5-8 mice per sex per genotype.

3.9 Loss of *I17rd* does not affect glucose metabolism.

Since our data show that *I17rd-/-* mice have decreased proportion of body fat, we evaluated whether loss of *I17rd* affects glucose metabolism by performing a GTT after 12 weeks of WD or CD feeding. As shown in Figure 14, our results show that WD-fed *I17rd-/-* mice did not show any significant difference in the rate of glucose clearance either at 30, 60, or 120 minutes post glucose administration as compared to *I17rd+/+* mice either in a males or in females as shown in Figures 14a and 14b. We also observed no differences in glucose tolerance in male and female *I17rd-/-* and *I17rd+/+* mice that were maintained on CD as shown in Figure 14c and 14d, suggesting *I17rd* does not affect glucose metabolism *in vivo*.

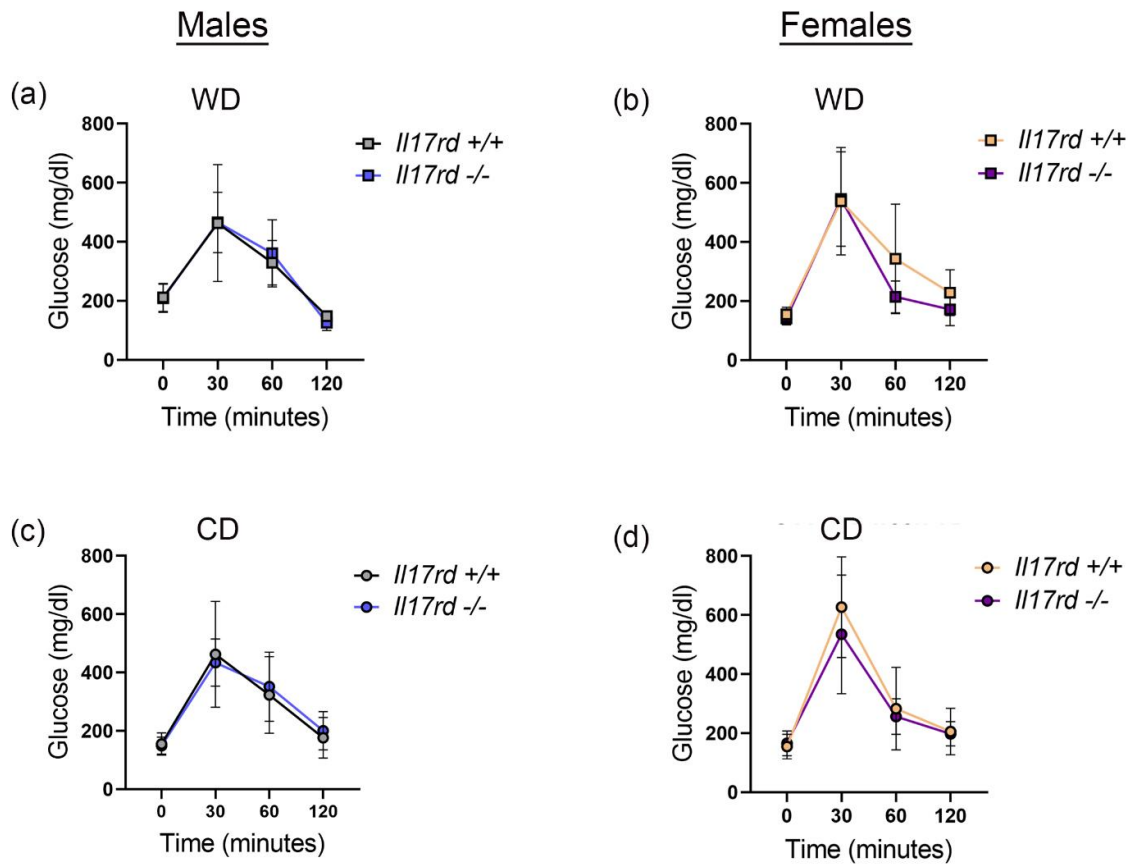


Figure 14: Loss of *Il17rd* does not affect glucose metabolism. GTT after 12 week WD feeding in (a) males and (b) females and 12-week CD feeding in (a) males and (b) females. Data were analyzed using two-way ANOVA with Sidak's post-hoc test. Results are presented as Mean \pm S.D. n=5-8 mice per sex per genotype.

3.10 Effect of loss of *Il17rd* on the levels of circulating IL17A and cholesterol in male and female mice upon WD feeding.

We first analyzed serum levels of circulating IL17 in our experimental groups. In males, WD feeding induced an increase in serum levels of IL17A in *Il17rd*+/+ mice as compared with *Il17rd*+/+ mice fed a CD, consistent with previous findings (104). However, the deletion of *Il17rd* did not significantly affect WD-induced upregulation in serum IL17A levels, as shown in Figure

15a. In females, WD feeding did not induce any differences in serum levels of IL17A in either *Il17rd+/+* or *Il17rd-/-* mice experimental groups, as shown in Figure 15b, indicating that WD-induced upregulation of IL17A is dependent on biological sex.

We subsequently analyzed serum levels of circulating cholesterol as previous studies have shown that cholesterol is essential for the differentiation of Th17 cells and induction of IL17 signaling *in vivo* (105). As shown in Figures 15c-d, total cholesterol levels were elevated in male *Il17rd+/+* and *Il17rd-/-* mice upon WD feeding as compared to CD, and the levels were not significantly different between the two groups. Whereas in females, the levels of cholesterol were significantly decreased in WD-fed *Il17rd-/-* mice as compared to WD-fed *Il17rd+/+* mice. Collectively, our results suggest that *Il17rd* upregulates IL17 in male mice, whereas females show no significant upregulation of IL17 signaling *in vivo*.

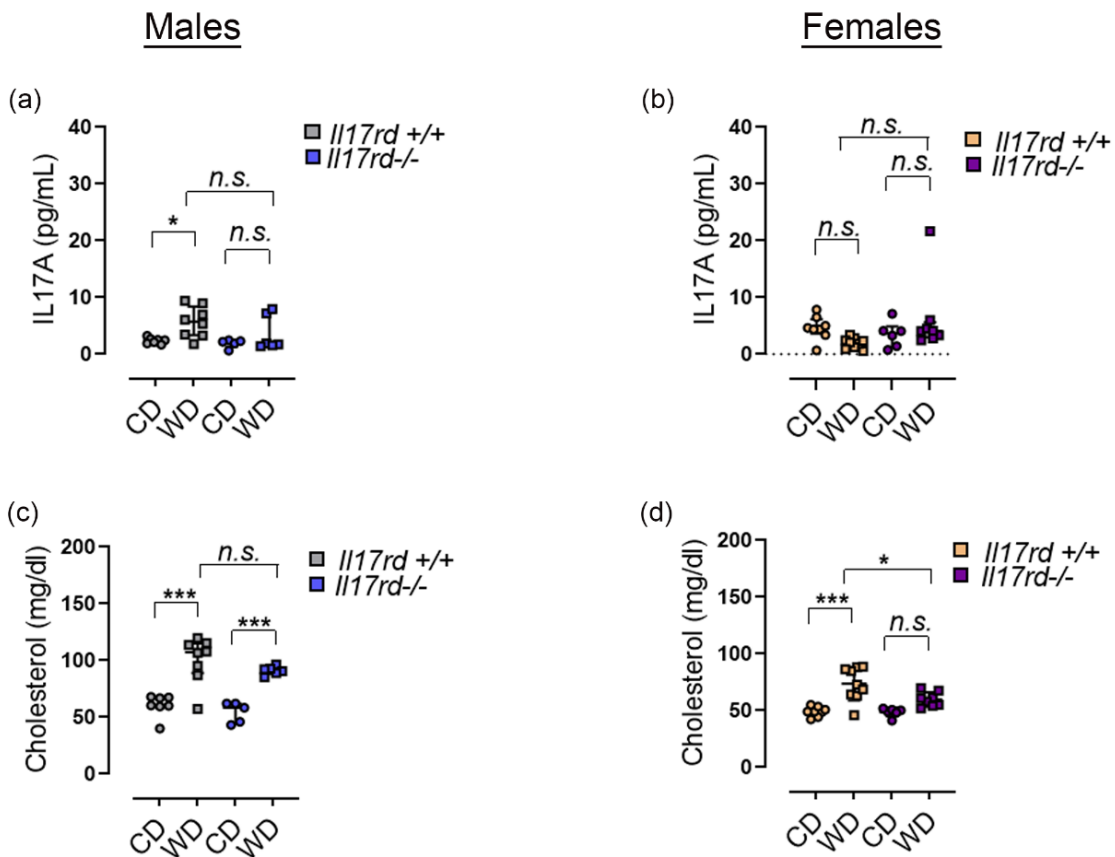


Figure 15: Effect of loss of *Il17rd* on the levels of circulating IL17A and cholesterol levels in male and female mice upon WD feeding.

Serum levels of IL17A in 8-11 week old (a) male and (b) female *Il17rd*^{-/-} and *Il17rd*^{+/+} mice fed a WD or CD for 14 weeks. Levels of total serum cholesterol in (c) male and (d) female *Il17rd*^{-/-} and *Il17rd*^{+/+} mice fed a WD or CD for 14 weeks. Data were analyzed by two-way ANOVA with Sidak's post-hoc test. For results in panel (a), data was analyzed with two-way ANOVA using absolute values, log transformed values did not demonstrate statistical significance. Results in panels (a,b,c) are presented as Median \pm I.Q.R, results in panel (d) are presented as Mean \pm S.D. * $p < 0.05$, ** $p < 0.005$, *** $p < 0.0005$. $n = 5-8$ mice per sex per genotype.

3.11 Loss of *Il17rd* decreases levels of FGF21 upon 14-week WD feeding.

FGF21 is a pleiotropic endocrine hormone that regulates multiple metabolic phenotypes, including adiposity, glucose metabolism, and weight gain (106, 107). Since our previous results suggest that *Il17rd*^{-/-} mice have a leaner phenotype and are resistant to weight gain as compared to *Il17rd*^{+/+} mice when fed with a WD, and since IL17RD was initially discovered as an inhibitor of FGF signaling (60, 61), we assessed the levels of circulating FGF21 in our mice. As shown in Figure 16a, WD feeding increased levels of circulating FGF21 in *Il17rd*^{+/+} male mice as has been previously reported (108). Concomitantly, we also observed an increase in levels of circulating FGF21 in WD-fed *Il17rd*^{-/-} male mice, however, these mice had significantly lower levels of circulating FGF21 upon WD feeding as compared to *Il17rd*^{+/+} mice. Whereas in females, although we observed an elevation in levels of circulating FGF21 in *Il17rd*^{+/+} and *Il17rd*^{-/-} mice upon WD feeding similar to males, there was no statistically significant difference in the levels of FGF21 although the trend remained consistent, as shown in Figure 16b. Thus, our results suggest that IL17RD regulates metabolic phenotype by regulating levels of FGF21.

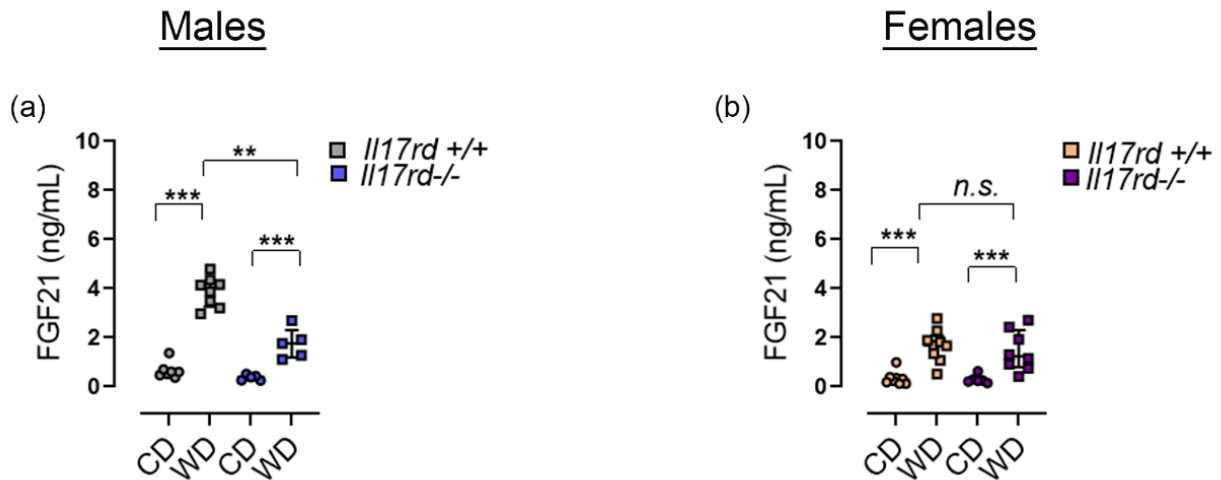


Figure 16: Loss of *Il17rd* decreases levels of FGF21 upon 14-week WD feeding. Serum levels of FGF21 in (a) male and (b) female *Il17rd*^{-/-} and *Il17rd*^{+/+} mice fed a WD or CD for 14 weeks. Data were analyzed by two-way ANOVA with Sidak's post-hoc test. Results are presented as Median ± I.Q.R *p<0.05, **p<0.005. n=5-8 mice per sex per genotype.

3.12 Loss of *Il17rd* decreases myeloid cell infiltration into the mouse aorta.

We then evaluated the extent of *in vivo* leukocyte infiltration into the aorta in our experimental cohorts of *Il17rd*^{-/-} or *Il17rd*^{+/+} mice fed with WD or CD for 14 weeks. Fresh blood was harvested from the mice and was subject to hematological analysis to determine circulating blood parameters, following which we collected the aortas and assessed the extent of differential leukocyte infiltration into the aorta by flow cytometry. As shown in Figures 17a and 17b, total aortic cell counts were similar between *Il17rd*^{-/-} and *Il17rd*^{+/+} mice fed with WD or CD in males as well as in females. We then analyzed leukocyte infiltration into the aorta in our experimental cohorts. As shown in Figure 17c, total circulating leukocyte counts were decreased in *Il17rd*^{-/-} mice fed with a WD, whereas in females, the number of circulating leukocytes was not significantly altered between male *Il17rd*^{-/-} and *Il17rd*^{+/+} mice fed either a WD or CD. Analysis

of leukocyte accumulation in the aorta showed that WD increased accumulation of CD11b^{pos} myeloid cells in the aortas of wild-type mice as has been previously described (109), whereas *Il17rd* deficient mice showed a significant decrease in relative accumulation of myeloid cells as shown in Figure 17d. We observed a similar phenotype in aortic infiltration of myeloid cells in females, suggesting that *Il17rd* regulation of leukocyte accumulation occurs independent of biological sex, indicated by Figures 17e and 17f. Next, we characterized the relative infiltration of Ly6C^{pos} proinflammatory monocytes. As shown in Figure 17g, in males, relative levels of circulating monocytes were not significantly different between *Il17rd* ^{-/-} and *Il17rd* ^{+/+} mice fed either a WD or CD for 14 weeks. Further, we observed an increase in aortic infiltration of Ly6C^{pos} monocytes upon WD feeding in *Il17rd*^{+/+} mice (110), and further loss of *Il17rd* was associated with a statistically significant decrease in Ly6C^{pos} proinflammatory monocyte accumulation in the aorta upon WD feeding as shown in Figure 17h. Whereas the relative number of F480/MHCII/CD11c macrophages remained unchanged, as shown in Figures 17k. In females, we did not obtain any statistical significance in proinflammatory monocyte infiltration amongst the experimental groups, as shown in Figures 17i and 17j, however, we observed an increased number of F480/MHCII/CD11c macrophages as shown in Figure 17l, indicating that *Il17rd* affects aortic recruitment of the monocyte-macrophage population upon WD feeding. (110). We also characterized the infiltration of neutrophils since previous findings have implicated IL17RD in promoting neutrophilia (54, 58). As shown in Figures 17m and 17n, we observed that WD-feeding induced a statistically significant increase in the infiltration of Ly6G^{pos} neutrophil cells in the aorta in males (111), and deletion of *Il17rd* significantly decreased neutrophil infiltration upon WD feeding. Whereas in females, WD feeding did not affect the infiltration of neutrophils, as shown in Figures 17o-17p. Summarily, our results suggest that *Il17rd* functions to promote IL17A-induced aortic infiltration of myeloid cells upon WD feeding *in vivo*.

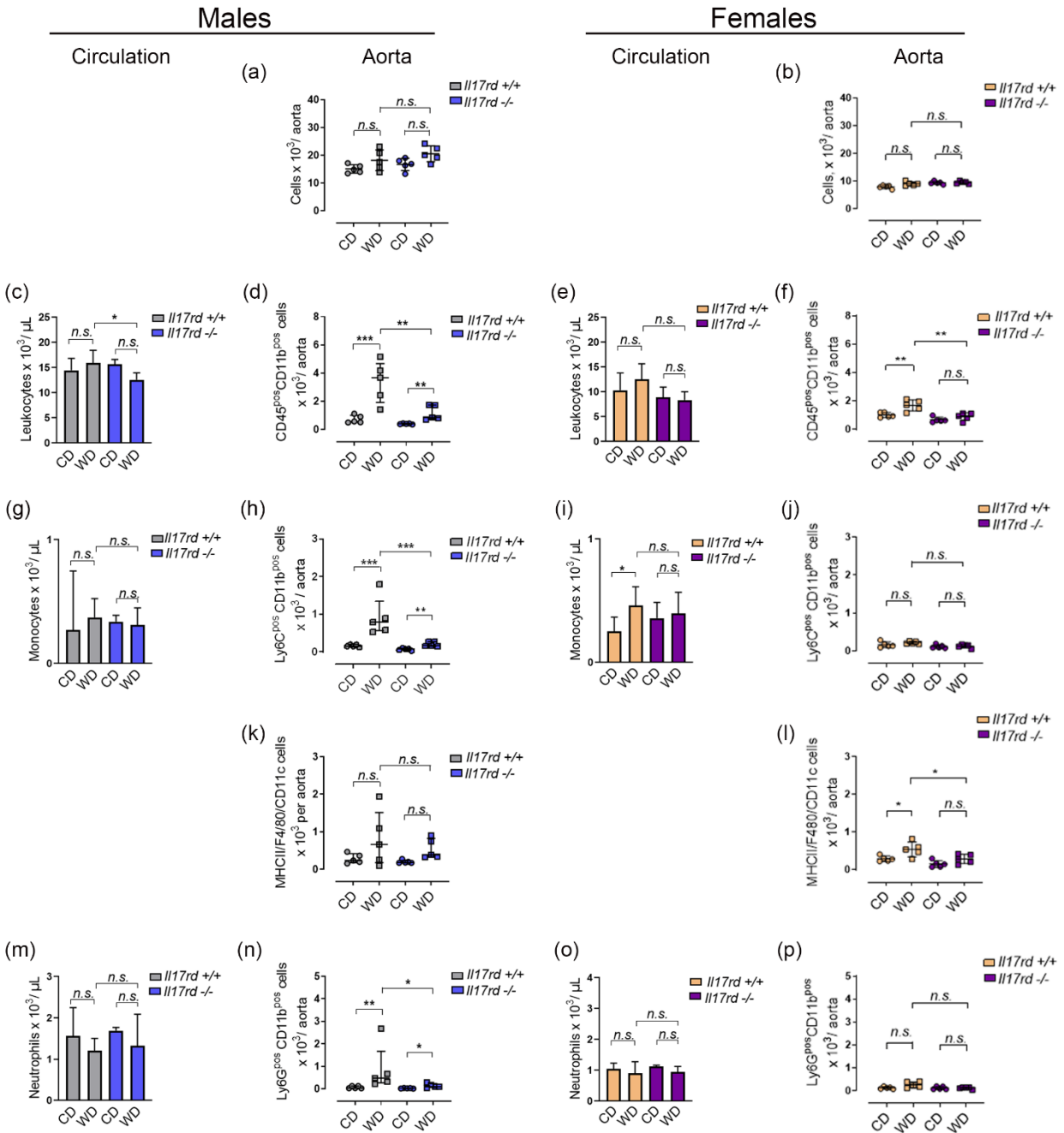


Figure 17: Loss of *Il17rd* decreases myeloid infiltration into the mouse aorta. Analysis of differential leukocyte subpopulations in circulating blood and aortic cell suspensions of 8-10 week old *Il17rd* ^{-/-} and *Il17rd* ^{+/+} mice maintained on a WD or CD for 14 weeks (n = 5-8 mice per group per sex). Total number of cells in aortic cell suspensions in (a) males and (b) females.

Figure 17 (continued)

Number of circulating and infiltrated leukocytes in (c,d) males and in (e,f) females. Total number of circulating and infiltrated monocytes in (g,h) males and in (i,j) females. Aortic cell counts of macrophages in (k) males and (l) females. Number of circulating and infiltrated neutrophils in (m,n) males and in (o,p) females. Data were analyzed by two-way ANOVA with Sidak's post-hoc test. Results in panels (d,g,h,k,m,n,o) are presented as Median \pm I.Q.R, results in panels (a,b,c,e,f,i,j,l,p) are presented as Mean \pm S.D. * $p < 0.05$, ** $p < 0.005$, *** $p < 0.0005$. $n = 5-8$ mice per sex per genotype.

3.13 Loss of *Il17rd* does not significantly affect the aortic endothelial expression levels of VCAM-1 and ICAM-1 upon WD feeding.

We further investigated *in vivo* aortic EC expression levels of VCAM-1 and ICAM-1 in aortic cell suspensions of our experimental cohorts of *Il17rd* $-/-$ and *Il17rd* $+/+$ mice maintained on a WD or CD for 14 weeks. As shown in Figures 18a and 18b, WD-fed *Il17rd* $+/+$ and *Il17rd* $-/-$ mice demonstrated no significant upregulation in aortic EC expression of VCAM-1 in males or in females. Next, we characterized the aortic EC expression of ICAM-1 in these mice. As shown in Figures 18c and 18d, expression of ICAM-1 was not significantly altered in *Il17rd* $+/+$ and *Il17rd* $-/-$ upon WD feeding, which corroborates our *in vitro* findings that IL17 signaling mediates proinflammatory monocyte accumulation independent of upregulation in CAM expression. Thus our results suggest that WD-induced upregulation in IL17 signaling did not affect the expression of VCAM-1 and ICAM-1 in aortic endothelial cells in mice.

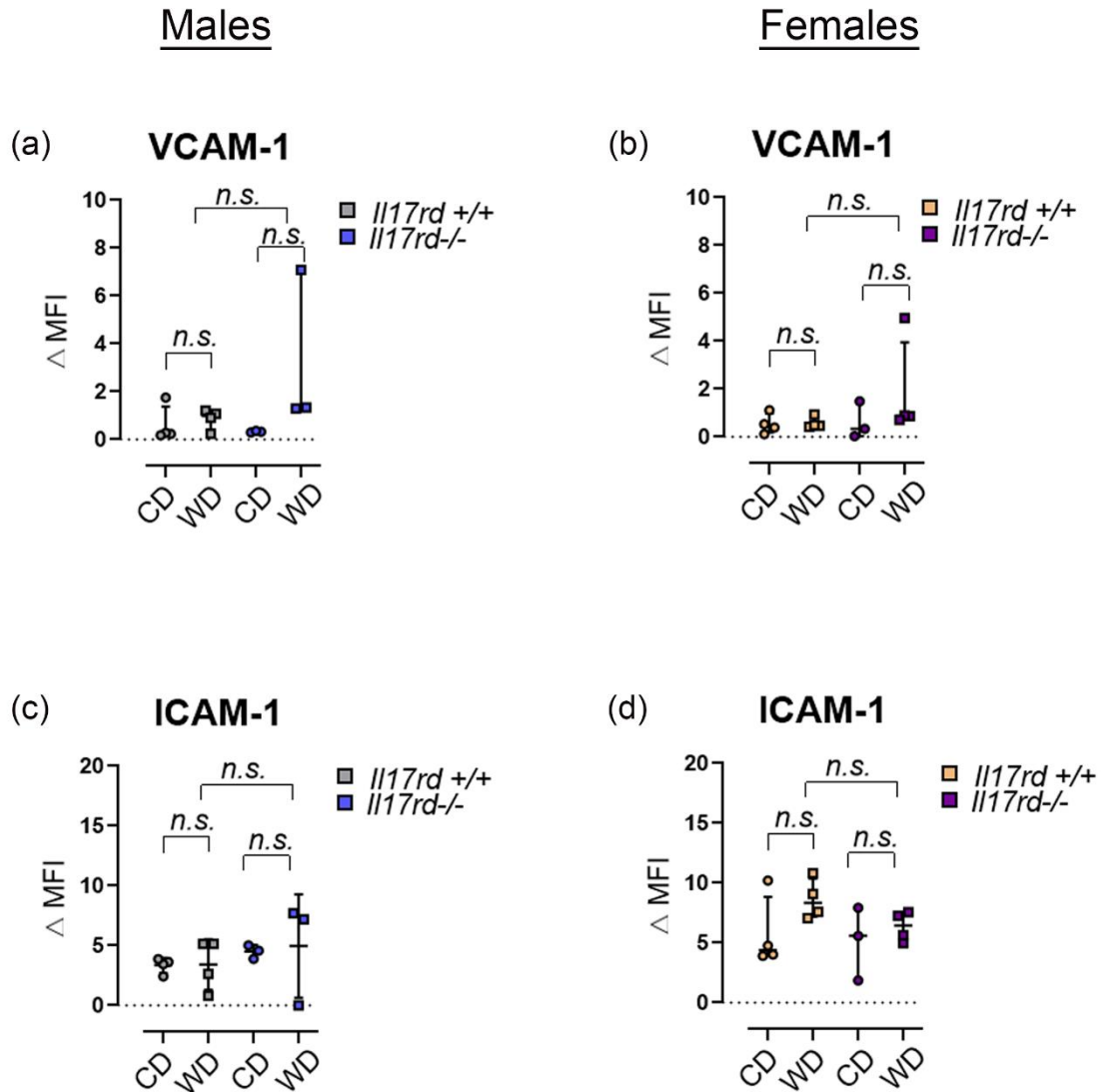


Figure 18: Loss of *Il17rd* does not affect the level of VCAM-1 and ICAM-1 expression on the aortic endothelial cells. Analysis of cell-surface expression of VCAM-1 and ICAM-1 on CD31^{pos} endothelial cells from aortic cell suspensions of 8-11 week-old *Il17rd* $^{-/-}$ and *Il17rd* $^{+/+}$ mice maintained on a WD or CD for 14 weeks (n = 5-8 mice per group per sex). Analysis of VCAM-1 expression in (a) males and (b) females, ICAM-1 expression in (c) males and (d) females, and CD38 expression in (e) males and (f) females. Each data point is representative of aortic ECs combined from 2 mice. Data were analyzed using two-way ANOVA with Sidak's

Figure 18 (continued)

post-hoc test. Results in panels (a,b,d) are presented as Median \pm I.Q.R, and results in panel (c) are presented as Mean \pm S.D.

3.14 Loss of *Il17rd* does not significantly affect the aortic endothelial expression levels of IL17RA and IL17RC upon WD feeding.

Since *Il17rd* has been shown to have overlapping functions with *Il17rc* in the context of IL17 signaling, we then characterized the expression of known receptors of IL17 signaling, including IL17RA and IL17RC in our experimental cohorts of *Il17rd* $-/-$ and *Il17rd* $+/+$ mice maintained on a WD or CD for 14 weeks. As shown in Figures 19a-d, we observed no difference in aortic EC expression of IL17RA and IL17RC upon WD feeding in *Il17rd* $+/+$ mice and *Il17rd* $-/-$ mice in males and in females. We then further characterized the expression of *Il17rc* in our experimental cohorts and observed no differences in aortic EC expression of *Il17rc* in our mice. Therefore, our results suggest that loss of *Il17rd* does not induce a compensatory upregulation in the expression of IL17RA and IL17RC *in vivo*.

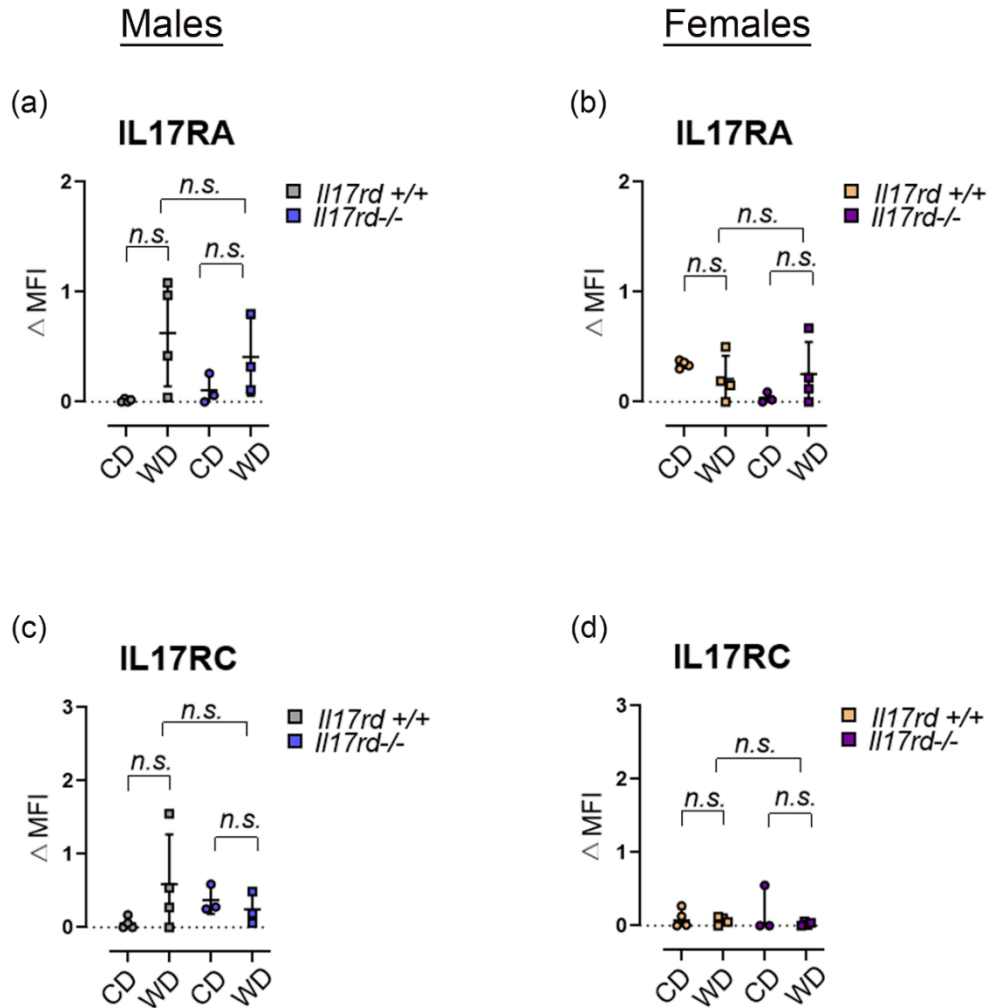


Figure 19: Loss of *Il17rd* does not significantly affect the aortic endothelial expression

levels of IL17RA and IL17RC upon WD feeding. Analysis of expression of IL17RA and

IL17RC in endothelial cells from aortic cell suspensions of 8-11 week old *Il17rd -/-* and *Il17rd +/+*

mice maintained on a WD or CD for 14 weeks (n = 5-8 mice per group per sex). Analysis of

IL17RA expression in (a) males and (b) females and IL17RC expression in (c) male and (d)

female mice. Each data point is representative of aortic ECs combined from 2 mice. Data were

analyzed by two-way ANOVA with Sidak's post-hoc test. Results in panels (a,b,c) are presented

as Mean \pm S.D., results in panel (d) are presented as Median \pm I.Q.R.

3.15 *I17rd* is expressed in atherosclerotic lesions in male mice *in vivo*.

Previous studies have established that leukocyte transmigration occurs as a function of endothelial cell activation during early atherosclerosis (109-111). Our previous findings suggest that deletion of *I17rd* decreases the accumulation of atherosclerotic cell populations under metabolic, inflammatory conditions, specifically myeloid cells. Therefore, we decided to investigate whether the expression of *I17rd* is upregulated within atherosclerotic lesions. Since *I17rd*^{-/-} mice express β -galactosidase under the control of the endogenous *I17rd* promoter, we injected 8-week-old male *I17rd*^{-/-} and *I17rd*^{+/+} mice with an adeno-associated viral vector encoding gain-of-function mouse PCSK9 (AAV-PCSK9^{DY}) (49) to initiate atherogenic plaque formation. After 12 weeks of feeding with either WD or CD, we analyzed differences in endogenous expression of *I17rd* by analyzing β -galactosidase activity within the aortic root. As shown in Figures 20a and 20b, expression of β -galactosidase was robustly upregulated in atherosclerotic lesions in *I17rd*^{-/-} mice fed a WD as compared to *I17rd*^{-/-} mice fed a CD, indicating that expression of *I17rd* was significantly increased during atherosclerotic conditions *in vivo*.

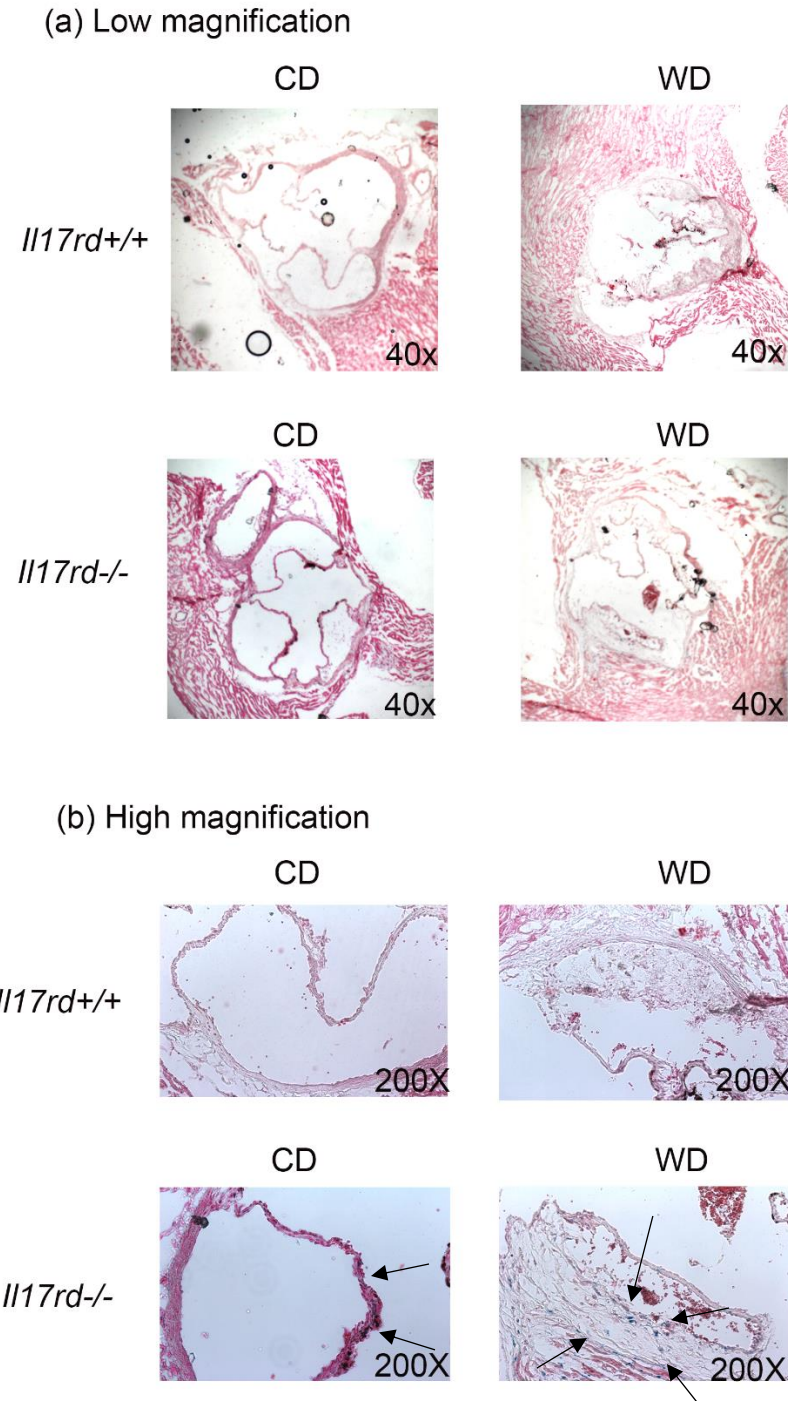


Figure 20: *Il17rd* is expressed in atherosclerotic lesions in male mice *in vivo*. 8 week-old male *Il17rd*^{+/+} and *Il17rd*^{-/-} mice were injected with AAV-mPCSK9^{D374Y} and fed a WD or CD for 12 weeks. Representative β -galactosidase staining of the aortic root at (a) 40X and (b) 200X. (n=4-5 mice per group). Arrowheads point towards β -galactosidase positive cells.

3.16 Loss of *Il17rd* does not affect atherosclerotic plaque formation *in vivo*.

Since our results suggest that *Il17rd* regulates aortic infiltration of myeloid cells upon WD feeding *in vivo*, which has been shown to function as a contributor to atherosclerotic plaque formation since our results suggest that *Il17rd* is expressed in aortic root lesions *in vivo*, we further investigated the functional relevance of the phenotype of WD-induced decreased myeloid cell infiltration by assessing aortic root lesion lipid deposition by Oil Red O staining. As shown in Figure 21a and 21b, loss of *Il17rd* did not affect atherosclerotic lesion area in our mice.

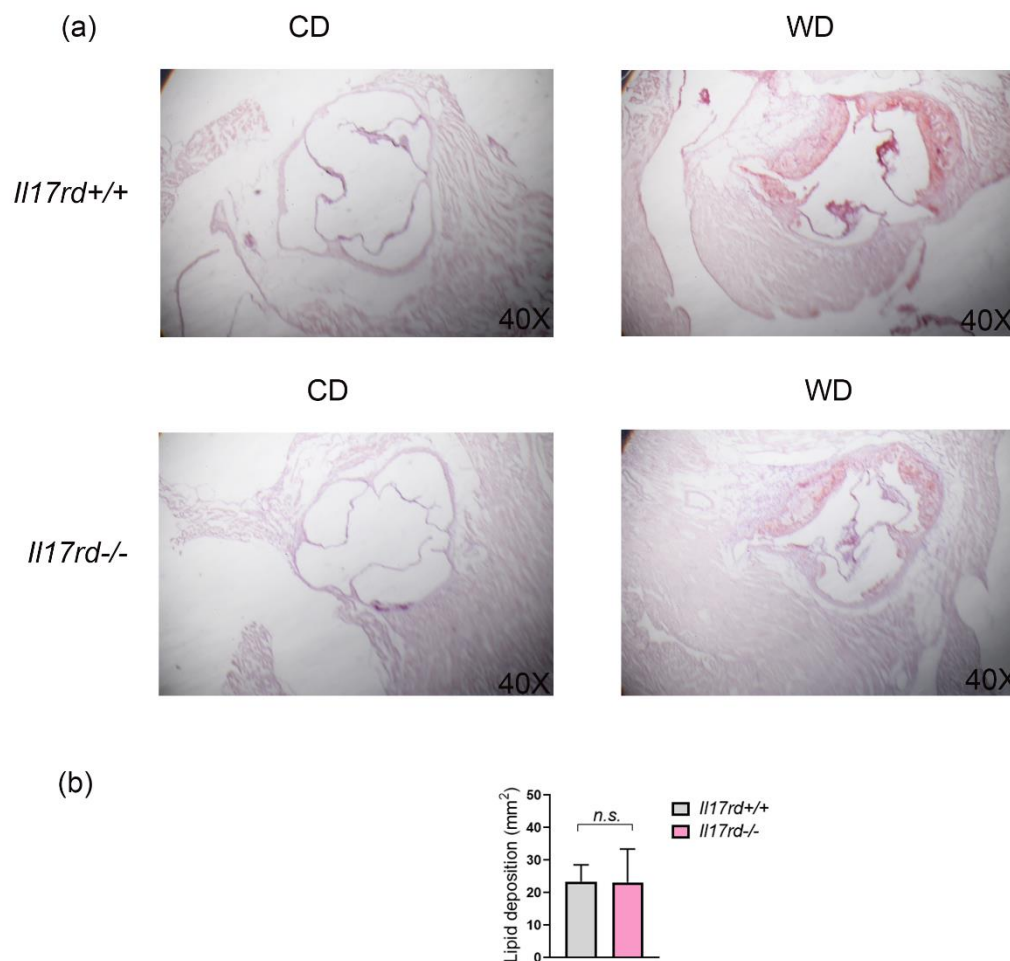


Figure 21: Loss of *Il17rd* does not affect atherosclerotic plaque formation *in vivo*.

Representative aortic root sections of AAV-mPCK9^{D374Y} injected *Il17rd*^{+/+} and *Il17rd*^{-/-} mice fed with a WD or CD for 12 weeks by Oil Red O staining (n=4-5 mice per group). (b)

Quantification of lipid deposition in aortic root sections of the mice. Since the experimental

Figure 21 (continued)

cohorts with a CD showed no plaque formation, we quantified the plaque area of WD-fed mice. Data were analyzed by using unpaired Student's t-test. Results are presented as Mean \pm S.D.

3.17 Analysis of atherogenesis in endothelial cell-specific *I17rd* loss of function mice.

Since our results showed that *I17rd* is expressed in multiple aortic cell subpopulations in vivo, we investigated the endothelial-specific *I17rd* loss of function mouse model. We created a conditional *I17rd* mouse construct containing exons 6 and 7 flanked by loxP sites as described in Figure 4, which is targeted in the extracellular domain. For the purpose of generating endothelial cell-specific *I17rd* loss-of-function mice, we used tamoxifen-inducible *Cdh5-Cre* mice (93). The *Cdh5-CreERT2* mice were first intercrossed with assessed for Cre expression using *Rosa26-Stopfl/fl- tdTomato* expressing mice, which is a Cre-reporter strain that expresses tdTomato fluorescence following Cre-mediated recombination (95). We then injected the *Rosa26-tdTomato-Cdh5CreERT2* positive mice with tamoxifen (1mg/mouse/day) for 5 days, following which the mice were injected with AAV-PCSK9^{D374Y} (49) to induce atherogenesis and were fed with a WD for 8 weeks. We then analyzed the expression of *tdTomato* in the aortic root of these mice. As shown in Figure 22, we observed robust expression of *tdTomato* in the *Rosa26-tdTomato-Cdh5CreERT2* these mice, validating our Cre-driver mice.

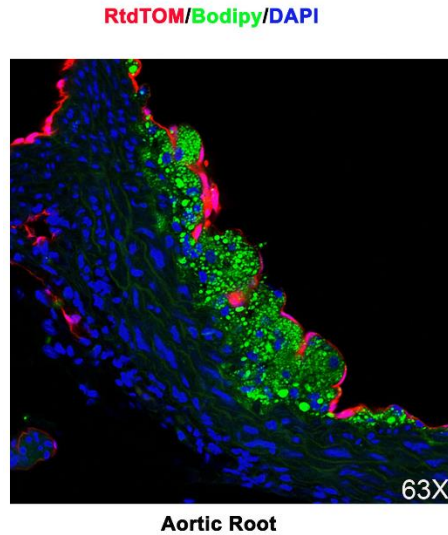


Figure 22: Efficiency of *Cdh5-CreERT2* mice.

Cdh5-CreERT2 mice were intercrossed with *Rosa26-Stopfl/fl- tdTomato* mice. 8 week old mice were injected with tamoxifen for 5 days and injected with AAV-PCSK9^{D374Y} to induce atherosclerosis. After 8 weeks of high-fat feeding, aortic roots were analyzed for tdTomato expression using a Leica SP8 confocal microscope. Blue represents nuclei stained with DAPI (nuclei), green represents lipids stained by BODIPY, red represents endothelial cell positive for tdTomato.

Next, we intercrossed the *Cdh5Cre-ERT2* mice with *Il17rdff* mice to generate *Il17rd ff, Cre-ERT2* positive (*Il17rdECKO*) and *Il17rd ff, Cre-ERT2* negative (*Il17rd ECWT*) mice. 8-10 week old *Il17rd ECWT* and *Il17rdECKO* mice were injected with 1mg/mouse/day of tamoxifen for 5 consecutive days to induce Cre-mediated recombination, following which the mice were injected with a single dose of 10^{11} genome copies/mouse of AAV-mPCSK9^{D374Y}. The mice were then fed with a WD for 16 weeks to induce atherosclerotic plaque formation, following which the aorta was harvested. We then assessed aortic root lesion size in these mice using Oil Red O staining. As shown in Figures 23a and 23b, mice with endothelial cell-specific loss of *Il17rd* did not show significant differences in plaque size as compared to littermate controls, indicating that

endothelial *Il17rd* does not affect atherosclerotic lesion formation in an AAV-PCSK9 model of atherosclerosis.

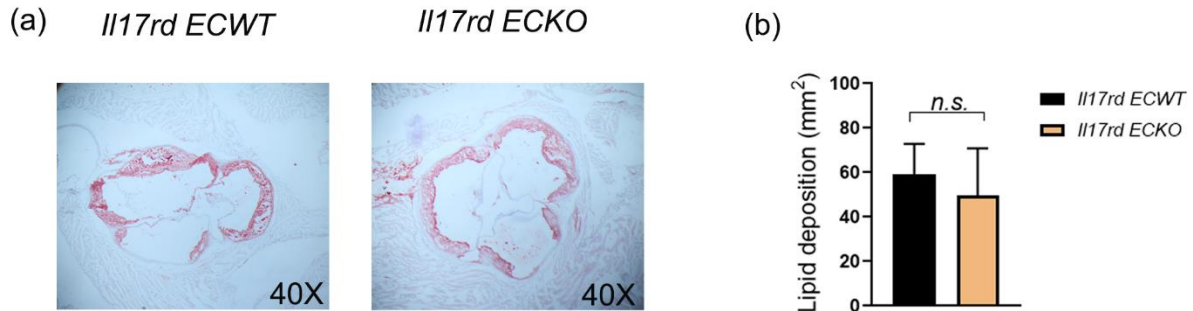


Figure 23: Endothelial specific deletion of *Il17rd* regulates atherosclerotic plaque formation. Male *Il17rd* ECWT and *Il17rd* ECKO mice (n=5-8 mice per group) were injected with tamoxifen followed by AAV-mPCSK9 and fed a western diet for 16 weeks. (a) Representative images of Oil Red O staining in aortic roots and (b) quantification of relative lipid deposition in the aorta. Data in panel b were analyzed using Student's unpaired t-test. Results are represented as Mean \pm S.D.

3.18 Circulating levels of IL23 and IL27 are altered in endothelial cell-specific *Il17rd* knockout mice during atherosclerosis.

Since our results indicate that endothelial cell-specific *Il17rd* does not affect lipid deposition in atherosclerotic plaque *in vivo*, we investigated whether loss of *Il17rd* affects circulating levels of proinflammatory mediators. In order to evaluate this, we first assessed levels of circulating cholesterol in AAV-PCSK9^{D374Y} injected *Il17rd*ECWT and *Il17rd*ECKO mice fed with WD for 16 weeks, however, we did not find any significant differences in levels of circulating cholesterol in these mice as shown in Figure 24a. Next, we assessed levels of known cytokine regulators of *Il17rd* function, including IL17A and FGF21 but did not find any significant differences in the

levels of these cytokines, as shown in Figures 24b and 24c. We then assessed levels of IL23, which functions as an upstream mediator of IL17 signaling in Figure 24d, and found that loss of *Il17rd* significantly enhanced levels of IL23 during atherosclerotic conditions in these mice. We then analyzed levels of proinflammatory interleukin family members, including IL1 α , IL1 β , IL6, IL10, and IL27, and determined that loss of *Il17rd* showed borderline significance towards decreased levels of IL27 in these mice as shown in Figures 24e-i. We also evaluated levels of CCL2 (MCP1) in our experimental cohort since our previous results showed decreased levels of proinflammatory monocytes in WD-fed *Il17rd ECKO* mice in Figure 24j, however, their levels were unaffected in these mice. Lastly, we also analyzed levels of other inflammatory mediators, including TNF α and GM-CSF in Figures 24k and 24l, however, we did not find any significant differences in levels of these cytokines in our experimental cohorts. Collectively, our results suggest that EC specific loss of *Il17rd* modulates levels of inflammatory cytokines IL23 and IL27 during atherosclerosis *in vivo*.

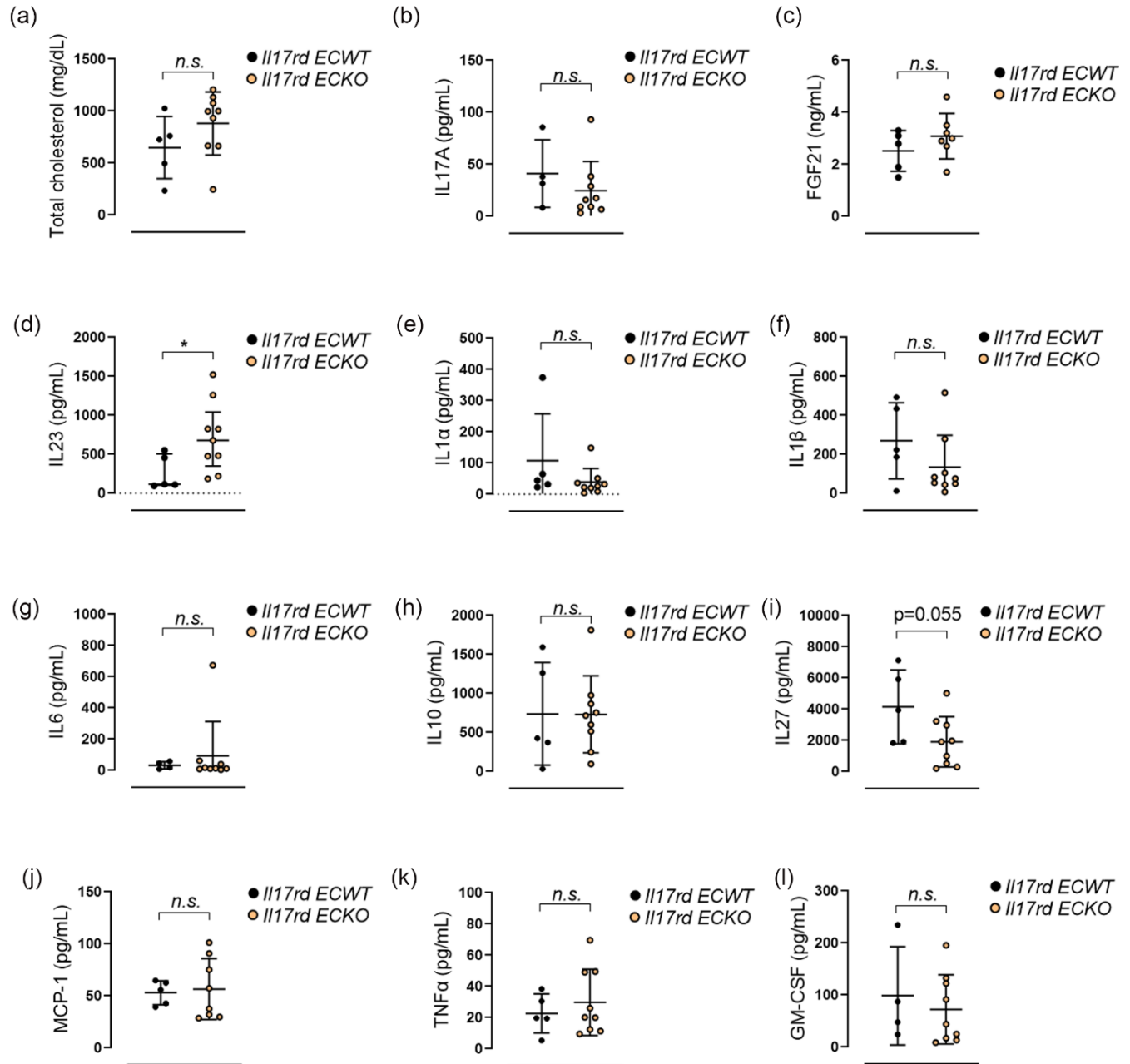


Figure 24: Circulating levels of IL23 and IL27 are altered in endothelial cell-specific *Il17rd* knockout mice during atherosclerosis. Serum levels of (a) cholesterol (b) IL17A (c) FGF21 (d) IL23 (e) IL1 α (f) IL1 β (g) IL6 (h) IL10 (i) IL27 (j) MCP1 (k) IL10 (k) TNF α (l) GM-CSF in 8-10 week old *Il17rd*ECWT and *Il17rd*ECKO mice (n=5-8 mice/group) injected with AAV-PCSK9^{D374Y} and fed a WD for 16 weeks. Results in panels (a-c, e-l) were analyzed using unpaired t-test and

Figure 24 (continued)

represented as Mean \pm S.D., results in panel (d) were analyzed using Mann-Whitney's test and are represented as Median \pm I.Q.R. *p<0.05.

CHAPTER 5: DISCUSSION AND FUTURE PERSPECTIVES

IL17RD was originally identified as an inhibitor of FGF signaling (60, 61) and was determined to be ubiquitously expressed in several cellular subtypes, with high levels of expression in endothelial cells (63, 86). However, the functional role of IL17RD in endothelial cells has not yet been elucidated. Our study attempts to delineate the functional significance of IL17RD in the regulation of inflammatory phenotype by focusing on its regulation of aortic leukocyte infiltration and EC activation by *in vitro* and *in vivo* analyses. We further investigated the pathophysiological relevance of our findings by investigating the role of IL17RD during the phenomenon of atherosclerotic plaque formation using global and endothelial cell-specific *Il17rd* loss-of-function mouse models. We report the novel findings that IL17RD is expressed in aortic ECs *in vitro* and *in vivo*. Additionally, our results demonstrate for the first time that IL17RD promotes the adhesion of monocytic cells in HAECs *in vitro*. Further, IL17RD promotes aortic myeloid cell accumulation, specifically proinflammatory monocytes, macrophages, and neutrophils upon WD feeding *in vivo*, and is expressed in atherogenic plaques in mice. However, endothelial IL17RD does not affect atherosclerotic plaque formation in a PCSK9 model of atherogenesis.

IL17A has been previously shown to promote myeloid cell accumulation and promote atherosclerotic plaque formation in *Apoe*^{-/-} mice. Specifically, deletion of IL17A was shown to ameliorate infiltration of neutrophils, monocytes, and macrophages into the aorta in both male and female mice (112). In our results, we observed that WD induced upregulation of IL17 levels only in males, whereas females showed no appreciable differences in the levels of IL17A. Our results suggest that in females, *Il17rd* promotes leukocyte infiltration by IL17-independent mechanisms, such as low cholesterol signaling, which has been shown to decrease myeloid cell infiltration onto the endothelium (34, 58, 113, 114). In our study, WD feeding enhanced aortic infiltration of proinflammatory monocytes and neutrophils in males, and macrophages in females, which is different from previous findings and might be attributable to differences in

genetic models (*Apoe*^{-/-} mice used in (112) vs BL6 mice used in our study). We observed that deletion of *Il17rd* ameliorated aortic infiltration of WD-induced myeloid cells, including monocytes and neutrophils in males and macrophages in females.

We also observed no difference in aortic expression levels of IL17RA and IL17RC in our mice, indicating that the phenotype of decreased myeloid cell infiltration in our mice occurs specifically due to the deletion of *Il17rd* and not due to a compensatory upregulation in the expression of *Il17ra* and *Il17rc* *in vivo*. In this respect, our study is novel since we demonstrate IL17RD regulation of endogenous IL17A signaling as opposed to previous studies focused on the administration of IL17A (54, 58). Our results also underscore an important role for biological sex in the IL17A-IL17RD signaling axis. In terms of disease relevance, although we observed expression of *Il17rd* within the atherosclerotic lesion, we did not find a significant difference in plaque size upon endothelial cell-specific deletion of *Il17rd* in our experimental cohorts, which might occur due to enhanced FGF signaling in ECs, which has been previously demonstrated to have anti-atherogenic effects (94, 115). Further, our findings implicate IL17RD in the regulation of serum levels of proinflammatory cytokines IL23 and IL27, which have been shown to function as upstream effectors of the IL17A signaling pathway (116).

EC activation encompasses molecular changes in the expression of endothelial Ig CAM molecules such as ICAM-1 and VCAM-1 (38). Given the established role of IL17A as a mediator of ICAM-1 and VCAM-1 expression in macrovascular ECs to enhance adhesion of leukocyte adhesion onto the endothelial monolayer (83, 85), and the high expression levels of IL17RD, we observed in aortic ECs, our results suggest an important role for this receptor in modulating aortic EC function, validating the utility of our *in vitro* model. However, in our results, we observed that IL17 did not upregulate the expression of VCAM-1 and ICAM-1 in endothelial cells in our study. We postulate that these differences might arise due a number of factors, including a) differences in cell type used for analysis (HUVECs vs. HAECs) (85), b) differences in methods of analysis used (number of ICAM^{POS} cells in (83) vs. total cellular expression levels

in our study) and c) donor-specific effects. Further, we did not observe any increase in aortic EC expression of VCAM-1 and ICAM-1 upon WD feeding despite enhanced IL17 levels, validating our *in vitro* findings that IL17 promotes EC activation independent of CAM expression in our model.

Our results also indicate that *Il17rd* promotes lipid accumulation and weight gain upon WD feeding in mice. Further, loss of *Il17rd* decreases levels of FGF21 in WD-fed mice despite a protective effect on weight gain and adiposity, suggestive of enhanced FGF21 sensitivity (60, 61, 117). Our findings highlight a novel role for *Il17rd* in regulating metabolic phenotype *in vivo*. We therefore postulate that IL17RD binds with FGFR1 and displaces β -Klotho from the FGFR1/ β -Klotho complex, given its intrinsic ability to inhibit FGFR1 dimerization and tyrosine kinase activity. In support of this, previous studies with *in vivo* overexpression of β -Klotho in hepatocytes and adipose tissue in mice showed similar results as WD-fed *Il17rd*^{-/-} mice with respect to glucose tolerance and enhanced FGF21 sensitivity (117).

Taken together, our study attempts to deepen the contextual understanding of the molecular mechanisms and regulation of functional phenotypes by IL17 involving its recently identified receptor IL17RD. Our findings suggest that IL17RD functions as a molecular and cellular mediator of IL17 and FGF signaling to functionally regulate phenotypic outcomes in inflammatory disease in a cell-type-dependent manner. Future experiments could focus on whether *Il17rd* regulates aortic infiltration of other known leukocyte subpopulations that have been previously shown to be differentially regulated by IL17 signaling, such as T cells (58). Further since FGF and IL17 signaling have also been shown to regulate leukocyte infiltration to regulate atherogenic plaque stability, it is possible that IL17RD mediates plaque stability rather than plaque size (94, 104, 118-123). Overall, our results emphasize the importance of characterizing IL17RD expression in other disease models, including IL17A and FGF-regulates models of disease involving endothelial activation, and provide impetus to future research to understanding the crosstalk between FGF and IL17 biology with a focus on IL17RD (124).

REFERENCES

1. Matienzo D, Bordoni B. Anatomy, Blood Flow. StatPearls. Treasure Island (FL)2023.
2. Chaudhry R, Miao JH, Rehman A. Physiology, Cardiovascular. StatPearls. Treasure Island (FL)2023.
3. Choi K, Kennedy M, Kazarov A, Papadimitriou JC, Keller G. A common precursor for hematopoietic and endothelial cells. *Development*. 1998;125(4):725-32.
4. Migliaccio G, Migliaccio AR, Petti S, Mavilio F, Russo G, Lazzaro D, et al. Human embryonic hemopoiesis. Kinetics of progenitors and precursors underlying the yolk sac----liver transition. *J Clin Invest*. 1986;78(1):51-60.
5. McGrath KE, Koniski AD, Malik J, Palis J. Circulation is established in a stepwise pattern in the mammalian embryo. *Blood*. 2003;101(5):1669-76.
6. Bautch VL, Caron KM. Blood and lymphatic vessel formation. *Cold Spring Harb Perspect Biol*. 2015;7(3):a008268.
7. Udan RS, Culver JC, Dickinson ME. Understanding vascular development. *Wiley Interdiscip Rev Dev Biol*. 2013;2(3):327-46.
8. De Smet F, Segura I, De Bock K, Hohensinner PJ, Carmeliet P. Mechanisms of vessel branching: filopodia on endothelial tip cells lead the way. *Arterioscler Thromb Vasc Biol*. 2009;29(5):639-49.
9. Taylor AM, Bordoni B. Histology, Blood Vascular System. StatPearls. Treasure Island (FL)2023.
10. dela Paz NG, D'Amore PA. Arterial versus venous endothelial cells. *Cell Tissue Res*. 2009;335(1):5-16.
11. Hennigs JK, Matuszcak C, Trepel M, Korbelen J. Vascular Endothelial Cells: Heterogeneity and Targeting Approaches. *Cells*. 2021;10(10).
12. Feletou M. The Endothelium: Part 1: Multiple Functions of the Endothelial Cells-Focus on Endothelium-Derived Vasoactive Mediators. *Integrated Systems Physiology: from Molecule to Function to Disease*. San Rafael (CA)2011.

13. Gimbrone MA, Jr., Garcia-Cardena G. Endothelial Cell Dysfunction and the Pathobiology of Atherosclerosis. *Circ Res.* 2016;118(4):620-36.
14. Murakami M, Simons M. Regulation of vascular integrity. *J Mol Med (Berl).* 2009;87(6):571-82.
15. Tabas I, Garcia-Cardena G, Owens GK. Recent insights into the cellular biology of atherosclerosis. *J Cell Biol.* 2015;209(1):13-22.
16. Kruger-Genge A, Blocki A, Franke RP, Jung F. Vascular Endothelial Cell Biology: An Update. *Int J Mol Sci.* 2019;20(18).
17. Komarova Y, Malik AB. Regulation of endothelial permeability via paracellular and transcellular transport pathways. *Annu Rev Physiol.* 2010;72:463-93.
18. Dejana E. Endothelial cell-cell junctions: happy together. *Nat Rev Mol Cell Biol.* 2004;5(4):261-70.
19. Lizama CO, Zovein AC. Polarizing pathways: balancing endothelial polarity, permeability, and lumen formation. *Exp Cell Res.* 2013;319(9):1247-54.
20. Aird WC. Phenotypic heterogeneity of the endothelium: I. Structure, function, and mechanisms. *Circ Res.* 2007;100(2):158-73.
21. Aird WC. Endothelial cell heterogeneity. *Cold Spring Harb Perspect Med.* 2012;2(1):a006429.
22. den Braanker H, van Stigt AC, Kok MR, Lubberts E, Bissoendial RJ. Single-Cell RNA Sequencing Reveals Heterogeneity and Functional Diversity of Lymphatic Endothelial Cells. *Int J Mol Sci.* 2021;22(21).
23. Jalkanen S, Salmi M. Lymphatic endothelial cells of the lymph node. *Nat Rev Immunol.* 2020;20(9):566-78.
24. Petrova TV, Koh GY. Biological functions of lymphatic vessels. *Science.* 2020;369(6500).
25. Oliver G, Kipnis J, Randolph GJ, Harvey NL. The Lymphatic Vasculature in the 21(st) Century: Novel Functional Roles in Homeostasis and Disease. *Cell.* 2020;182(2):270-96.

26. Kalluri AS, Vellarikkal SK, Edelman ER, Nguyen L, Subramanian A, Ellinor PT, et al. Single-Cell Analysis of the Normal Mouse Aorta Reveals Functionally Distinct Endothelial Cell Populations. *Circulation*. 2019;140(2):147-63.
27. You LR, Lin FJ, Lee CT, DeMayo FJ, Tsai MJ, Tsai SY. Suppression of Notch signalling by the COUP-TFII transcription factor regulates vein identity. *Nature*. 2005;435(7038):98-104.
28. Fish JE, Wythe JD. The molecular regulation of arteriovenous specification and maintenance. *Dev Dyn*. 2015;244(3):391-409.
29. Davies PF, Civelek M, Fang Y, Guerraty MA, Passerini AG. Endothelial heterogeneity associated with regional athero-susceptibility and adaptation to disturbed blood flow in vivo. *Semin Thromb Hemost*. 2010;36(3):265-75.
30. Virani SS, Alonso A, Benjamin EJ, Bittencourt MS, Callaway CW, Carson AP, et al. Heart Disease and Stroke Statistics-2020 Update: A Report From the American Heart Association. *Circulation*. 2020;141(9):e139-e596.
31. Libby P, Buring JE, Badimon L, Hansson GK, Deanfield J, Bittencourt MS, et al. Atherosclerosis. *Nat Rev Dis Primers*. 2019;5(1):56.
32. Gistera A, Hansson GK. The immunology of atherosclerosis. *Nat Rev Nephrol*. 2017;13(6):368-80.
33. Libby P, Hansson GK. From Focal Lipid Storage to Systemic Inflammation: JACC Review Topic of the Week. *J Am Coll Cardiol*. 2019;74(12):1594-607.
34. Goldstein JL, Brown MS. A century of cholesterol and coronaries: from plaques to genes to statins. *Cell*. 2015;161(1):161-72.
35. Reglero-Real N, Colom B, Bodkin JV, Nourshargh S. Endothelial Cell Junctional Adhesion Molecules: Role and Regulation of Expression in Inflammation. *Arterioscler Thromb Vasc Biol*. 2016;36(10):2048-57.
36. Granger DN, Senchenkova E. Inflammation and the Microcirculation. *Integrated Systems Physiology-From Cell to Function*. San Rafael (CA)2010.
37. Ley K, Huo Y. VCAM-1 is critical in atherosclerosis. *J Clin Invest*. 2001;107(10):1209-10.

38. Galkina E, Ley K. Vascular adhesion molecules in atherosclerosis. *Arterioscler Thromb Vasc Biol.* 2007;27(11):2292-301.
39. Timmerman I, Daniel AE, Kroon J, van Buul JD. Leukocytes Crossing the Endothelium: A Matter of Communication. *Int Rev Cell Mol Biol.* 2016;322:281-329.
40. Nakashima Y, Raines EW, Plump AS, Breslow JL, Ross R. Upregulation of VCAM-1 and ICAM-1 at atherosclerosis-prone sites on the endothelium in the ApoE-deficient mouse. *Arterioscler Thromb Vasc Biol.* 1998;18(5):842-51.
41. Bui TM, Wiesolek HL, Sumagin R. ICAM-1: A master regulator of cellular responses in inflammation, injury resolution, and tumorigenesis. *J Leukoc Biol.* 2020;108(3):787-99.
42. Martinelli R, Gegg M, Longbottom R, Adamson P, Turowski P, Greenwood J. ICAM-1-mediated endothelial nitric oxide synthase activation via calcium and AMP-activated protein kinase is required for transendothelial lymphocyte migration. *Mol Biol Cell.* 2009;20(3):995-1005.
43. Daugherty A, Tall AR, Daemen M, Falk E, Fisher EA, Garcia-Cardena G, et al. Recommendation on Design, Execution, and Reporting of Animal Atherosclerosis Studies: A Scientific Statement From the American Heart Association. *Circ Res.* 2017;121(6):e53-e79.
44. Granada JF, Kaluza GL, Wilensky RL, Biedermann BC, Schwartz RS, Falk E. Porcine models of coronary atherosclerosis and vulnerable plaque for imaging and interventional research. *EuroIntervention.* 2009;5(1):140-8.
45. Emini Veseli B, Perrotta P, De Meyer GRA, Roth L, Van der Donckt C, Martinet W, et al. Animal models of atherosclerosis. *Eur J Pharmacol.* 2017;816:3-13.
46. Brousseau ME, Hoeg JM. Transgenic rabbits as models for atherosclerosis research. *J Lipid Res.* 1999;40(3):365-75.
47. Plump AS, Smith JD, Hayek T, Aalto-Setälä K, Walsh A, Verstuyft JG, et al. Severe hypercholesterolemia and atherosclerosis in apolipoprotein E-deficient mice created by homologous recombination in ES cells. *Cell.* 1992;71(2):343-53.
48. Ishibashi S, Goldstein JL, Brown MS, Herz J, Burns DK. Massive xanthomatosis and atherosclerosis in cholesterol-fed low density lipoprotein receptor-negative mice. *J Clin Invest.* 1994;93(5):1885-93.

49. Roche-Molina M, Sanz-Rosa D, Cruz FM, Garcia-Prieto J, Lopez S, Abia R, et al. Induction of sustained hypercholesterolemia by single adeno-associated virus-mediated gene transfer of mutant hPCSK9. *Arterioscler Thromb Vasc Biol.* 2015;35(1):50-9.
50. Teupser D, Persky AD, Breslow JL. Induction of atherosclerosis by low-fat, semisynthetic diets in LDL receptor-deficient C57BL/6J and FVB/NJ mice: comparison of lesions of the aortic root, brachiocephalic artery, and whole aorta (en face measurement). *Arterioscler Thromb Vasc Biol.* 2003;23(10):1907-13.
51. Shi W, Wang NJ, Shih DM, Sun VZ, Wang X, Lusis AJ. Determinants of atherosclerosis susceptibility in the C3H and C57BL/6 mouse model: evidence for involvement of endothelial cells but not blood cells or cholesterol metabolism. *Circ Res.* 2000;86(10):1078-84.
52. Gaffen SL. Structure and signalling in the IL-17 receptor family. *Nat Rev Immunol.* 2009;9(8):556-67.
53. Li X, Bechara R, Zhao J, McGeachy MJ, Gaffen SL. IL-17 receptor-based signaling and implications for disease. *Nat Immunol.* 2019;20(12):1594-602.
54. Mellett M, Atzei P, Horgan A, Hams E, Floss T, Wurst W, et al. Orphan receptor IL-17RD tunes IL-17A signalling and is required for neutrophilia. *Nat Commun.* 2012;3:1119.
55. Monin L, Gaffen SL. Interleukin 17 Family Cytokines: Signaling Mechanisms, Biological Activities, and Therapeutic Implications. *Cold Spring Harb Perspect Biol.* 2018;10(4).
56. McGeachy MJ, Cua DJ, Gaffen SL. The IL-17 Family of Cytokines in Health and Disease. *Immunity.* 2019;50(4):892-906.
57. Amatya N, Garg AV, Gaffen SL. IL-17 Signaling: The Yin and the Yang. *Trends Immunol.* 2017;38(5):310-22.
58. Su Y, Huang J, Zhao X, Lu H, Wang W, Yang XO, et al. Interleukin-17 receptor D constitutes an alternative receptor for interleukin-17A important in psoriasis-like skin inflammation. *Sci Immunol.* 2019;4(36).
59. Toy D, Kugler D, Wolfson M, Vanden Bos T, Gurgel J, Derry J, et al. Cutting edge: interleukin 17 signals through a heteromeric receptor complex. *J Immunol.* 2006;177(1):36-9.
60. Tsang M, Friesel R, Kudoh T, Dawid IB. Identification of Sef, a novel modulator of FGF signalling. *Nat Cell Biol.* 2002;4(2):165-9.

61. Furthauer M, Lin W, Ang SL, Thisse B, Thisse C. Sef is a feedback-induced antagonist of Ras/MAPK-mediated FGF signalling. *Nat Cell Biol.* 2002;4(2):170-4.
62. Harduf H, Halperin E, Reshef R, Ron D. Sef is synexpressed with FGFs during chick embryogenesis and its expression is differentially regulated by FGFs in the developing limb. *Dev Dyn.* 2005;233(2):301-12.
63. Yang RB, Ng CK, Wasserman SM, Komuves LG, Gerritsen ME, Topper JN. A novel interleukin-17 receptor-like protein identified in human umbilical vein endothelial cells antagonizes basic fibroblast growth factor-induced signaling. *J Biol Chem.* 2003;278(35):33232-8.
64. Xiong S, Zhao Q, Rong Z, Huang G, Huang Y, Chen P, et al. hSef inhibits PC-12 cell differentiation by interfering with Ras-mitogen-activated protein kinase MAPK signaling. *J Biol Chem.* 2003;278(50):50273-82.
65. Novatchkova M, Leibbrandt A, Werzowa J, Neubuser A, Eisenhaber F. The STIR-domain superfamily in signal transduction, development and immunity. *Trends Biochem Sci.* 2003;28(5):226-9.
66. Mellett M, Atzei P, Bergin R, Horgan A, Floss T, Wurst W, et al. Orphan receptor IL-17RD regulates Toll-like receptor signalling via SEFIR/TIR interactions. *Nat Commun.* 2015;6:6669.
67. Kovalenko D, Yang X, Nadeau RJ, Harkins LK, Friesel R. Sef inhibits fibroblast growth factor signaling by inhibiting FGFR1 tyrosine phosphorylation and subsequent ERK activation. *J Biol Chem.* 2003;278(16):14087-91.
68. Torii S, Kusakabe M, Yamamoto T, Maekawa M, Nishida E. Sef is a spatial regulator for Ras/MAP kinase signaling. *Dev Cell.* 2004;7(1):33-44.
69. Fuchs Y, Brunwasser M, Haif S, Haddad J, Shneyer B, Goldshmidt-Tran O, et al. Sef is an inhibitor of proinflammatory cytokine signaling, acting by cytoplasmic sequestration of NF-kappaB. *Dev Cell.* 2012;23(3):611-23.
70. Ren Y, Cheng L, Rong Z, Li Z, Li Y, Zhang X, et al. hSef potentiates EGF-mediated MAPK signaling through affecting EGFR trafficking and degradation. *Cell Signal.* 2008;20(3):518-33.

71. Korsensky L, Haif S, Heller R, Rabinovitz S, Haddad-Halloun J, Dahan N, et al. The tumor suppressor Sef is a scaffold for the classical NF-kappaB/RELA:P50 signaling module. *Cell Signal*. 2019;59:110-21.
72. Kovalenko D, Yang X, Chen PY, Nadeau RJ, Zubanova O, Pigeon K, et al. A role for extracellular and transmembrane domains of Sef in Sef-mediated inhibition of FGF signaling. *Cell Signal*. 2006;18(11):1958-66.
73. Yang S, Wang Y, Mei K, Zhang S, Sun X, Ren F, et al. Tumor necrosis factor receptor 2 (TNFR2).interleukin-17 receptor D (IL-17RD) heteromerization reveals a novel mechanism for NF-kappaB activation. *J Biol Chem*. 2015;290(2):861-71.
74. Boros J, Newitt P, Wang Q, McAvoy JW, Lovicu FJ. Sef and Sprouty expression in the developing ocular lens: implications for regulating lens cell proliferation and differentiation. *Semin Cell Dev Biol*. 2006;17(6):741-52.
75. Grothe C, Claus P, Haastert K, Lutwak E, Ron D. Expression and regulation of Sef, a novel signaling inhibitor of receptor tyrosine kinases-mediated signaling in the nervous system. *Acta Histochem*. 2008;110(2):155-62.
76. Preger E, Ziv I, Shabtay A, Sher I, Tsang M, Dawid IB, et al. Alternative splicing generates an isoform of the human Sef gene with altered subcellular localization and specificity. *Proc Natl Acad Sci U S A*. 2004;101(5):1229-34.
77. Rong Z, Ren Y, Cheng L, Li Z, Li Y, Sun Y, et al. Sef-S, an alternative splice isoform of sef gene, inhibits NIH3T3 cell proliferation via a mitogen-activated protein kinases p42 and p44 (ERK1/2)-independent mechanism. *Cell Signal*. 2007;19(1):93-102.
78. Ziv I, Fuchs Y, Preger E, Shabtay A, Harduf H, Zilpa T, et al. The human sef-a isoform utilizes different mechanisms to regulate receptor tyrosine kinase signaling pathways and subsequent cell fate. *J Biol Chem*. 2006;281(51):39225-35.
79. Yang X, Kovalenko D, Nadeau RJ, Harkins LK, Mitchell J, Zubanova O, et al. Sef interacts with TAK1 and mediates JNK activation and apoptosis. *J Biol Chem*. 2004;279(37):38099-102.
80. Ron D, Fuchs Y, Chorev DS. Know thy Sef: a novel class of feedback antagonists of receptor tyrosine kinase signaling. *Int J Biochem Cell Biol*. 2008;40(10):2040-52.
81. Rong Z, Wang A, Li Z, Ren Y, Cheng L, Li Y, et al. IL-17RD (Sef or IL-17RLM) interacts with IL-17 receptor and mediates IL-17 signaling. *Cell Res*. 2009;19(2):208-15.

82. Wang J, Wang C, Liu L, Hong S, Ru Y, Sun X, et al. Adverse events associated with anti-IL-17 agents for psoriasis and psoriatic arthritis: a systematic scoping review. *Front Immunol.* 2023;14:993057.
83. Mai J, Nanayakkara G, Lopez-Pastrana J, Li X, Li YF, Wang X, et al. Interleukin-17A Promotes Aortic Endothelial Cell Activation via Transcriptionally and Post-translationally Activating p38 Mitogen-activated Protein Kinase (MAPK) Pathway. *J Biol Chem.* 2016;291(10):4939-54.
84. Allam G, Abdel-Moneim A, Gaber AM. The pleiotropic role of interleukin-17 in atherosclerosis. *Biomed Pharmacother.* 2018;106:1412-8.
85. Roussel L, Houle F, Chan C, Yao Y, Berube J, Olivenstein R, et al. IL-17 promotes p38 MAPK-dependent endothelial activation enhancing neutrophil recruitment to sites of inflammation. *J Immunol.* 2010;184(8):4531-7.
86. Pande S, Yang X, Friesel R. Interleukin-17 receptor D (Sef) is a multi-functional regulator of cell signaling. *Cell Commun Signal.* 2021;19(1):6.
87. Hwang SY, Kim HY. Expression of IL-17 homologs and their receptors in the synovial cells of rheumatoid arthritis patients. *Mol Cells.* 2005;19(2):180-4.
88. Meng H, Wang S, Tang X, Guo J, Xu X, Wang D, et al. Respiratory immune status and microbiome in recovered COVID-19 patients revealed by metatranscriptomic analyses. *Front Cell Infect Microbiol.* 2022;12:1011672.
89. McGovern DP, Rotter JI, Mei L, Haritunians T, Landers C, Derkowski C, et al. Genetic epistasis of IL23/IL17 pathway genes in Crohn's disease. *Inflamm Bowel Dis.* 2009;15(6):883-9.
90. Wang K, Zhao S, Liu B, Zhang Q, Li Y, Liu J, et al. Perturbations of BMP/TGF-beta and VEGF/VEGFR signalling pathways in non-syndromic sporadic brain arteriovenous malformations (BAVM). *J Med Genet.* 2018;55(10):675-84.
91. Park ES, Kim S, Yao DC, Savarraj JPJ, Choi HA, Chen PR, et al. Soluble Endoglin Stimulates Inflammatory and Angiogenic Responses in Microglia That Are Associated with Endothelial Dysfunction. *Int J Mol Sci.* 2022;23(3).

92. Anunciado-Koza RP, Manuel J, Mynatt RL, Zhang J, Kozak LP, Koza RA. Diet-induced adipose tissue expansion is mitigated in mice with a targeted inactivation of mesoderm specific transcript (Mest). *PLoS One*. 2017;12(6):e0179879.
93. Wang Y, Nakayama M, Pitulescu ME, Schmidt TS, Bochenek ML, Sakakibara A, et al. Ephrin-B2 controls VEGF-induced angiogenesis and lymphangiogenesis. *Nature*. 2010;465(7297):483-6.
94. Chen PY, Qin L, Baeyens N, Li G, Afolabi T, Budatha M, et al. Endothelial-to-mesenchymal transition drives atherosclerosis progression. *J Clin Invest*. 2015;125(12):4514-28.
95. Madisen L, Zwingman TA, Sunkin SM, Oh SW, Zariwala HA, Gu H, et al. A robust and high-throughput Cre reporting and characterization system for the whole mouse brain. *Nat Neurosci*. 2010;13(1):133-40.
96. Leighton PA, Mitchell KJ, Goodrich LV, Lu X, Pinson K, Scherz P, et al. Defining brain wiring patterns and mechanisms through gene trapping in mice. *Nature*. 2001;410(6825):174-9.
97. Abaira VE, Hyun N, Tucker AF, Coling DE, Brown MC, Lu C, et al. Changes in Sef levels influence auditory brainstem development and function. *J Neurosci*. 2007;27(16):4273-82.
98. Girondel C, Levesque K, Langlois MJ, Pasquin S, Saba-EI-Leil MK, Rivard N, et al. Loss of interleukin-17 receptor D promotes chronic inflammation-associated tumorigenesis. *Oncogene*. 2021;40(2):452-64.
99. He Q, Yang X, Gong Y, Kovalenko D, Canalis E, Rosen CJ, et al. Deficiency of Sef is associated with increased postnatal cortical bone mass by regulating Runx2 activity. *J Bone Miner Res*. 2014;29(5):1217-31.
100. de Waard V, Gijbels MJ, Lutgens E, de Winther MP, de Vries CJ. Models and Analysis of Atherosclerosis, Restenosis, and Aneurysm Formation in the Mouse. *Curr Protoc Mouse Biol*. 2012;2(4):317-45.
101. Hu D, Yin C, Mohanta SK, Weber C, Habenicht AJ. Preparation of Single Cell Suspensions from Mouse Aorta. *Bio Protoc*. 2016;6(11).
102. Liu R, Lauridsen HM, Amezcua RA, Pierce RW, Jane-Wit D, Fang C, et al. IL-17 Promotes Neutrophil-Mediated Immunity by Activating Microvascular Pericytes and Not Endothelium. *J Immunol*. 2016;197(6):2400-8.

103. Yang Y, Smith DL, Jr., Keating KD, Allison DB, Nagy TR. Variations in body weight, food intake and body composition after long-term high-fat diet feeding in C57BL/6J mice. *Obesity (Silver Spring)*. 2014;22(10):2147-55.
104. Erbel C, Chen L, Bea F, Wangler S, Celik S, Lasitschka F, et al. Inhibition of IL-17A attenuates atherosclerotic lesion development in apoE-deficient mice. *J Immunol*. 2009;183(12):8167-75.
105. Varshney P, Narasimhan A, Mittal S, Malik G, Sardana K, Saini N. Transcriptome profiling unveils the role of cholesterol in IL-17A signaling in psoriasis. *Sci Rep*. 2016;6:19295.
106. Tezze C, Romanello V, Sandri M. FGF21 as Modulator of Metabolism in Health and Disease. *Front Physiol*. 2019;10:419.
107. Staiger H, Keuper M, Berti L, Hrabe de Angelis M, Haring HU. Fibroblast Growth Factor 21-Metabolic Role in Mice and Men. *Endocr Rev*. 2017;38(5):468-88.
108. Fisher FM, Chui PC, Antonellis PJ, Bina HA, Kharitononkov A, Flier JS, et al. Obesity is a fibroblast growth factor 21 (FGF21)-resistant state. *Diabetes*. 2010;59(11):2781-9.
109. Koltsova EK, Hedrick CC, Ley K. Myeloid cells in atherosclerosis: a delicate balance of anti-inflammatory and proinflammatory mechanisms. *Curr Opin Lipidol*. 2013;24(5):371-80.
110. Swirski FK, Libby P, Aikawa E, Alcaide P, Luscinskas FW, Weissleder R, et al. Ly-6Chi monocytes dominate hypercholesterolemia-associated monocytosis and give rise to macrophages in atheromata. *J Clin Invest*. 2007;117(1):195-205.
111. Osaka M, Ito S, Honda M, Inomata Y, Egashira K, Yoshida M. Critical role of the C5a-activated neutrophils in high-fat diet-induced vascular inflammation. *Sci Rep*. 2016;6:21391.
112. Butcher MJ, Gjurich BN, Phillips T, Galkina EV. The IL-17A/IL-17RA axis plays a proatherogenic role via the regulation of aortic myeloid cell recruitment. *Circ Res*. 2012;110(5):675-87.
113. Westerterp M, Tsuchiya K, Tattersall IW, Fotakis P, Bochem AE, Molusky MM, et al. Deficiency of ATP-Binding Cassette Transporters A1 and G1 in Endothelial Cells Accelerates Atherosclerosis in Mice. *Arterioscler Thromb Vasc Biol*. 2016;36(7):1328-37.

114. Xiao H, Lu M, Lin TY, Chen Z, Chen G, Wang WC, et al. Sterol regulatory element binding protein 2 activation of NLRP3 inflammasome in endothelium mediates hemodynamic-induced atherosclerosis susceptibility. *Circulation*. 2013;128(6):632-42.
115. Kokkinos J, Tang S, Rye KA, Ong KL. The role of fibroblast growth factor 21 in atherosclerosis. *Atherosclerosis*. 2017;257:259-65.
116. Wang RX, Yu CR, Mahdi RM, Egwuagu CE. Novel IL27p28/IL12p40 cytokine suppressed experimental autoimmune uveitis by inhibiting autoreactive Th1/Th17 cells and promoting expansion of regulatory T cells. *J Biol Chem*. 2012;287(43):36012-21.
117. Samms RJ, Cheng CC, Kharitononkov A, Gimeno RE, Adams AC. Overexpression of beta-Klotho in Adipose Tissue Sensitizes Male Mice to Endogenous FGF21 and Provides Protection From Diet-Induced Obesity. *Endocrinology*. 2016;157(4):1467-80.
118. Durand E, Scoazec A, Lafont A, Boddaert J, Al Hajzen A, Addad F, et al. In vivo induction of endothelial apoptosis leads to vessel thrombosis and endothelial denudation: a clue to the understanding of the mechanisms of thrombotic plaque erosion. *Circulation*. 2004;109(21):2503-6.
119. Wang Y, Zang J, Liu C, Yan Z, Shi D. Interleukin-17 Links Inflammatory Cross-Talks Between Comorbid Psoriasis and Atherosclerosis. *Front Immunol*. 2022;13:835671.
120. Erbel C, Dengler TJ, Wangler S, Lasitschka F, Bea F, Wambsganss N, et al. Expression of IL-17A in human atherosclerotic lesions is associated with increased inflammation and plaque vulnerability. *Basic Res Cardiol*. 2011;106(1):125-34.
121. Danzaki K, Matsui Y, Ikesue M, Ohta D, Ito K, Kanayama M, et al. Interleukin-17A deficiency accelerates unstable atherosclerotic plaque formation in apolipoprotein E-deficient mice. *Arterioscler Thromb Vasc Biol*. 2012;32(2):273-80.
122. Gistera A, Robertson AK, Andersson J, Ketelhuth DF, Ovchinnikova O, Nilsson SK, et al. Transforming growth factor-beta signaling in T cells promotes stabilization of atherosclerotic plaques through an interleukin-17-dependent pathway. *Sci Transl Med*. 2013;5(196):196ra00.
123. Mao Y, Liu XQ, Song Y, Zhai CG, Xu XL, Zhang L, et al. Fibroblast growth factor-2/platelet-derived growth factor enhances atherosclerotic plaque stability. *J Cell Mol Med*. 2020;24(1):1128-40.
124. Shao X, Chen S, Yang D, Cao M, Yao Y, Wu Z, et al. FGF2 cooperates with IL-17 to promote autoimmune inflammation. *Sci Rep*. 2017;7(1):7024.

BIOGRAPHY OF THE AUTHOR

Shivangi Pande was born and raised in Mumbai, India. She obtained her Bachelor's (B.Sc.) and Master of Science (M.Sc.) in Biochemistry in 2010 and 2012 respectively, from the University of Mumbai. She began her doctoral studies at the University of Maine's Graduate School of Biomedical Sciences and Engineering (GSBSE) in September 2013. Shivangi is a candidate for the Doctor of Philosophy degree in Biomedical Sciences from the University of Maine in August 2023.